UNIVERSITY OF TWENTE.

Shifting Shorelines

Finding relations between hydrodynamic forcing and seaward edge erosion rate of a semi-natural salt marsh in a meso-tidal environment

Juliana Bruil

Enschede,
February 2025

Shifting Shorelines

Finding relations between hydrodynamic forcing and seaward edge erosion rate of a semi-natural salt marsh in a meso-tidal environment

Master Thesis Water Engineering and Management

Author:
Juliana Bruil

Supervisors:
Dr.ir. V. Kitsikoudis (Vasileios)
S. Dzimballa MSc (Sarah)
Dr.ir. E.M. Horstman (Erik)

Civil Engineering
University of Twente, the Netherlands
February 28, 2025

Picture front page taken by Juliana Bruil in June 2024.

Shifting Shorelines

Finding relations between hydrodynamic forcing and seaward edge erosion rate of a semi-natural salt marsh in a meso-tidal environment

Juliana Bruil

Summary

This master's thesis investigates the processes driving edge retreat of salt marshes with a particular focus on the relationships between erosion rates and hydrodynamic forcing. Salt marshes are critical coastal ecosystems, valued for their ability to attenuate wave energy, reduce hydraulic loads on engineered defenses, and support biodiversity. However, global trends reveal increasing lateral retreat of marsh edges, driven by the tide and waves, which reduces their surface area and compromises their ecological and protective functions. The Wierum salt marsh in the Wadden Sea, formed through historical semi-natural land reclamations, experiences erosion at its seaward edge. This edge has the shape of a near-vertical cliff with a characteristic height of 0.5 m.

The study addresses key questions on the relationships between spatially averaged hydrodynamic forcing and both average and spatial variability of erosion rate. It also explores the potential influence of edge morphology and vegetation density on localized erosion rates. The methodology integrates morphological and hydrodynamic data spanning from 2016 to 2024. Marsh edge retreat was quantified using aerial imagery and digital elevation models. Hydrodynamic forcing was analysed using the metrics wave power and wave thrust, calculated from wave height and water depth. The findings point towards a positive relationship between both hydrodynamic forcing variables and average marsh edge erosion rate, using both a linear and power law relationship. The results of the linear relationship are in good agreement with comparable studies in the literature, although the number of data points is limited and quite widely distributed, which leads to substantial uncertainties. A negative relation was found between the frequency of inundation (i.e. the percentage of hours per year with cliff inundation) and dimensionless erosion rate. This indicates that the wave intensity during inundation rather than the total period of inundation influences lateral cliff retreat.

The spatial variability of erosion rates shows a slight difference between different sections of the marsh. However, no notable differences were observed in the relationship between erosion rates and hydrodynamic forcing among these sections. Vegetation density and marsh boundary complexity, quantified through the Normalized Difference Vegetation Index (NDVI) and fractal dimensions of the edge shape were also compared to spatial differences in erosion rate. The marsh edge complexity was found to correlate negatively with erosion rate, indicating that a marsh with a more smooth marsh edge erodes faster than a marsh with a more complex marsh edge shape. Although the data were widely scattered, this result is supported by theories found in literature. Along the marsh edge, very low values for NDVI were determined, which indicates that there is barely any vegetation growing at the marsh edge. Nevertheless, a weakly negative relation was found between vegetation density and erosion rate, which supports theories stating a stabilizing effect of vegetation against erosion.

By focusing on the Wierum marsh as a case study, this study contributes to understanding the mechanisms of salt marsh edge retreat in meso-tidal environments. The results provide an addition to the available knowledge about salt marsh edge erosion. Moreover, they offer valuable information for parties responsible for conservation and maintenance of the Wierum salt marsh.

Keywords: Salt marsh, edge retreat, wave power, wave thrust, inundation frequency, vegetation density, salt marsh edge complexity.

Preface

This master thesis marks the end of my time as student Civil Engineering at the University of Twente. I very much enjoyed my time here during both the Bachelor and Master and I am glad to have been a part of such a welcoming and inspiring community. Diving into the process of salt marsh erosion, I gained new insights into the complexity of hydrodynamics, I learned to always be critical on results and I gained some useful skills regarding academic writing, python coding and data analysis.

While the actual content of my thesis was quite different than what I first was hoping to do, I am still happy with the result and proud to see what I have achieved in the last nine months. To that end, I would like to thank my supervisors from the University of Twente for their advice during our bi-weekly meetings. I would like to thank Erik Horstman, for guiding me at key moments during the process, Vasileios Kitsikoudis for his critical view and efforts to reach my fullest potential, and lastly Sarah Dzimballa who gave me many practical insights into the ins and outs of the Wierum marsh. A special thanks goes to Pim Willemsen, for our field trip to the Wierum marsh where I got to see the study site in real life.

I would also like to thank my family for their support during the whole process, their encouragements during tougher times and their views on the topic. I would also like to express my appreciation to friends who were always willing to give their opinion on wording, figure clarity and general layout, or to help me with a quick question. In particularly I would like to thank all fellow students from 'UT HOK' who joined the lunch walks and with whom I enjoyed numerous cups of our very own coffee. I want to give a quick shout-out to the people from 'de gezellige tafel' for all the fun intermezzo's in between the serious work.

I hope that the findings of my thesis may lead to a better understanding of salt marsh erosion processes and add a valuable addition to both the scientific community and practitioners in coastal management.

Juliana Bruil

14-02-2025
Enschede

Table of Contents

Table of Figures

Table of Tables

Chapter 1

Introduction

Salt marshes are found all around the globe in low-lying coastal regions with mild hydrodynamic conditions, for example behind sandbars or barrier islands, or in lagoons, deltas and estuaries. They are vegetated intertidal wetlands that are usually only inundated during high tide (Allen, 2000; Belknap & Kelley, 2021; FitzGerald & Hughes, 2021). The topic of this thesis is the lateral movement of the seaward salt marsh edge, that often has the shape of a cliff subject to erosion (Bouma et al., 2016; Wang et al., 2024).

Salt marshes are valuable coastal protection features because they are able to attenuate the incoming waves from the sea by increasing the drag on the flow through vegetation (Allen, 2000; D'Alpaos et al., 2021; Francalanci et al., 2013; Wilson et al., 2021). This decreases the hydraulic load on any engineered coastal protection structures landward of the marsh, meaning that their crest height could be lower, which saves cost (Schoonees et al., 2019; Vuik et al., 2016). Moreover, salt marshes provide a rich environment for halophytic plants and animals, like birds and macrobenthos. Therefore, salt marshes are important in enhancing and maintaining biodiversity (Belknap & Kelley, 2021). A global trend, unfortunately, is erosion of the marsh at the seaward edge by the incoming tide and waves. The marsh edge tends to move laterally towards the shore which leads to a decrease in marsh surface area (Bendoni et al., 2021; Houttuijn Bloemendaal et al., 2023) and hampers the effectiveness of wave-attenuation. Maintaining healthy, well-functioning salt marshes is therefore important.

In this document, firstly the research context is presented in Chapter 2, which includes the literature review on relevant processes that influence lateral cliff movement, the knowledge gaps that follow from this literature review, the scope and the introduction of the study area (the salt marsh near Wierum). Then, Chapter 3 considers the research structure, consisting of the research objective, research questions and methods. After that, the results are presented (Chapter 4), divided into a marsh-averaged scale and a marsh section scale. The results are discussed in Chapter 5, which also includes a comparison to other literature and some important limitations. Finally, in Chapter 6 the main conclusions of this study are drawn and relevant recommendations for further research are posed. There are three appendices that provide extra background information on the input data, the marsh-averaged scale and the marsh section scale (Appendix A, B and C, respectively).

Chapter 2

Research Context

2.1 Literature Review

2.1.1 Edge erosion in salt marshes

On the seaward side, salt marshes often transition into low-lying mudflats or sandflats that are frequently exposed to tidal and wave action, as they are only dry during low tide (see Figure 2.1) (Allen, 2000; Francalanci et al., 2013; Quaresma et al., 2007). This is the area where there is an opportunity for seedlings to settle and sprout and hence for expansion of the salt marsh. It is also the source and sink of the sediment that enters and exits the marsh (D'Alpaos et al., 2021). The border between the marsh and the flat can be formed by a steep, near-vertical cliff (or scarp) or a gentler slope from the marsh towards the flat (Bouma et al., 2016; Wang et al., 2024). In marshes with a cliff, the exact location of the cliff can be stable in time or retreat towards the mainland (laterally), which means that the marsh shrinks in surface area. In marshes without a cliff, there is often marsh expansion by means of sediment trapping by pioneer vegetation. On top of the lateral edge dynamics of the marsh, there is also vertical erosion or accumulation of sediment which is mostly caused by the hydrodynamic forcing (Dzimballa et al., 2025).

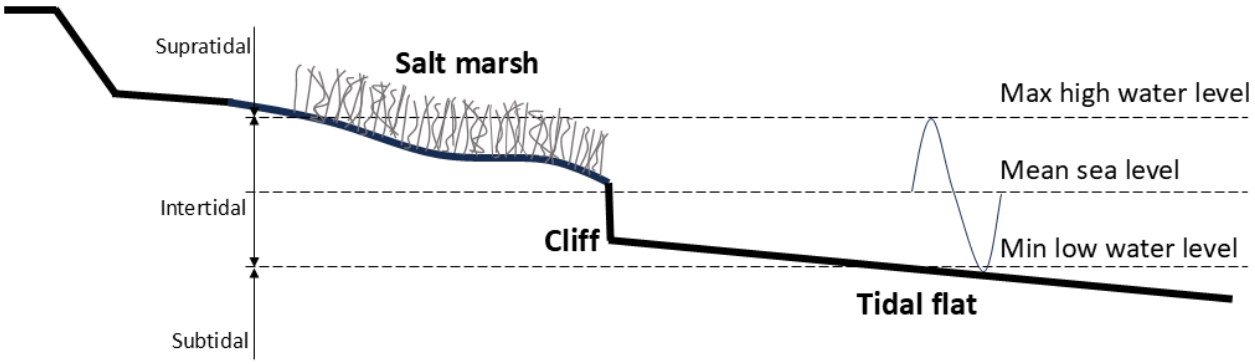

Figure 2.1: Schematic drawing of a salt marsh and tidal flat and inundation depth relative to the tide (not to scale).

The transition over time from gentle seaward slope to steep cliff is characterised by different processes at the top and bottom part of the marsh edge that lead to an increase of this slope. At the bottom part of the slope there is erosion due to hydrodynamic action. Also the tidal flat right in front of the marsh is eroded, which further increases the existing slope. At the same time, at the upper part of the slope the roots of the vegetation prevent sediment from eroding and the aboveground vegetation ensures vertical marsh growth due to sediment trapping. These processes combined support the steepening of the slope between the marsh and the tidal flat, which could

ultimately transform in a vertical cliff (Callaghan et al., 2010; Koppel et al., 2005; Willemsen et al., 2018).

The key characteristics involved in edge retreat are categorized into external forcing (tides, currents, and waves) and internal resistance (biota and soil properties) (Bendoni et al., 2014). These characteristics are interconnected and the whole system influences lateral erosion of the marsh edge and the morphology of the marsh. Figure 2.2 shows all characteristics and processes and will be used to create the structure of this literature review, except for soil characteristics, fauna and shells.

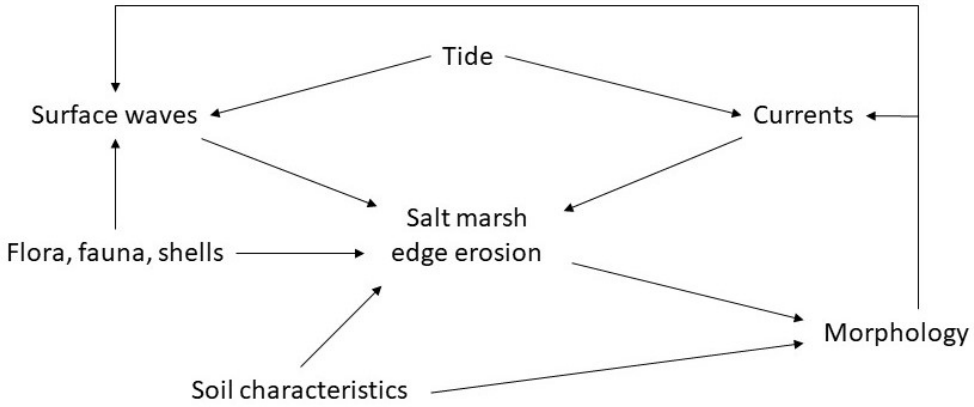

Figure 2.2: Processes involved in salt marsh edge erosion. Adapted and simplified from Bendoni et al. (2014).

2.1.2 Hydrodynamic processes

As Figure 2.2 indicates, hydrodynamic processes impacting salt marsh edge erosion originate from tidal actions, generating both cross-shore and along-shore currents. Besides that, there are smaller surface waves that are wind-generated and hit the marsh edge (Bendoni et al., 2014). Inside the marsh, there is a difference between creek flow (through the channels in the marsh) and sheet flow (through the vegetation). The channels cut through the cliffs at the marsh's edge, meaning that the water enters the marsh first through the channels during rising tide (D'Alpaos et al., 2021). This is one location where edge erosion is happening.

Tidal movement

The influence of the tide is twofold: vertical (the fluctuation in water level from low to high tide) and horizontal (the alongshore and cross-shore current). The tidal fluctuation in water level can cause large cliff erosion failure. During high tide, the soil in the salt marsh is saturated resulting in high pore water pressures. When the water level drops towards low tide there is consequently an excess pore water pressure. This can result in vertical tension cracks in the soil where a block of soil can get loose and topple (Figure 2.3) (Francalanci et al., 2013). This is an example of mass failure, which is mentioned before. Also the alongshore current that the tide generates could cause cliff erosion. When the bed shear stress is larger than the critical bed shear stress, soil particles can be entrained from the bed, resulting in erosion (Bendoni et al., 2021). The same process mechanisms are at play at the cliff edge.

The relative height of the salt marsh with respect to the tidal range influences the rate of cliff erosion. Marsh edge erosion is highest when the marsh elevation level is equal to the water level (Fagherazzi et al., 2013). At low tide, when the water does not reach the marsh edge there is no edge erosion. As soon as the water level is above the marsh platform level, on the other hand, the water flows on top of the marsh (Callaghan et al., 2010). Instead of lateral erosion, surface erosion due to the current and orbital wave motion is occurring more (Bendoni et al., 2021). Depending on the local tidal climate these water level conditions might be more or less

common (Bendoni et al., 2016). Lateral edge retreat is therefore unlikely to be affected by sea level rise. Sea level rise does, however, decrease the wave attenuation capabilities of the marsh (Tonelli et al., 2010).

Wind-waves

The effect of wind-waves on salt marsh cliff erosion is more significant than the tidal water level fluctuation, but only on top of the tidal movement they cause significant bank failure (Callaghan et al., 2010; Francalanci et al., 2013; Karimpour et al., 2016; Mel et al., 2022; Willemsen et al., 2018). Incoming waves are often generated by the wind blowing over the water in front of the marsh. The larger the fetch length and wind speed, the larger the waves (higher wave height and longer wave length). The wind direction also determines the wave direction. Depending on the topography, a maximum wave height at the coast can be determined using the largest fetch length with the maximum wind speed in that direction. Approaching the marsh edge, the wave energy is dissipated due to bottom friction and wave breaking or white capping (Callaghan et al., 2010). This happens on the tidal flat that is slightly sloping towards the marsh. If this dissipation is significant the wave loses (almost) all its energy and cannot erode the marsh edge (Zhu et al., 2024). The bathymetry of the tidal flat in front of the salt marsh therefore influences the lateral erosion rate (Callaghan et al., 2010).

Wave power or wave energy flux (P in W/m) is used most often as the metric for wave climate because it includes the significant wave height (H_s in m), the water density (ρ in kg/m^2), the gravitational acceleration (g in m/s^2), the wave group celerity (c_g in m/s) and wave direction (α in degrees with respect to North) as input variables (Equations 2.1 and 2.2, where the wave group celerity is equal to the wave celerity c_w, assuming shallow water conditions). This makes it an easily usable and comprehensive variable to quantify the hydrodynamic forcing with.

$$P = \frac{1}{8}\rho g H_s^2 c_g \cos(\alpha) \tag{2.1}$$

$$c_g = c_w = \sqrt{gh} \tag{2.2}$$

The wave thrust also gives insight into the effects of wave action on the cliff. Wave thrust (T in kN/m) is a similar concept as wave power (Equation 2.3), but also takes into account the relative water depth with respect to the cliff. This is done by including the area of the cliff that is subject to wave impact, usually determined per meter boundary width (meaning A in m^2/m, Equation 2.4). This means that when the water level is lower than the cliff bottom the impacted area is zero and the area reaches a maximum once the water level is equal or higher than the cliff top level. Also included in the wave thrust are the wave height, water density and gravitational acceleration constant.

$$T = \left(\frac{1}{2}\rho g H_s\right) \cdot A \cdot \cos(\alpha) \tag{2.3}$$

With:

$$A = \begin{cases} 0 & \text{if } h_{water} < h_{cliff,bottom} \\ h_{water} & \text{if } h_{cliff,bottom} < h_{water} < h_{cliff,top} \\ \mathrm{h}_{cliff,top} & \text{if } h_{water} > h_{cliff,top} \end{cases} \tag{2.4}$$

In literature, wave thrust has mostly been used in relation to effects on ships and wind-turbines in the open sea and ocean. Regarding salt marsh edge retreat, wave thrust has been implemented in modelling studies (Donatelli et al., 2019; Tonelli et al., 2010). Results of those studies show that the wave thrust is maximum when the water level is equal to the top of the marsh edge cliff. These water levels have therefore the largest impact on cliff retreat (Fagherazzi et al., 2013). As soon as the water level is above the marsh surface, the wave thrust decreases rapidly. The magnitude of this effect decreases with a decreasing wave height (Tonelli et al., 2010).

2.1.3 Physical processes of marsh edge erosion

The two types of erosion that occur at the marsh edge are particle-by-particle erosion and mass failure. The water from the waves can enter the tension cracks that were created by the rising and falling tide, which weakens the soil and speeds up the erosion process in the cracks. This results in a block of soil toppling or sliding from the edge (Francalanci et al., 2013). Another type of bulk failure is undercutting, when the waves erode the lower part of the cliff and the cantilever part falls down (Fagherazzi et al., 2013). All three mass failure mechanisms are visualized in Figure 2.3.

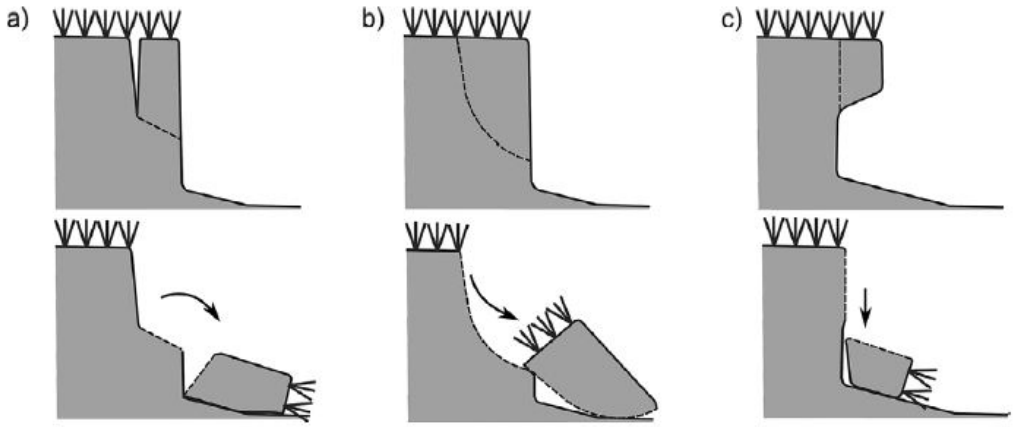

Figure 2.3: Types of mass failure. a) toppling; b) sliding; c) cantilever. Adopted from Bendoni et al. (2014).

Particle-by-particle erosion on a salt marsh cliff is a more or less continuous process where individual soil particles or very small clumps are entrained by the water flow (Bendoni et al., 2014). This type of erosion happens when water flows along the cliff or when waves reach the cliff. The relative water level with respect to the cliff is therefore important. When the water level is quite low particle erosion only happens at the bottom of the cliff and a cantilever shape can be formed (Figure 2.3) (Francalanci et al., 2013). Even though the process of particle-by-particle erosion is slower than mass-failure, Francalanci et al. (2013) found in their lab experiments that in total, the volume of eroded marsh cliff was similar for mass failure and particle erosion.

The edge erosion is often quantified as lateral retreat rate in meter per year (Sanford & Gao, 2018; Schwimmer, 2001; WinklerPrins et al., 2024), but also volumetric erosion in m^3 per meter edge length per year is used (Bendoni et al., 2016; Finotello et al., 2020; Marani et al., 2011; Mel et al., 2022). The volumetric erosion rate gives more insight in the amount of sediment that the marsh is losing, but requires additional detailed information about elevation of the marsh over time. The lateral retreat is a simpler way of quantifying edge erosion.

Leonardi, Defne, et al. (2016) state that in slowly eroding marshes the frequency-magnitude distribution of erosion rate indicates a non-normal distribution with a long tail to the right (high erosion rate). This means that while the mean erosion rate is quite low, there are extreme events that have a large impact on the erosion rate (Leonardi, Defne, et al., 2016; Leonardi & Fagherazzi, 2015). In rapidly eroding salt marshes, on the other hand, the frequency-magnitude distribution is more normally distributed with a larger mean. However, the variation around the mean is smaller and there is a more even erosion rate (Leonardi, Defne, et al., 2016).

Erosion rate - Wave power relationship

A linear relationship between wave power and marsh edge erosion rate is widely accepted. Different methods are used to determine this varying from field measurements, modelling, remote sensing analysis, to historical data analysis (Bendoni et al., 2016; Finotello et al., 2020; Marani et al., 2011; Mel et al., 2022; Sanford & Gao, 2018). Very often, the linear fit is forced to go through the origin (0,0) because no wave power (no waves) should lead to no erosion. The slope of the linear trend is α and includes intrinsic marsh parameters that represent the marsh resistance against the wave power. This results in a simple model for marsh edge erosion rate, where E denotes erosion rate and P wave power. The dimensionless wave power and erosion rate were determined by dividing by the average value ($E^* = E/E_{avg}$ and $P^* = P/P_{avg}$). This means that also α becomes dimensionless: α^* (Equation 2.5).

$$E^* = \alpha^* P^* \tag{2.5}$$

Leonardi, Ganju, and Fagherazzi (2016) evaluated measurements of marsh erosion and wave power at eight salt marshes around the world and found an overarching linear relationship with an α^* of 0.67 (Figure 2.4).

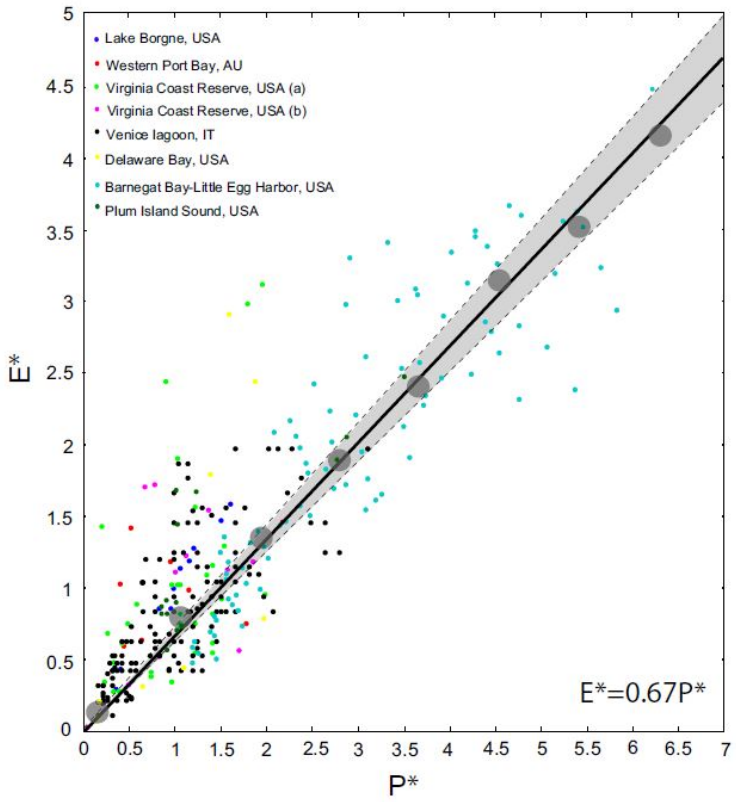

Figure 2.4: Linear relationship between dimensionless wave power (P^*) and dimensionless lateral erosion rate (E^*) with a dimensionless intrinsic marsh parameter (α^*) of 0.67. From Leonardi, Ganju, and Fagherazzi (2016).

Recent research (Houttuijn Bloemendaal et al., 2023) analyzed data from different studies (e.g. Bendoni et al. (2016), Marani et al. (2011), Mel et al. (2022), and Sanford and Gao (2018)) that presented a linear relationship between erosion rate and wave power and found that many use non-normally distributed wave power and/or erosion rate data. Since linear regression assumes normally distributed data, the linear relationships found were not accurate. Transforming and re-fitting the data shows that only three out of the 10 studies examined correctly presented a linear relation. An exponential curve (2 out of 10) or power curve (5 out of

10, including the four studies mentioned above) are in the other cases the best fit. Additional data from the Great Marsh in Massachusetts that Houttuijn Bloemendaal et al. collected also showed a power relation as best fit between dimensionless wave power and dimensionless edge retreat rate. The exact relationship is very dependent on local characteristics such as wind-wave climate, marsh edge orientation, and bathymetry (Houttuijn Bloemendaal et al., 2023).

Erosion rate - Wave thrust relationship

Leonardi, Defne, et al. (2016) evaluated the erosion rate between 1930 and 2013 of 10 sections of the Barnegat Bay salt marsh and used modelled values of wave thrust as hydrodynamic forcing. They found a positive correlation with a slope of the linear fit of 11.915 (Figure 2.5). To the author's knowledge, this is the only study that specified a relationship between wave thrust and salt marsh edge erosion using field data. The wave thrust - erosion rate relationship is very site-specific, as it is dependent on the relative cliff height with respect to the tidal range.

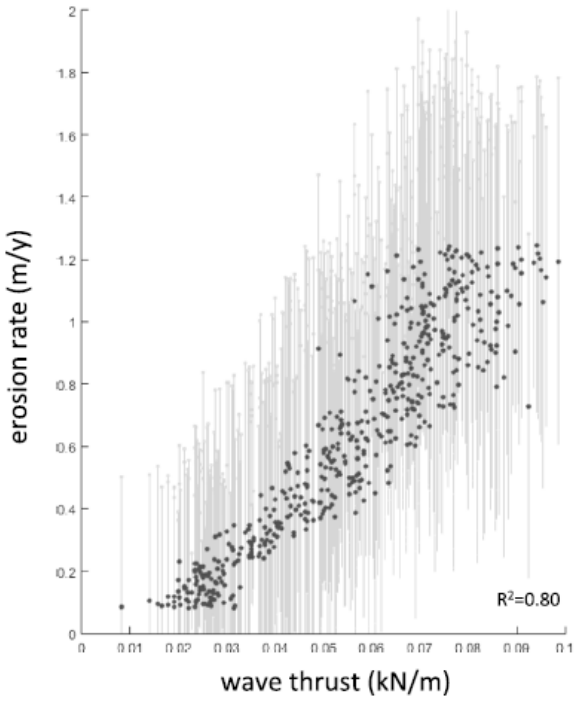

Figure 2.5: Linear relationship between wave thrust (T in Kn/m) and lateral erosion rate (E in m/year) with a slope of 11.915 m^2/kN/year. Grey lines are error bars. From Leonardi, Defne, et al. (2016).

2.1.4 Effects of vegetation

There are different types of halophytic vegetation that grow on the marsh bank and tolerate saline conditions, both as inundation by salt water and salty soil. The type of vegetation depends, amongst other factors, on the inundation period that is determined by marsh elevation and tidal amplitude, and latitude. In cooler regions grasses dominate the lower parts of the marsh where cliff erosion might be happening (Belknap & Kelley, 2021) and will therefore be the focus in this section.

Next to the aboveground biomass (stems, leaves), also the below-ground parts of the vegetation play an important role in the process of cliff erosion. In general, plant roots increase the soil shear strength, which reduces particle erosion (Francalanci et al., 2013). Often only the top part of the cliff is held together by plant roots and will erode slower than the bottom part, which results in undercutting, tension cracks (Schwimmer,

2001) and cantilever mass failure (Figure 2.3) (Bendoni et al., 2016). This is dependent on the water level, because a too high or too low water level will not result in waves hitting the marsh cliff. In general, the roots of vegetation on the cliff bank seems to decrease and delay bulk erosion, but studies on this topic are difficult to compare, as the methods are ambiguous and the results are not always straightforward (Feagin et al., 2009; Francalanci et al., 2013).

The presence of vegetation is often quantified by the Normalized Vegetation Index (NDVI) (Davranche et al., 2010; Martinez et al., 2024; Sun et al., 2018; WinklerPrins et al., 2024). The NDVI is a parameter that quantifies the presence of vegetation using (sattelite) imagery by extracting the reflectance wavelengths of the near-infrared band (NIR) and the red band of the RGB image. A higher value for NDVI indicates that the evaluated pixel has denser vegetation and a value below 0.1 means that there is (almost) no vegetation (Viana et al., 2019). Furthermore, the type of vegetation can roughly be determined using the NDVI. Viana et al. (2019) state that a NDVI between 0.2 and 0.3 indicates that there is grass and a NDVI above 0.6 indicates very dense vegetation, such as shrubs and trees. In salt marshes the NDVI typically ranges between 0.15 at the low marsh and up to 0.7 at the high marsh (Martinez et al., 2024; Sun et al., 2018). Hladik et al. (2013) use a threshold value for NDVI of 0.3 to differentiate between short and tall vegetation (*Spartina alterniflora*) in an area with salt marshes around the Duplin River, Georgia, USA. Closer to the Wierum marsh, on the island Schiermonnikoog in the Wadden Sea, NDVI values between 0.2 in winter and 0.9 in summer were found (Vrieling et al., 2018).

2.1.5 Alongshore variations

The shape of the marsh boundary is not always straight. Some marsh boundaries show a very irregular, jagged shape (Leonardi & Fagherazzi, 2015) or a more regular, wavy pattern (Schwimmer, 2001). The cause of these different shapes has been researched, but there is no real consensus. Most often, the local wave climate is assumed to be the cause. A modelling study by Leonardi and Fagherazzi (2015) showed that when the wave power is high, the marsh boundary erodes quite uniformly and predictably. When the wave power is low, on the other hand, there are irregularities visible because the volume and location of the failures is hard to predict. This is probably due to small-scale heterogeneities in marsh resistance factors in the model (such as soil strength). Moreover, the occurrence of extreme event also has an impact: a higher frequency of extreme events leads to a smoother marsh edge shape, both for low and high wave power (Leonardi, Defne, et al., 2016). Figure 2.6 shows the results of the model that was used.

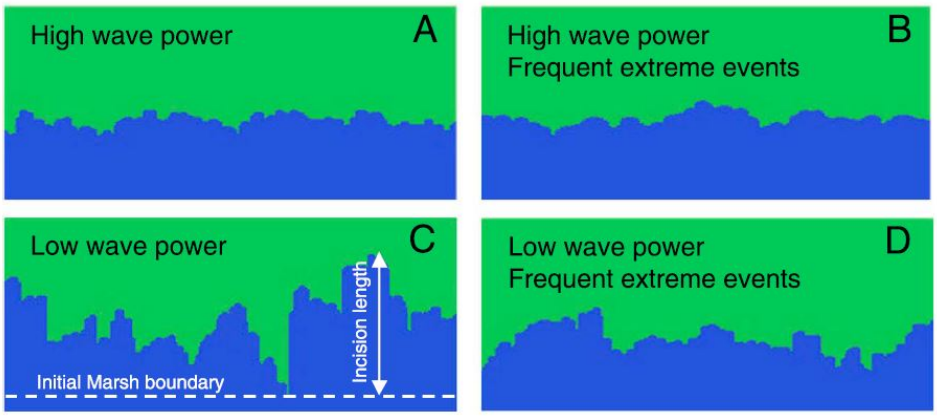

Figure 2.6: Relation between marsh edge shape, wave power and extreme event frequency. From Leonardi and Fagherazzi (2015).

Another characteristic that is observed is a more regular, wavy edge pattern. This happens when there are two small V-shaped erosion cuts (or clefts) in a formerly straight marsh boundary. The area in between is called

a neck, which experiences erosion along the length, widening the cleft. This makes the neck narrower until it is cut off and a small island (called a stack) emerges in front of the new salt marsh boundary (Schwimmer, 2001). The different stages of this process are schematized in Figure 2.7, which is based on field measurements and observations in Rehoboth Bay, Delaware, USA. The rootmat hole in this figure represents the process of undercutting and tension crack failure, as described in Section 2.1.3. An alternative theory of the process that happens after the initial formation of necks and clefts is that the shape of the marsh boundary could remain the same. This occurs when there is wave attenuation in the cleft that limits erosion. Then, there is more lateral erosion at the tip of the neck and the cleft becomes less deep. This process is going on until there is also erosion again in the cleft and the geometry is maintained (Schwimmer, 2001). However, this is a speculation made by Schwimmer and no confirmation of these processes is given in literature.

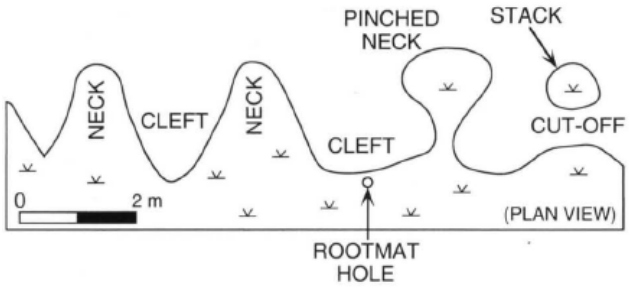

Figure 2.7: Schematization of the irregular cliff erosion in Rehoboth Bay, Delaware, USA. Adopted from Schwimmer (2001).

The irregularity of a salt marsh shoreline has been quantified by the fractal dimension (FD) (Bertassello et al., 2018; Leonardi, Defne, et al., 2016; Schwimmer, 2008; Simon & Simon, 1995). The fractal dimension is a measure of how fast complexity increases when the scale of evaluation decreases. Figure 2.8 shows an example of this process using the box counting method (Piera et al., 2005), further explained in Section 3.3.3. A larger fractal dimension indicates a more complex shape (Peitgen et al., 2004). In context to salt marsh edge erosion, Leonardi, Defne, et al. (2016) state that irregular shaped marsh boundaries retreat slower than more homogeneous marsh edges, using the wave thrust as forcing indicator. This negative relationship is also found in a study by Schwimmer (2008) that evaluated the geometry of six marshes in Rehoboth Bay, Delaware, USA.

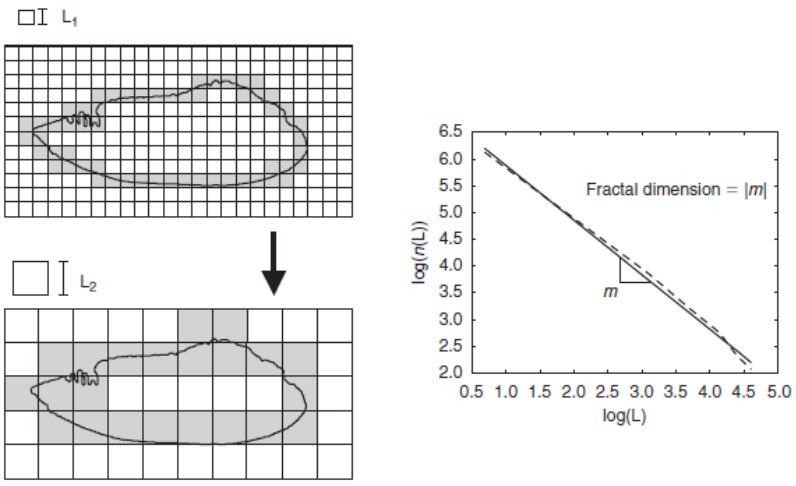

Figure 2.8: Visualization of the box counting method to determine the fractal dimension. Adopted from Piera et al. (2005).

The vertical profile of the salt marsh edge can have different shapes that have different erosion characteristics. Next to a vertical cliff, the marsh edge can also have a slope, or even a terraced profile. Especially for the latter, there is wave energy dissipation happening at the lower parts of the terrace. This means that the wave power and wave thrust at the upper part of the terrace is less strong and there is likely less lateral erosion (Tonelli et al., 2010). This vertical shape of the marsh edge could also explain some differences in alongshore erosion rate.

2.2 Knowledge gaps

Although salt marsh edge erosion is a widely researched topic, there are some knowledge gaps.

There is little known about salt marsh edge erosion in a meso-tidal environment (tidal range of 2 - 4 m). The most studied areas are micro-tidal environments with a tidal range under 2 m. Examples of these kinds of environments are the Venice Lagoon and coast of Florida and the Gulf of Mexico (Whitfield & Elliott, 2011). A meso-tidal environment leads to a different hydrodynamic forcing on the marsh edge that could have an impact on edge erosion rate and the relationships found in literature may not be applicable.

Very few studies have been done regarding the relationship between incoming wave thrust and salt marsh cliff retreat. There are some modeling studies done on this relationship that use real-world data to some extent (Donatelli et al., 2019; Tonelli et al., 2010), but they present a heavily simplified version of reality, regarding marsh morphology. To the author's knowledge, only one data analysis based solely on field data has been done (Leonardi, Defne, et al., 2016). Hence, the relationship between incoming wave thrust and salt marsh cliff retreat is understudied. Regarding wave power, there is much research done on the effects of wave power on the salt marsh edge. In literature often a linear relationship is presented (Leonardi, Ganju, & Fagherazzi, 2016; McLoughlin et al., 2015; Mel et al., 2022). However, a power law relation is found to result in a better fit in some cases (Houttuijn Bloemendaal et al., 2023). Therefore, there is no general consensus about the kind of relationship between wave power and marsh edge retreat rate.

There is a lack of knowledge on the spatial variability of salt marsh edge erosion and the processes that influence this. Along the marsh edge there can be significant differences in erosion rate. So far, there have only been theories (Schwimmer, 2001) and model studies (Leonardi & Fagherazzi, 2015) that tried to explain this phenomenon. Again, to the author's knowledge, no research based solely on field data has been done relating marsh characteristics such as edge complexity and vegetation density to the spatial difference in marsh edge erosion rate.

2.3 Research Aim

The research aim follows from the knowledge gaps: This research aims to investigate how hydrodynamic forcing influences salt marsh cliff erosion in a meso-tidal environment at both a marsh-averaged and a local scale, examining temporal variability and alongshore differences in erosion rate and marsh characteristics.

2.4 Study area

The area of interest for this thesis is a salt marsh in the Wadden Sea, in the north of the Netherlands (see Figure 2.9). It is located just east of the village of Wierum, right next to the sea dike. It is approximately 1.2 km long, 150 m wide at its widest and only a couple meters wide at is narrowest with an area of about 11.5 ha.

The Wadden Sea is a mesotidal back-barrier basin consisting of a large tidal flat with channels cutting through. The tide is predominantly semi-diurnal with an average tidal range of 2.2 m that is increased/decreased by 0.7 m by the spring/neap cycle (Siemes et al., 2020). The wave energy in the Wadden Sea is low, as waves are mostly wind-generated, with a mean significant wave height of 1.3 m and a period of 5 s. During storms this may increase up to 6 m high waves. The sediment in the Wadden Sea consists of mostly sand (90%) and mud (10%) (Elias et al., 2012).

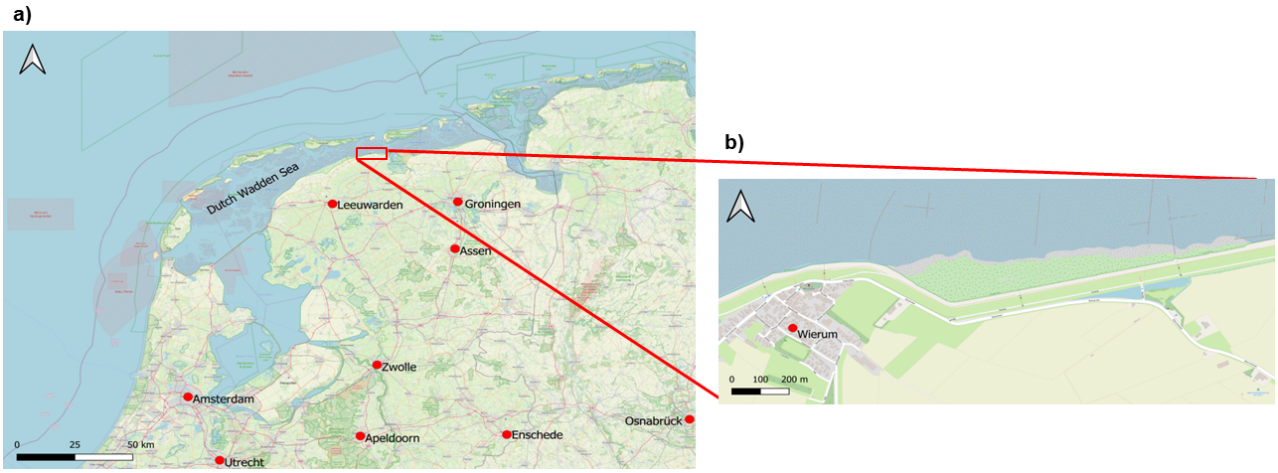

Figure 2.9: Map of the study area. a) overview; b) zoomed in.

The seaward border of the marsh has an irregular shape with necks and clefts visible of up to 2 m length (Figure 2.10 a). Along the border there are mostly cliffs of 0.5 m to almost 1 m tall, while at some locations there is no cliff but a gradual or stair-shaped slope towards the water. Also the vegetation is not uniformly spread over the marsh at the edge. At some locations, there is grass growing on top of the cliff (mostly *Puccinellia maritima*), while at some locations there is bare soil. In front of the cliff there is some pioneer vegetation: samphire (*Salicornia europaea*). Moreover, there are sheep grazing on the marsh that might limit the vegetation growth. At low tide the water is far from the marsh edge and even at regular high tide the water does not reach the marsh surface. This only happens during storms. This means that at many cliff locations, undercutting as failure mechanism is visible (Figure 2.10 b).

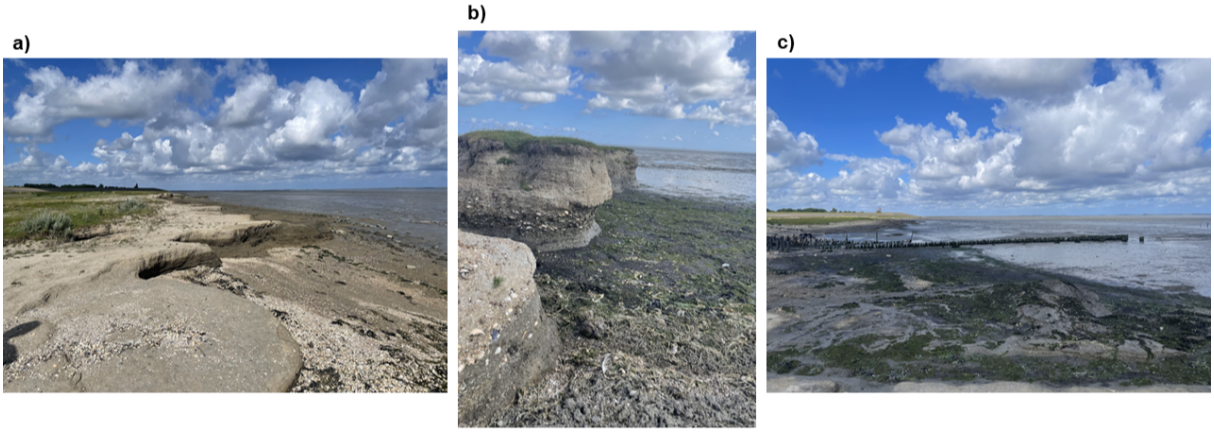

Figure 2.10: Pictures from the salt marsh at Wierum taken by Juliana Bruil (June 2024). a) irregular shaped marsh edge, no vegetation on top of the cliff; b) undercutting in the cliff, vegetation on top of the cliff; c) remains of a brushwood dam.

The Wierum salt marsh was formed as a result of historical semi-natural land reclamations (Elschot et al., 2020). This was done by constructing small, semi-permeable brushwood dams that were constructed in a rectangular shape with a small inlet at the sea side, which ensures that the water from the tide is able to enter and exit the marsh but it limits flow velocity and wave energy (Siemes et al., 2020). As a result, sedimentation increases and the bed was elevated until it is not flooded by the tide any more. Then, a taller and stronger dike was built in the place of the brushwood dams and there are new brushwood dams constructed further into the sea (Beintema et al., 2007). However, the brushwood dams were not maintained for the last decennia. There are remains of degraded brushwood dams present that extend up to 500 m into the Wadden Sea. As a result, the stabilizing effects are negligible and the marsh experiences lateral erosion. Within the marsh, parallel to the sea dike there is still such a low summer dike consisting of brickwork (Figure 2.11). This dike has not been maintained for a long time, which resulted in erosion of the dike on the east side of the marsh. The dike is completely washed away there and the marsh behind it has also eroded. There is one main channel in the marsh that has an inlet under the summer dike and splits in two channels within the marsh.

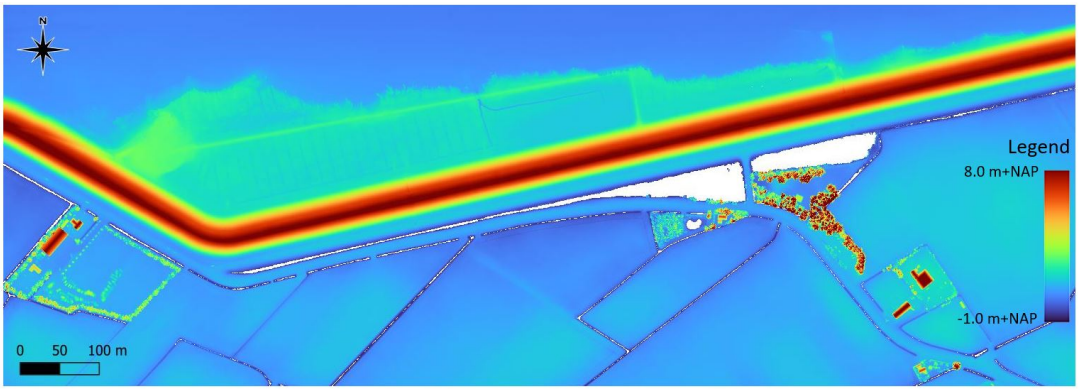

Figure 2.11: Elevation map of the study area (Rijksdienst voor het Cultureel Erfgoed, 2023). The summer dike is visible as a light green line, the channels as a darker blue line.

The Dutch Department of Waterways and Public Works (Rijkswaterstaat) formulated a need for more up-to-date knowledge on the quality and quantity of the salt marshes in the Wadden Sea to be able to maintain them (Elschot et al., 2020). Studying the erosion at the Wierum marsh and the relating processes is a first step in this process.

Chapter 3

Research Structure

3.1 Research objectives

There are two main objectives in this research, which are divided into two scales: a larger, marsh-averaged scale and a smaller, marsh section scale.

The first objective of this research relates to the marsh-averaged scale and is to investigate the relationship between temporal changes in spatially averaged hydrodynamic forcing and the salt marsh cliff retreat rate in a meso-tidal environment. The second objective relates to the marsh section scale and is to determine the spatial differences in cliff retreat rates by separating the marsh edge into sections that have similar properties and to investigate the contribution of temporal changes in spatially averaged hydrodynamic forcing and local alongshore variations in marsh edge characteristics.

3.2 Research questions

There are three main research questions that are linked to the two scales.

How is the spatially average salt marsh cliff retreat rate related to the spatially averaged hydrodynamic forcing at the Wierum site?

1. What is the relationship between incoming wave power and average cliff retreat rate?
2. What is the relationship between incoming wave thrust and average cliff retreat rate?
3. How does the frequency of inundation relate to the average rate of cliff retreat?

How are local alongshore variations in cliff erosion rate at the Wierum site related to spatially averaged hydrodynamic processes and local differences in marsh edge characteristics?

1. How does the cliff retreat rate vary along the Wierum marsh edge?
2. What is the relationship between temporal hydrodynamic forcing variability and spatiotemporal cliff retreat rate variability?
3. How does the shape of the marsh edge relate to local cliff retreat rate?
4. What are the vegetation characteristics near the marsh cliff and what is the effect on local variation of cliff retreat rate along the marsh boundary?

3.3 Methods

3.3.1 Data sets

For both scales there are two types of data needed: morphological marsh data and hydrodynamic forcing data. The data sets that are used are described below, including information on the quality and preprocessing done on the data.

Data sources and availability

The morphological marsh data is retrieved from aerial images and elevation measurements. Aerial imagery from the Publieke Dienstverlening Op de Kaart (PDOK) covers the years from 2016 to 2024. Imagery taken before 2016 is generally lower in resolution, so 2016 was chosen as the starting point for the analysis. Additional elevation data from the Actueel Hoogtebestand Nederland (AHN) and drone-captured Digital Elevation Models (DEMs) were used for comparison to the aerial images. AHN data from 2020 and 2023 were used and the drone DEMs were conducted in November 2022, September 2023, and January 2024. Figure A.1 in Appendix A provides more information about exact timestamps of these images.

The hydrodynamic forcing variables that are needed are water depth (h), significant wave height (H_s) and wave direction. Three main sources were used: Rijkswaterstaat's waterinfo website (RWS, https://waterinfo.rws.nl), the MATROOS platform (https://noos.matroos.rws.nl) was utilized, also by Rijkswaterstaat, and additional data from KNMI was used. Data recorded by a buoy near the marsh at Wierum (Wierum buoy in Figure 3.1) were used. Between June 2017 and September 2019 and from June 2022 onward, water level data were not available for the Wierum buoy, so data from the nearby station at Holwerd (Holwerd buoy in Figure 3.1) was used. From October 2020 onward, the wave height data is generated by a SWAN model that spans the entire Wadden Sea. This very extensive numerical model was constructed by Deltares and calibrated and validated multiple times in 2013, 2014 and 2018. It has a grid of approximately 35 m and includes parameters such as water levels, flow, wave propagation and breaking (Deltares, 2023). As measurement location the the same as the Wierum buoy is chosen. Wave direction data is available from 2020 onward, so for earlier periods wind direction data from KNMI is used (Lauwersoog weather station in Figure 3.1) and there is assumed that the wave direction is equal to the wind direction. More information about the data sources and availability is given in Figure A.1 in Appendix A.

Figure 3.1: Map of the locations of the different measurement stations.

Data quality

The quality of both the morphological datasets is assessed based on consistency, resolution, and completeness. The PDOK images taken between 2016 and 2020 offer a resolution of 25 cm, while later images improved to 8 cm, providing sufficient detail to observe annual cliff retreats. However, some images lack precise dates and in that case an estimate of the date was made, based on the knowledge that the image was made either in summer (2016-2020) or in winter (2020-2024). AHN data have a lower resolution at 50 cm horizontally and 5 cm vertically, while the drone-derived DEMs add high-resolution elevation details (0.5 cm horizontally, 1.0 cm vertically).

Hydrodynamic data quality was evaluated based on resolution, missing data points and outlier presence. The resolution amongst the datasets varied from one measurement every 10 minutes to four observations per day. The exact accuracy of measurement methods is unknown but assumed to be sufficient. Certain RWS datasets showed outliers in water depth, such as unlikely negative depths or extreme wave heights, which were flagged for removal. The percentage of missing data in the data sets varies between 0.0 % (no missing data) and 25 % for the MATROOS data.

Data preprocessing

Preprocessing of the hydrodynamic data was undertaken to align all datasets from July 2016 to December 2023, at a consistent interval. Water depth data from the Holwerd station were adjusted using the spatially average seabed level of the mudflat at Wierum, ensuring uniformity between stations. Moreover, the water depth data was filtered to contain only depths between (but excluding) zero and the top of the cliff. Wave height data were merged from the two sources (observations and modeled values) to also create one time series. Wave direction was adjusted to the marsh's angle relative to North and incorporated as a cosine factor to refine wave power calculations. More information about the preprocessing steps is given in Appendix A. The final datasets contain hourly values for water depth and daily averages for wave height and wave direction.

3.3.2 Marsh-averaged scale

Marsh edge erosion rate

The erosion rate of the salt marsh edge was determined using PDOK aerial images, AHN data and drone DEMs independently. This is done in the program QGIS by tracking the marsh boundary manually and thus digitalizing the marsh edge. In the PDOK images the location of the cliff was visible as a darker color (Figure 3.2). In the AHN and drone DEMs the same approach was taken, now using the elevation of the marsh to determine the edge.

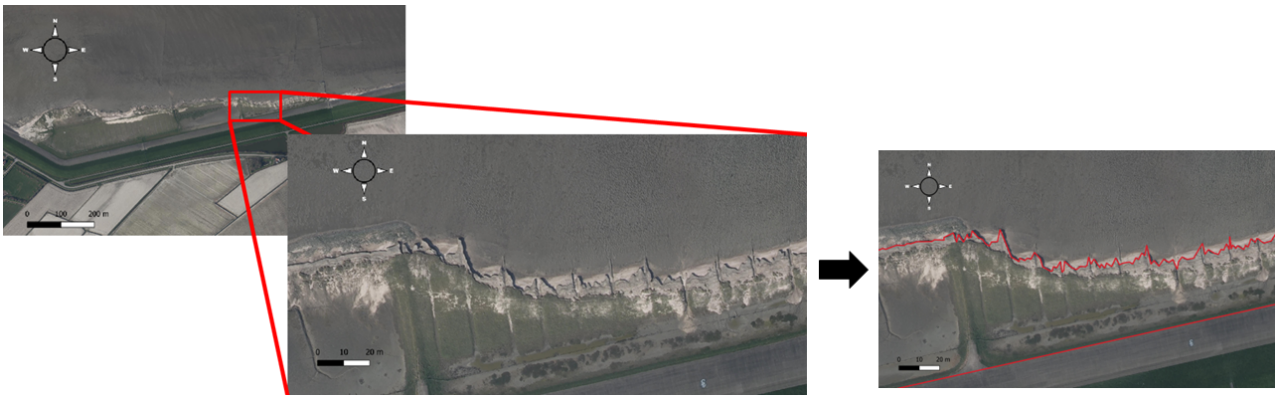

Figure 3.2: Example of the determination of the marsh edge on the PDOK image of 2023. The red line is the digitization of the marsh edge.

The local width of the marsh is determined along cross-shore transects with a 10 m spacing interval. The starting points are positioned at the seaward toe of the dike, where the transects go perpendicularly seawards from the dike. The transects are parallel to each other, which means that at the westernmost part of the marsh in the dent of the dike, the transects are not perpendicular with respect to the dike but rather follow the same orientation as the other transects (visualized in Figure 3.3). This is done to prevent intersections of transects which leads to a messy and confusing marsh width at the west side of the marsh. Consecutively, the marsh width is determined as the distance from the seawards toe of the dike to the marsh edge along the transect. This process is done for all three data sources separately. A final data set of marsh widths is made by combining the three data sets where possible and desired. This final configuration is based on the quality and availability of the data sources. Finally, the average marsh edge retreat rate over the whole marsh boundary is determined by averaging over all transects and subtracting two consecutive series from each other. The yearly retreat is taken as the retreat of the marsh in one calendar year (1st of January to 31st of December).

Using the elevation data from AHN4 the cliff height is determined. This is done by creating cross-sections of the marsh at the locations of the transects showing the elevation of the marsh and the part of the mudflat in front of the marsh. The cliff is then defined as the (near) vertical part of the seaward marsh boundary and the cliff height is determined for each cross-section. Appendix B.3 shows these cross-sections at selected transects.

Hydrodynamic forcing

Following the research questions, the incoming hydrodynamic forcing onto the salt marsh near Wierum is quantified as the wave power, wave thrust and the inundation frequency.

Both the wave power (P in W/m, Equation 3.1 and 3.2) and wave thrust (T in N/m, Equation 3.3) are calculated using linear wave theory, assuming shallow water conditions near the marsh edge (Timmerman et al., 2021). Hourly water depth data and daily wave height and wave direction data are used to create hourly values for wave power and wave thrust.

$$P = \frac{1}{8}\rho g H_s^2 c_g \cos(\alpha) \tag{3.1}$$

Where:

$$c_g = c_w = \sqrt{gh} \tag{3.2}$$

$$T = \left(\frac{1}{2}\rho g H_s\right) \cdot h \cdot \cos(\alpha) \tag{3.3}$$

Only the wave power and wave thrust that act on the cliff surface are considered. This means that the water depth data set is first cropped to only include values larger than (so excluding) 0.0 m and smaller than or equal to 0.5 m (the cliff height). This is also why the impacted area in Equation 2.3 is transformed in just the water depth in Equation 3.3.

The third quantification of hydrodynamic forcing used is the frequency of inundation of the salt marsh. This is defined as the percentage of hours per year that the water depth is above a certain threshold. Equation 3.4 is used to determine this, where $n_{hours>threshold}$ is the number of hours in a year that the water depth is larger than the threshold, $n_{hours,year}$ is the total amount of hours that there are in a year (8766). Two thresholds of inundation are used to do the analysis with: 0 m (meaning any water at the marsh edge) and 1.0 m (ensuring that the whole cliff is inundated).

$$f = \frac{n_{hours>threshold}}{n_{hours,year}} \cdot 100\% \tag{3.4}$$

Relation erosion rate and hydrodynamic forcing

The resulting hourly wave power and wave thrust data are linked to the erosion rate by first taking the yearly average value and then creating dimensionless variables P^*, T^* and E^* for wave power, wave thrust and erosion rate, respectively. This is done by dividing the variable by its average value over the whole time series (Equation 3.5, where P, T and E are inserted for X).

$$X^* = \frac{X}{X_{avg}} \tag{3.5}$$

The relationships between incoming wave power and erosion rate and incoming wave thrust and erosion rate are tested using two different fitting functions: a linear model and a power law model. Both fits are optimized using a least square difference algorithm. The assumption is made that at zero wave power and wave thrust, there is no erosion and vice versa. This means that the fit must go through the point (0,0). The linear model for the erosion rate - wave power (wave thrust) relationship has the shape $E^* = \alpha^* P^*$ ($E^* = \alpha^* T^*$) where α^* is the slope of the graph and represents intrinsic marsh conditions (Leonardi, Ganju, & Fagherazzi, 2016). The power law model has the shape $E^* = kP^{*n}$ ($E^* = kT^{*n}$). In a way, k and n also include unknown intrinsic marsh parameters. All three parameters (α^*, k and n) are dimensionless.

The relation between erosion rate and inundation frequency is tested by taking the dimensionless erosion (E^*) per year and the percentage of hours that the water level surpasses the threshold. A linear fit to the data points is made to find a relation.

As goodness-of-fit metrics the root-mean-square-error (RMSE) and the R-squared (R^2) are used (Equations 3.6 and 3.7, respectively, where O are observed values, F are modeled values using a fitting method and n is the total number of data points. The value of RMSE uses the absolute difference between the fitted values and the observed points, where a vale of 0 means no difference, i.e. a perfect fit. R^2 represents a relative goodness-of-fit and the value of R^2 lies between 0 and 1. An R^2 of 0 means that there is no relation between the observed points and their fitted values and an R^2 of 1 means that there is a perfect relation.

$$RMSE = \sqrt{\Sigma_{i=1}^{n} \left(\frac{O_i - F_i}{n} \right)^2} \tag{3.6}$$

$$R^2 = \left(\frac{\sum \left(O_i - O_{avg} \right) \left(F_i - F_{avg} \right)}{\sqrt{\sum \left(O_i - O_{avg} \right)^2 \sum \left(F_i - F_{avg} \right)^2}} \right)^2 \tag{3.7}$$

3.3.3 Marsh section scale

Relation between erosion rate and hydrodynamic forcing

To determine the local variation in marsh edge retreat the marsh is divided in sections that have similar properties being the presence or absence of a cliff and the presence or absence of a summer dike (Table 3.1). This resulted in six sections named A to F, as presented in Figure 3.3. The yearly retreat of the sections is determined using the same approach as for the marsh averaged scale, but now including only the transects that lie in the section. The summer dike is best visible on the AHN image and drone DEMs (for example Figure 2.11).

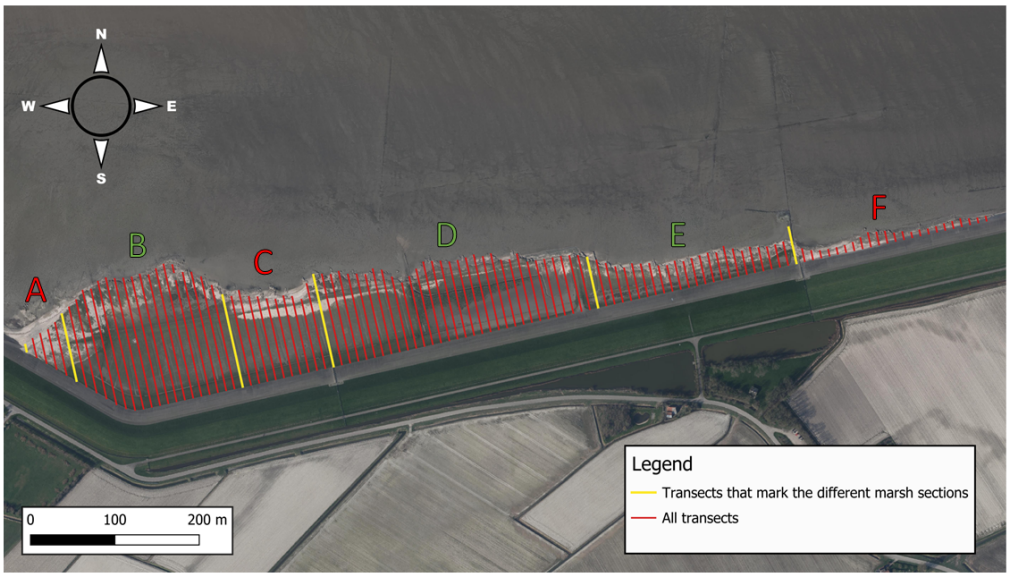

Figure 3.3: Division of the six marsh sections where a red letter indicates a section (almost) without cliff (A, C and F) and a green letter indicates a section with cliff (B, D and E). As background the PDOK image of 2023 is used.

Table 3.1: Characteristic properties of the six marsh sections

Section	Characteristics
A	no cliff, no summer dike
B	cliff and summer dike
C	no cliff, summer dike
D	cliff and summer dike
E	cliff, no summer dike
F	no cliff, no summer dike

The marsh width of the sections is determined in the same way as for the marsh-averaged scale, using the final configuration of data sets. The marsh edge retreat rate per section is determined using the same methods as for the marsh-averaged scale (Section 3.3.2). The hydrodynamic forcing is assumed to be equal over the whole marsh boundary, so the marsh-averaged data is used.

For the relation between erosion rate and hydrodynamic forcing a very similar approach is used as for the marsh-averaged scale: the dimensionless marsh cliff retreat rate per section is plotted against the dimensionless

hydrodynamic forcing using Equation 3.5. The goodness-of fit between a linear fit and a power law fit through the data points is then determined using the RMSE and R^2 (Equations 3.6 and 3.7, respectively).

Relation erosion rate and shape of the marsh boundary

The marsh boundary of the six sections is different in shape. Sections without a cliff tend to have a more smooth boundary and sections with a cliff seem more complex and curved. To test whether a relation exists between marsh edge complexity and erosion rate, the marsh edge complexity is quantified using Mandelbrot's fractal dimension (FD). The FD is determined using the box-counting method in a Python algorithm per marsh section for the nine different years. The marsh edge of one section is filled with a number of boxes (q) of a certain size (L). Then, step by step, the size of the boxes is decreased and more and more boxes needed to fill the whole boundary. The complexity of the boundary shape influences this process, as a more complex shape requires more boxes to fill the whole marsh boundary for a certain box size. The FD is found by taking the slope in the graph of $log(q)$ against $log(L)$ (Equation 3.8 (Leonardi, Defne, et al., 2016)).

$$FD = \frac{\Delta log(q)}{\Delta log(L)} \tag{3.8}$$

The erosion rate is plotted against the FD for the six different sections and the nine years. A linear trend line is fitted through these data points to find a relationship. Again, the RMSE and R^2 are used as goodness-of-fit metrics.

Relation erosion rate and vegetation along the marsh edge

The vegetation near the marsh edge is quantified using the NDVI which uses the reflectance of the earth surface using the near-infrared (NIR) band with a wavelength around 0.86 μm and the red band with a wavelength around 0.66 μ m. The NDVI is then computed using Equation 3.9, where ρ_{NIR} indicates the reflectance of the near-infrared band and ρ_{red} indicates the reflectance of the red band (Viana et al., 2019).

$$NDVI = \frac{\rho_{NIR} - \rho_{red}}{\rho_{NIR} + \rho_{red}} \tag{3.9}$$

Where:
NDVI < 0.1 indicates no vegetation
0.2 < NDVI < 0.3 indicates grass
NDVI > 0.6 indicates very dense vegetation

Sattelite images of the NIR and red band are retrieved from sattelietdataportaal.nl. The sattelite images of the summer months (between June and September) were used to ensure that there is vegetation present on the marsh. These images were available for the years 2019 until 2023, where the image with the least cloud cover of each year was selected. The NDVI is then determined for every cell in the image using the program QGIS. Per section, the 90th percentile value for NDVI of the marsh edge is determined, using a width of 2 m landward from the actual marsh edge. Then, the relation between erosion rate and NDVI of the marsh edge is determined per section. Again, the RMSE and R^2 are used as goodness-of-fit metrics.

Chapter 4

Results

4.1 Input data

4.1.1 Topographic marsh data

Figure 4.1 visualizes the retreating marsh edge over time using the PDOK aerial images as data source and following the method as described in Section 3.3.2. In the aerial images the marsh edge was very well visible at locations where there was a cliff, but difficult to determine at locations of a sloping or stair-shaped descend onto the mud flat. In that case the marsh edge was digitalized as a straight line to the next presence of a cliff. This is also visible in Figure 4.1, for example at the most western part of the marsh. There the edge retreat is sometimes even negative (meaning expansion), probably because there was no exact edge location, which led to discrepancies between years. Also note the large difference between 2023 and 2024. Reasons for this could be that a big storm hit the marsh that year, but also the 2024 image was still under revision at the time of this analysis, so it may not be very accurate.

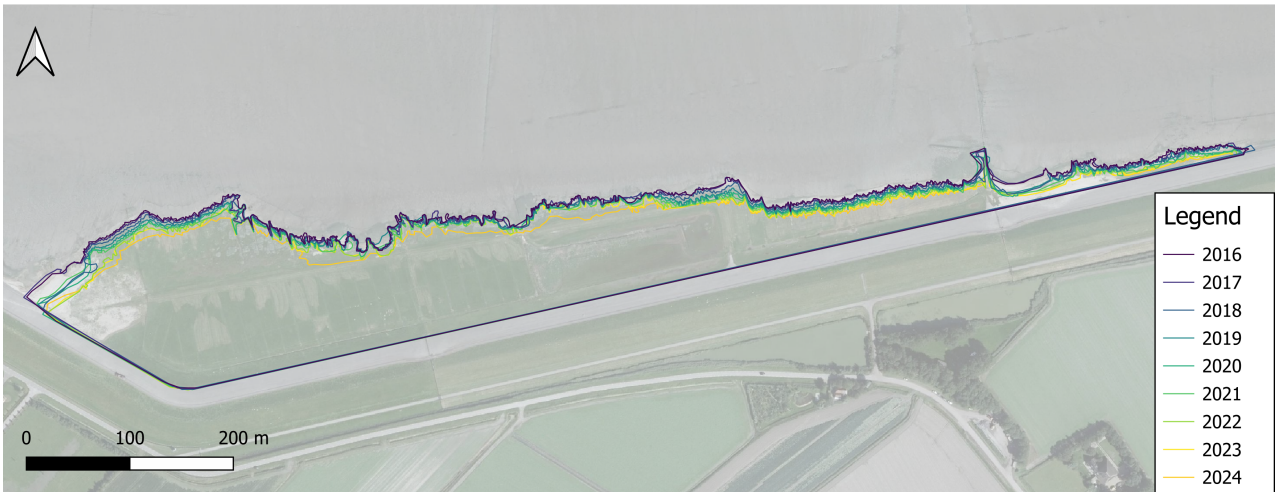

Figure 4.1: Map of the Wierum marsh edge retreat from 2016 until 2024 using PDOK data. As background map the aerial image of 2016 is used.

The average cliff height in the Wierum marsh is 0.49 m (Figure 4.2) with a maximum of 0.74 m and a minimum of 0.1 m, which can be interpreted as no cliff. Some of the very high values for cliff height are found at the easternmost side of the marsh (Appendix B.3). At some transects at this location there is no marsh area which means that the location of the "cliff" is placed right at the toe of the dike and this makes the results unreliable. Excluding the low and high values results in an average cliff height of 0.51 m. This value for cliff

height is used for the marsh-averaged scale. Section 4.3 dives into these differences along the seaward marsh edge using different cliff height for the different marsh sections.

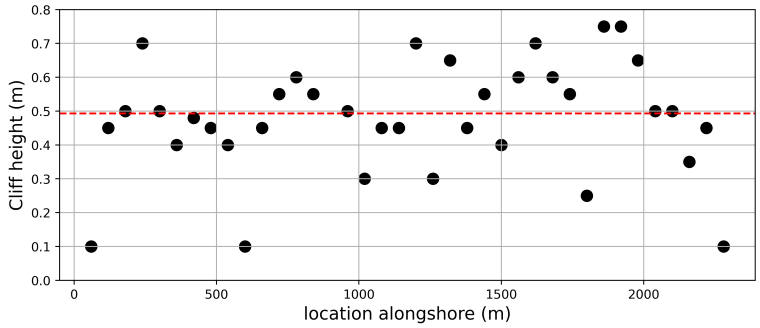

Figure 4.2: Measured cliff height along the marsh edge using AHN4 data. The average cliff height is 0.5 m (red, dotted).

4.1.2 Hydrodynamic forcing

The hourly values of water depth and daily average values for significant wave height are plotted over time in Figure 4.3 and the wave direction is presented in a wind rose in Figure 4.4.

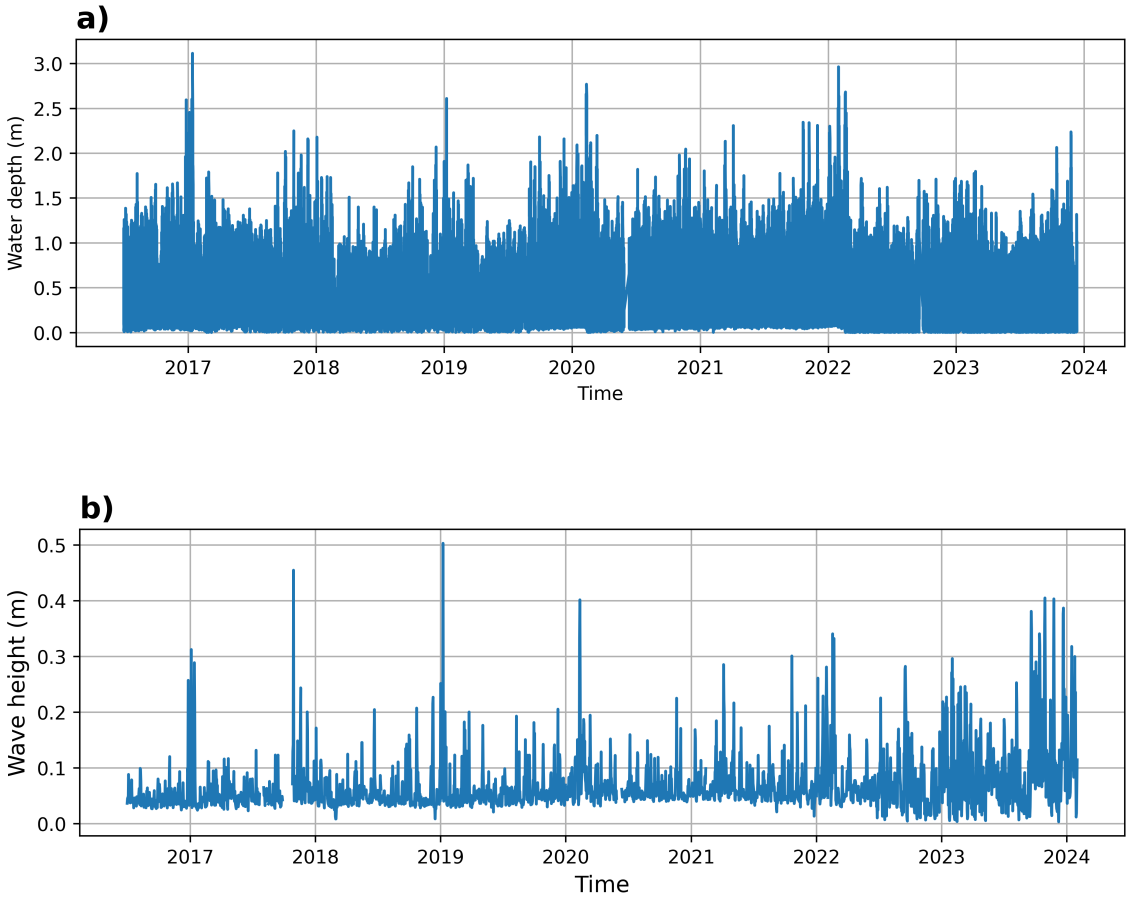

Figure 4.3: Time series plot of hourly water depth (a) and daily wave height (b) modified to the location of the Wierum marsh.

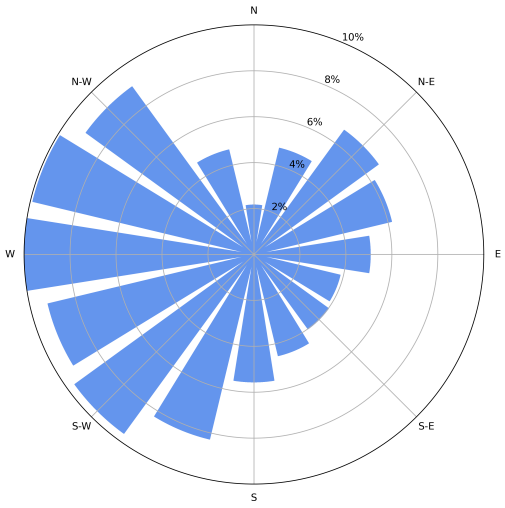

Figure 4.4: Wave direction at the Wierum marsh in percentage of days that a certain direction occurs.

The plots for water depth and wave height (Figure 4.3) reveal a seasonal trend: in winter the water depths and wave heights are larger than in summer. Starting from June 23rd 2022, water level data from the Holwerd station was used instead of directly at Wierum. This change is clearly visible in the plotted data. The water depth is on average 11 cm lower in the modified Holwerd water depth than the Wierum water depth. Also between June 2017 and September 2019 water level data from the Holwerd station is used, but this is not visible in Figure 4.3 a. The wave height data was available for the Wierum location for the whole time series. Still, there is a difference visible between data before and after mid-2022. The average and standard deviation are both 3 cm higher in the first part compared to the second part of the wave height data. This difference in wave height can be explained by the fact that until the 21st of June 2022 the data set contains observed values, whereas after that date the data originates from a SWAN numerical model. Another observation is a slight increase in minimum water depth and wave height in the period between mid 2019 and mid 2022. Reasons for this are unknown: to the authors knowledge the measurement locations and methods are equal for that time period. Figure 4.4 reveals that the dominant wave directions are between North-West and South-West.

The distributions of the daily data of water depth and significant wave height are presented below as histograms (Figure 4.5). To determine the amount of bins the Freedman-Diaconis rule is used, which includes the interquartile range of the data. This resulted in 40 bins for h and 51 bins for H_s. The data is tested against four theoretical distributions: normal, log-normal, gamma and beta. Water depth follows a beta distribution with parameters α = 0.91 and β = 24.44. The significant wave height is distributed according a log-normal distribution with parameters μ = 0.0028 and σ = 0.53. These distributions are also plotted in Figure 4.5.

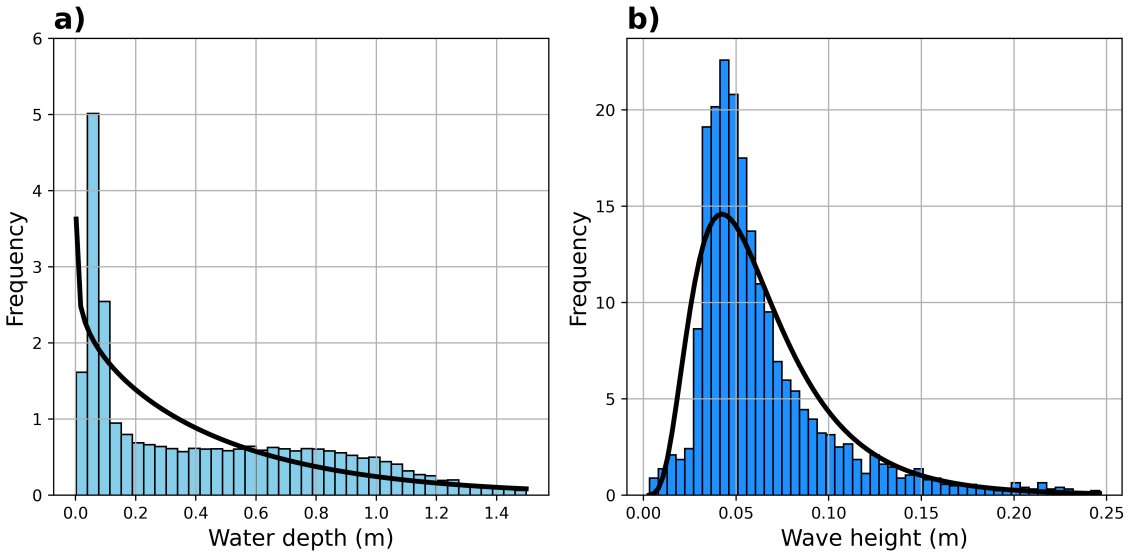

Figure 4.5: Distributions of the hydrodynamic variables including the best-fitting distribution: a) hourly water depth with beta distribution (n=44405), and b) daily significant wave height with log-normal distribution (n=2603).

Comparison between data sources

From October 11th until December 11th 2023 water level and wave height measurements were done on the mudflat in front of the Wierum marsh using a wave logger with a pressure sensitive disk (Wave logger winter 2023 in Figure 3.1). From this, the water level, significant wave height, wave period and orbital velocity can be determined. Figure 4.6 shows plots of the water level and significant wave height using different data sources. The sensor of the locally measured data was placed at a level of 0.26 m+NAP, which is why there are no water levels below that value recorded.

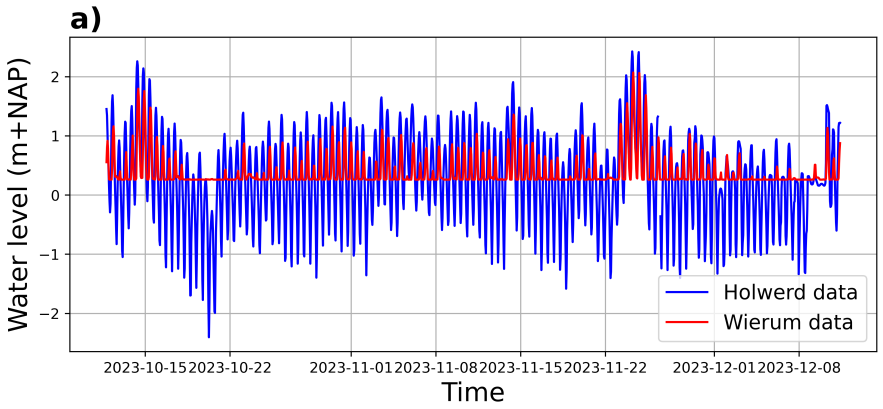

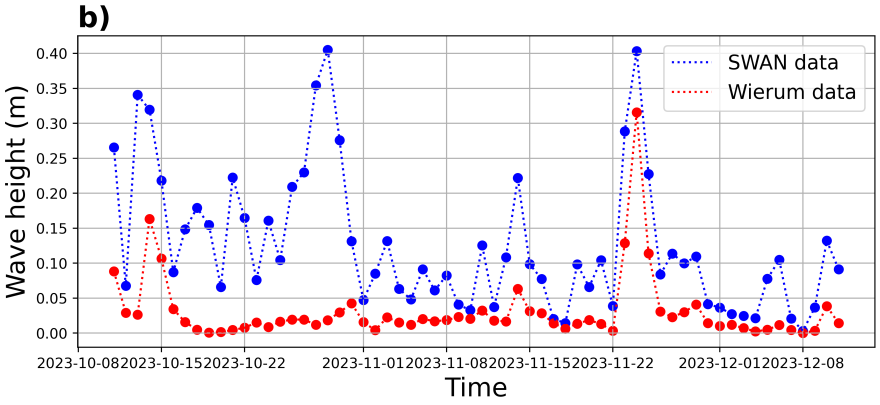

Figure 4.6: Comparison between data sources (locations in Figure 3.1): a) hourly water level from Holwerd station (blue, Holwerd buoy) and the local measurements (red, wave logger winter 2023); b) daily wave height from the SWAN model (blue, Wierum buoy) and the local measurements (red, wave logger winter 2023).

The sensor of the locally measured data consistently shows lower values for water level than the Holwerd station. The instances of high water depth and low water depth do seem to coincide very well between the two data sets. Also the wave height is much lower in the local measured data set than the SWAN-generated data (averages of 0.03 m and 0.13 m, respectively). Moreover, there are much higher peaks in the SWAN data that are not measured by the wave logger. This difference probably originates from a difference in measurement location. The location for which the SWAN data was extracted lies further out on the mud flat, where water depths are generally larger leading to taller waves. Close to the shore, where the local measurements were conducted, the waves have dissipated more and are therefore smaller. Furthermore, there is a difference in measuring method which could explain the difference. The SWAN data was generated by a numerical model and the local data was measured using a wave logger. To ensure continuity of the data sets, the Holwerd data is used instead of the local measurements.

4.2 Marsh Averaged Scale

For the marsh averaged scale the whole stretch of marsh edge is considered, meaning that the average erosion rate is used and the hydrodynamic forcing is considered equal over the whole marsh edge.

4.2.1 Erosion rate

Configuration using three data sources

Figure 4.7 and Table 4.1 show the average marsh width and yearly erosion rate of the three data sources.

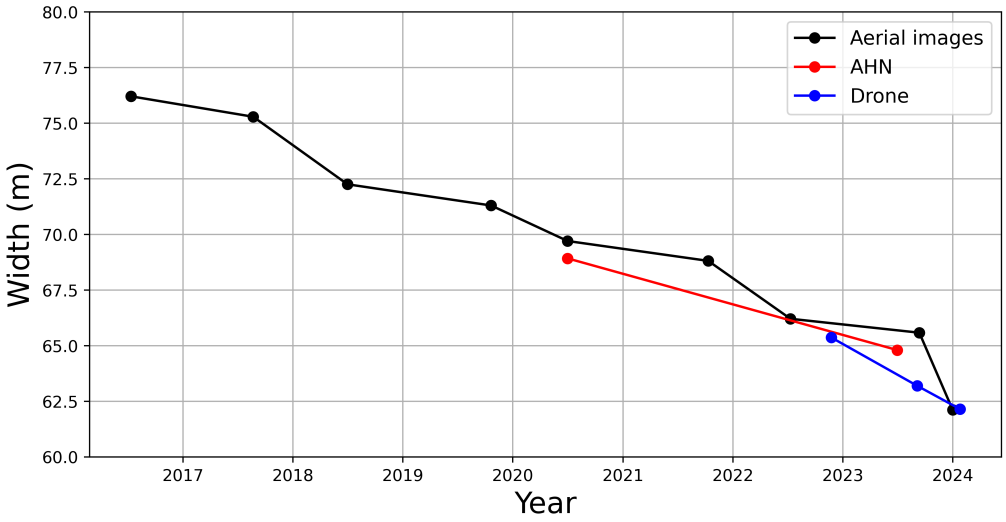

Figure 4.7: Comparison of average marsh width between PDOK images, AHN data, and drone DEMs.

Table 4.1: Comparison of the yearly retreat rates of the three different data sources.

	PDOK pictures	**AHN**	**Drone**
Start date or year	2016	2020	24-11-2022
End date or year	2024	2023	25-01-2024
Retreat (m/year)	1.11	1.37	2.75

The results of the three data sources show a similar trend, meaning a decline of average marsh width over the years and a positive yearly retreat. Table 4.1 shows that the retreat rate using AHN data is reasonably well in line with the PDOK pictures, but the yearly retreat is much larger using the drone data. This could be explained by the fact that the drone DEMs were taken only in the last 1.5 years and there was an increase in marsh erosion in those years. Looking at Figure 4.7, this explanation is reinforced since the marsh width decline using the PDOK images is similar to that of the drone data: 3.90 m and 3.22 m, respectively.

In general, the marsh width using the AHN data is smaller than the PDOK images (0.78 m in 2020 and 0.85 m in 2023). This could be explained by the uncertainty that lies in the dates that the AHN data was obtained (as explained in Section 3.3.1 and Appendix A). If this was later in the year, for both years the difference would be much smaller. Moreover, the PDOK image data point for 2023 presents a larger marsh width than the other two data sources. The drone DEMs are the most accurate and therefore the most reliable out of the three data sources. Therefore, the final configuration for marsh width consists of data from PDOK images until the data point in 2022. From that point onward the three drone data points are used for the marsh width and erosion rate.

Average marsh width and yearly retreat

The final configuration of data sources results in the plots below, showing average marsh width (Figure 4.8 a) and yearly retreat rate of the marsh edge (Figure 4.8 b).

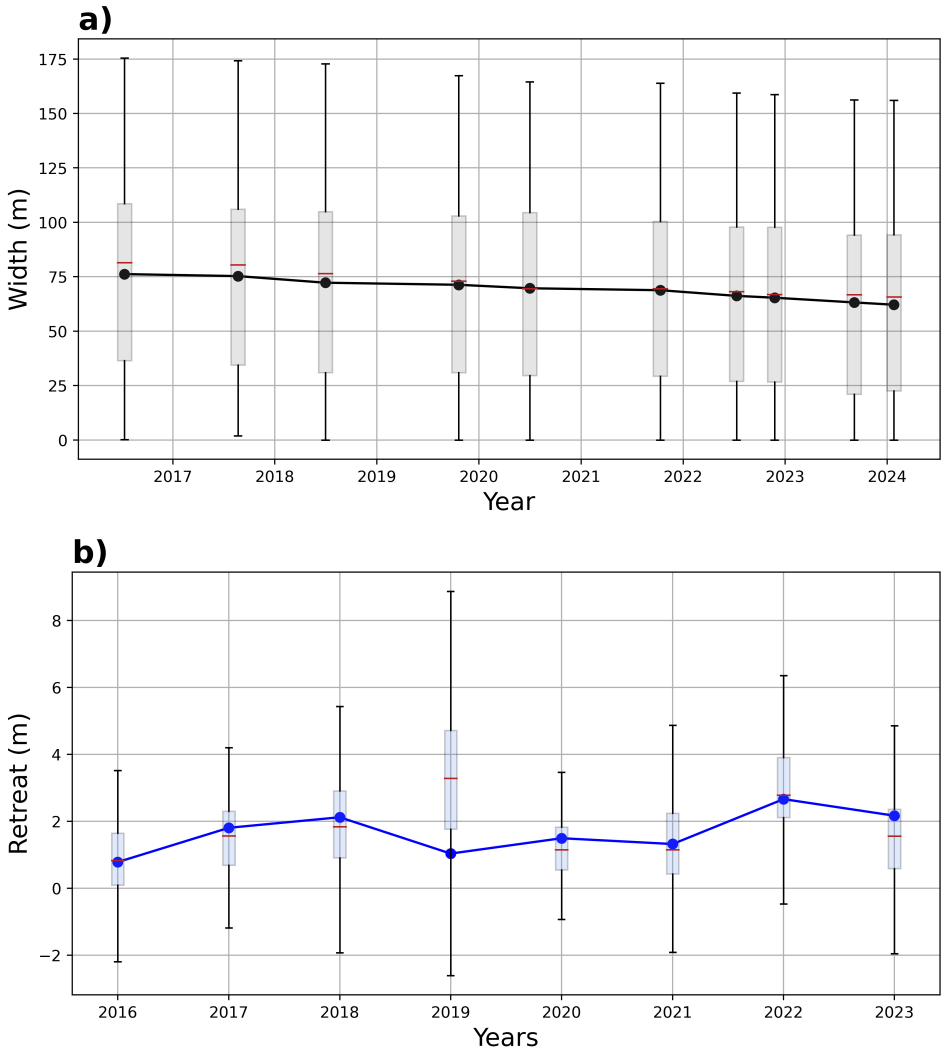

Figure 4.8: Average marsh width (a) and annual retreat (b) of the whole marsh using the final configuration of datasets, including a box-plot showing the minimum, first quartile, median, third quartile and maximum of the data per year outliers are excluded.

The average marsh width over all transects shows a clear decline throughout the years: from 76.2 m in 2016 to 62.1 m in 2024. Due to the irregular shape of the marsh, the box-plot is very large. At some points, the width is less than one meter, while at its widest in 2016, the marsh is more than 175 m wide. The box-plots do not vary much between the nine years: the standard deviation lies between 49.1 m in 2018 and 47.3 m in 2024. There is, however, a slight overall decline in standard deviation over the years. This might be caused by the marsh disappearing completely at some transects in later years. This results in a width of 0 and also a standard deviation of 0 and a lower average standard deviation.

The average retreat rate in the nine years that were included is 1.56 m/year. In total, in nine years the cliff has retreated 14.06 m (averaged over the whole marsh edge). However, there are large differences between the years, which is reflected in the sizes of the box-plots. Especially the year 2019 deviates from the other years,

with a very large box-plot and an average retreat rate that does not fall within the first and third quartile of the box-plot. Reasons for this are unknown. The relatively large box-plots indicate that the erosion of the marsh does not occur uniformly over the entire marsh edge. Local differences in marsh width and erosion rate are therefore considered in Section 4.3. However, the distribution of the marsh width and annual retreat over the marsh edge is examined and presented by Figure 4.9 for all years together. The data of the 119 transects is sorted into 11 bins for which the frequency of occurrence is determined.

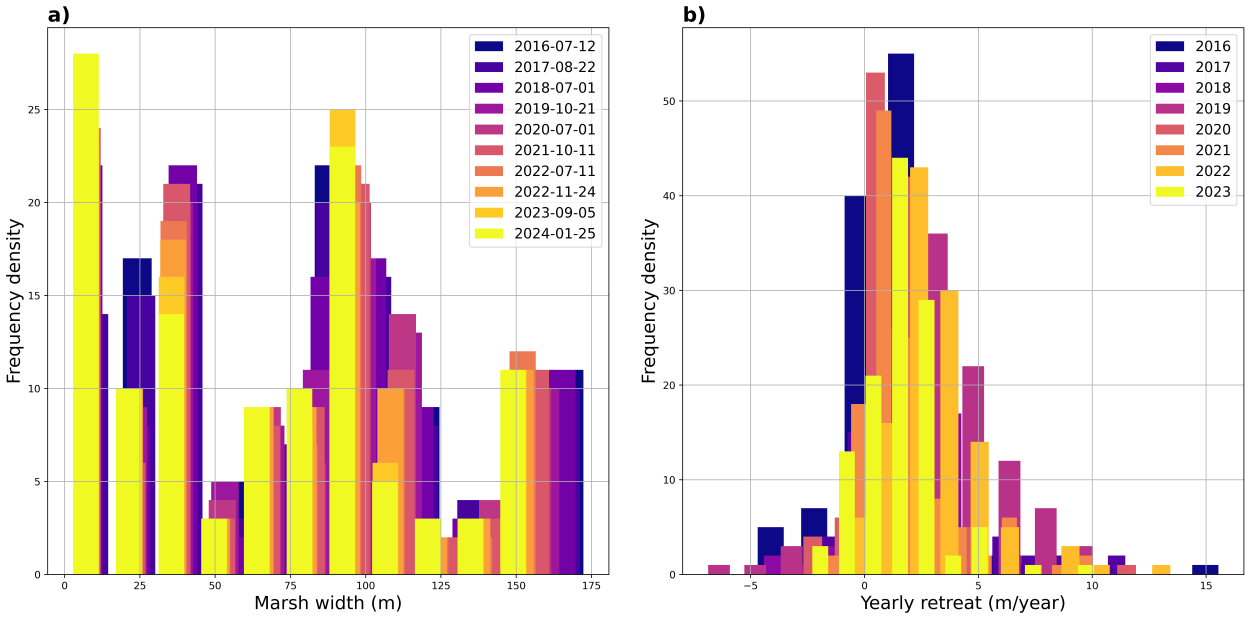

Figure 4.9: Frequency plotted for the average marsh width (a) and annual retreat (b) of the whole marsh per year.

The marsh width (Figure 4.9 a) is fairly randomly distributed over the whole marsh length. This makes sense because the marsh is very wide on the west side and decreases in width towards the east, meaning that all marsh widths are more or less present in the distribution. The distribution over the years is very similar. One thing that stands out is the large portion of very small marsh widths for 2024. An explanation for this is that the marsh has eroded so much that at more and more locations there is (almost) no salt marsh left in front of the dike. The most occurring widths lie between 80 m and 120 m, which are located in the middle of the marsh. There are two regions where the frequency is very low: around 50 m width and between 125 m and 140 m width. Appendix B shows the distribution of the separate years in detail.

The distribution of annual retreat is visualized the same way as the marsh width (Figure 4.9 b). The distribution of the annual retreat also shows consistency between the years. Contrary to the marsh width, the retreat data shows a bell-curve-like shape which suggests (close to) normal distributed data. The most occurring retreat for all years lies between 0 and 2 meters.

4.2.2 Hydrodynamic forcing

Wave power and wave thrust

The wave power and wave thrust were computed per hour using the hourly water level data and a daily average value for wave height and wave direction. The time series of the data are plotted in Figure 4.10 for wave power (a) and wave thrust (b).

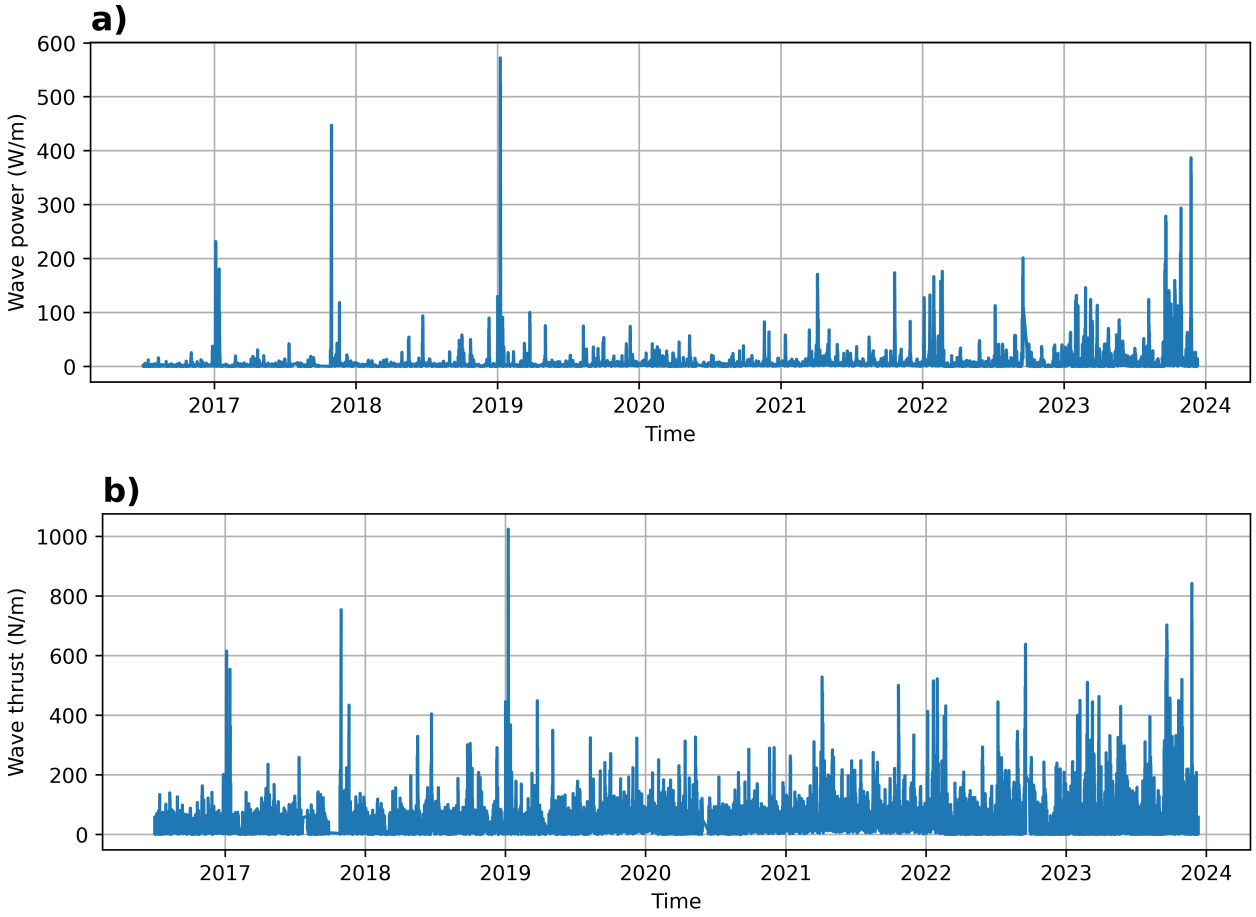

Figure 4.10: Plot of the time series of hourly averaged wave power (a) and wave thrust (b) for the Wierum salt marsh.

The average wave power is 5.37 W/m with a standard deviation of 15.39 W/m and the average wave thrust is 33.70 N/m with a standard deviation of 49.16 N/m. Both have a minimum value of 0 (rounded), and the maxima are 572.17 W/m for the wave power and 1023.82 N/m for the wave thrust. Both plots show a similar trend of mostly low values with some high extremes. These extremes correspond to events of high water depths and wave heights (Figure 4.3), for example on 04/01/2017, 29/10/2017, 08/01/2019 and the end of 2023. The difference in the time series between the available data from measurements at the Wierum marsh (up to June 23rd 2022) and the SWAN model-generated values for Holwerd (from June 23rd 2022) is less apparent in the graphs of the wave power and wave thrust (Figure 4.10) than it was in the graphs of the water depth and wave height (Figure 4.3). Both the wave power and wave thrust show a larger average in the last period compared to the first part, which could be a consequence of the high water depths and wave heights in the end of 2023. However, it could also be due to the difference in data sources (observed and SWAN modeled input variables).

The distributions of the daily data of the two hydrodynamic variables (wave power and wave thrust) are presented below as histograms (Figure 4.11). To determine the amount of bins the Freedman-Diaconis rule is used resulting in 144 bins for P and 73 bins for T. The histograms of wave power and wave thrust look very similar with a high count of low values and a long tail towards the right. The data is tested against four theoretical distributions: normal, log-normal, gamma and beta. Both the wave power and wave thrust are distributed following a log-normal distribution with parameters $\mu = 1.93 * 10^{-17}$ and $\sigma = 1.20$ for wave power and parameters $\mu = 6.41 * 10^{-17}$ and $\sigma = 1.18$. These distributions are also included in Figure 4.11.

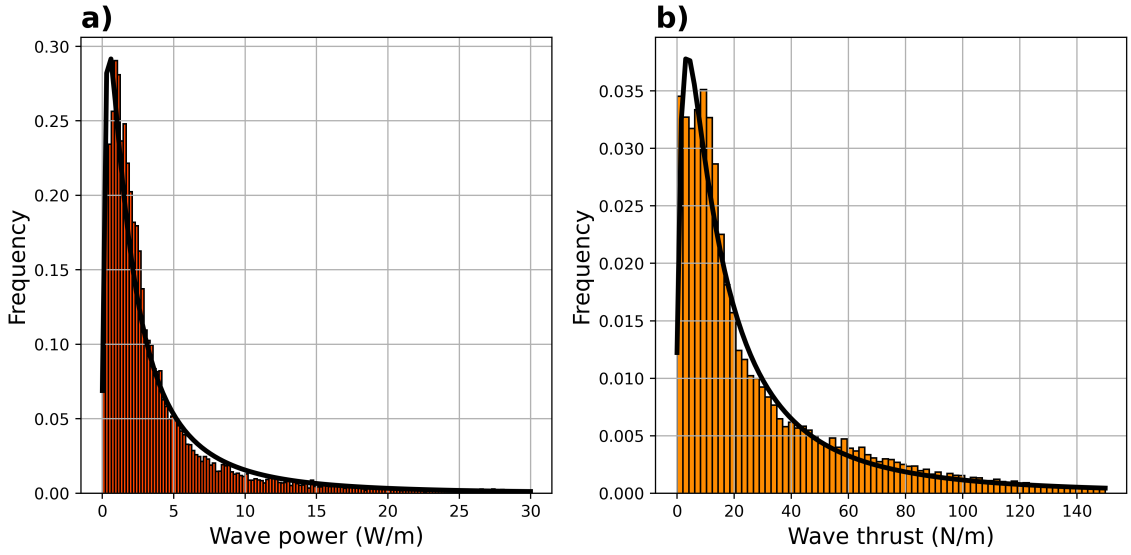

Figure 4.11: Distributions of the hydrodynamic variables including a plot of the best-fitting distribution: a) wave power with log-normal distribution (n=26071), and b) wave thrust with log-normal distribution (n=26002).

Inundation frequency

Figure 4.12 shows the variation of inundation frequency over the years of the two thresholds: h > 0.0 m and h > 1.0 m.

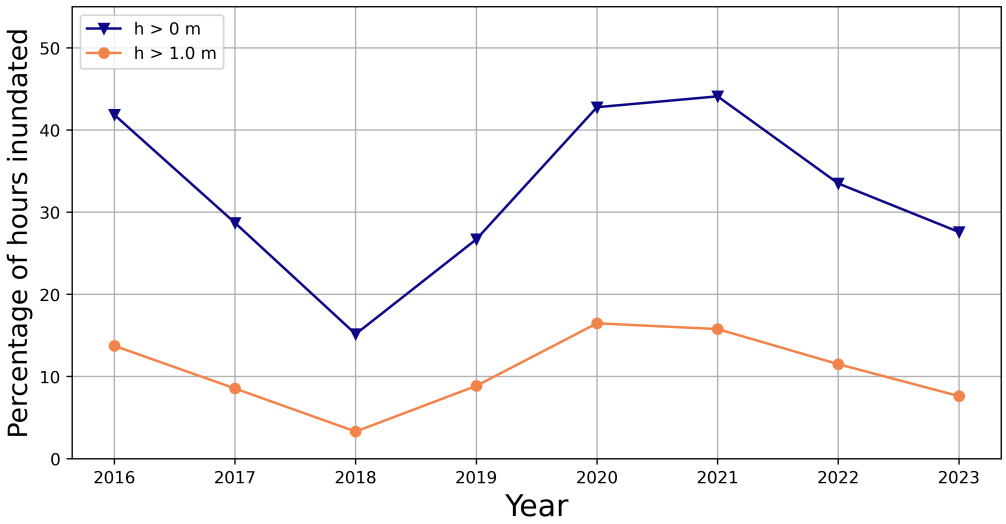

Figure 4.12: Inundation frequency (percentage of hours per year that the water depth exceeds a threshold) plotted for the two thresholds (h > 0.0 m and h > 1.0 m) over the 8 years.

The general trend is a decreasing inundation frequency with increasing water depth threshold (Table **??**). This makes sense as higher water depths occur less frequently within a tidal cycle. Figure 4.12 further shows that there are significant differences between the eight years. The year that stands out the most is 2018, where the percentage of hours in which the water depth is exceeded is very low. Only 15.2% of the hours that year there was any water at the marsh edge (threshold $h > 0$ m). The highest values are found for the years 2020 and 2021, where 16.5% and 15.8% of the hours in these years respectively the marsh was completely flooded (threshold $h > 1.0$ m).

4.2.3 Relations between erosion and hydrodynamic forcing

Wave power and wave thrust

Figure 4.13 shows the results of the yearly dimensionless wave power data plotted against yearly dimensionless erosion rate. It also includes a linear fit and a power law fit through the data points. Table 4.2 presents the standard deviations of the dimensionless erosion rate and dimensionless wave power.

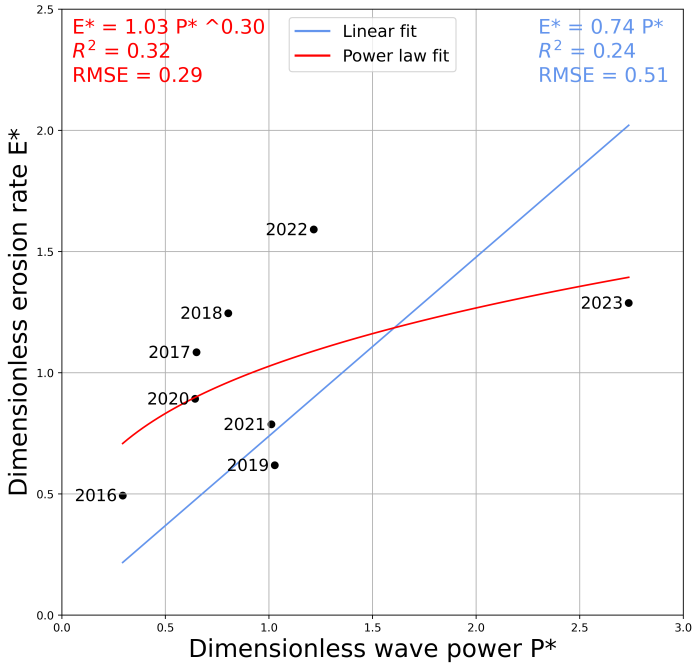

Figure 4.13: Relation between dimensionless wave power (P^*) and dimensionless erosion rate (E^*) including a linear fit of the shape $E* = \alpha^* P^*$ (blue) and a power law fit of the shape $E* = kP^{*n}$ (red).

Table 4.2: Dimensionless standard deviation of the erosion rate and wave power per year.

year	**2016**	**2017**	**2018**	**2019**	**2020**	**2021**	**2022**	**2023**
Stdev E^* (-)	0.75	1.38	0.95	0.82	1.00	1.31	0.42	1.38
Stdev P^* (-)	0.43	2.53	1.61	4.34	0.96	1.71	2.76	5.78

Both the linear function and the power law function show a positive relation between wave power and erosion rate. The fit of a linear line through the data points gives a slope α^* of 0.74. The RMSE is 0.51 and R^2 is 0.24. The power function shows a slightly better fit with an RMSE of 0.29 and an R^2 of 0.32. The power of the function n is 0.30 and k is 1.03. The year 2023 clearly stands out from the other points, because of the high value for wave power. The power law model catches this, whereas it lowers the performance of the linear model. The relatively large RMSE and low R^2 is partly explained by the standard deviations presented in Table 4.2. Apparently there is significant variation in erosion rate and wave power in the data. This spatial variation in erosion rate is explored more in Section 4.3.

The growth factor of the power model (n) lies well below 1.0. This means that an increase in hydrodynamic forcing does not result in a very large increase in marsh erosion. Hence, the marsh would be quite resilient against extreme hydrodynamic conditions such as storms and sea level rise. However, there were very little data points for this study and the power law function does not result in a very convincing fit to the data, so there is a

large uncertainty in this result.

Figure 4.14 shows the results of the yearly dimensionless wave thrust data plotted against yearly dimensionless erosion rate. It also includes a linear fit and a power law fit through the data points. Table 4.3 presents the standard deviations of the dimensionless erosion rate and dimensionless wave thrust.

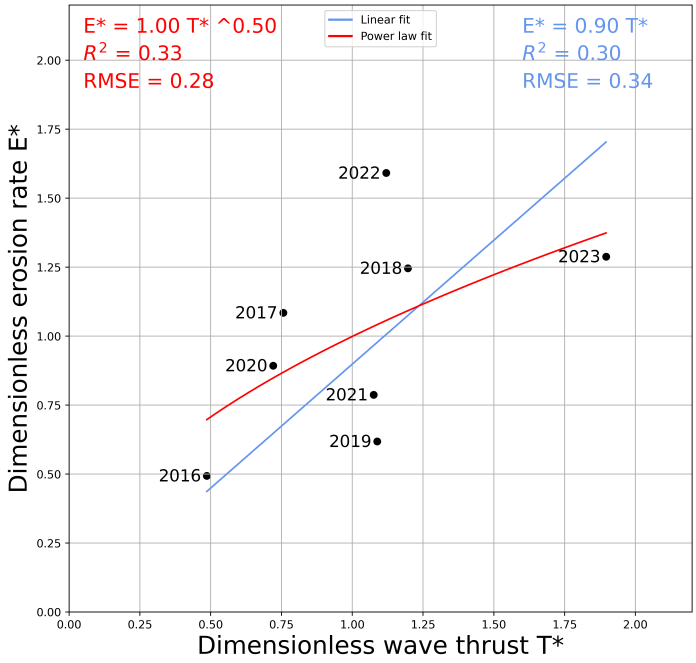

Figure 4.14: Relation between dimensionless wave thrust (T^*) and dimensionless erosion rate (E^*) including a linear fit of the shape $E* = \alpha^* T^*$ (blue) and a power law fit of the shape $E* = kT^{*n}$ (red).

Table 4.3: Dimensionless standard deviation of the erosion rate and wave thrust per year.

year	**2016**	**2017**	**2018**	**2019**	**2020**	**2021**	**2022**	**2023**
Stdev E^* (-)	0.75	1.38	0.95	0.82	1.00	1.31	0.42	1.38
Stdev T^* (-)	0.61	1.16	1.29	1.62	0.96	1.23	1.66	2.50

The results in Figure 4.14 show a positive relation between dimensionless wave thrust and dimensionless erosion rate. The data points of the wave thrust-erosion rate relation lie closer together than the wave power data points, which resulted in a better fit. The linear fit through the data points has a slope α^* of 0.90, a RMSE of 0.34 and an R^2 of 0.30. The power function results in similar goodness-of-fit metrics to the linear fit with a RMSE of 0.28 and an R^2 of 0.33. The power n is 0.50 and k is 1.00.

Inundation frequency

Figure 4.15 shows dimensionless erosion rate plotted against the percentage of hours that the water depth exceeds a certain threshold (h > 0.0 m and h > 1.0 m).

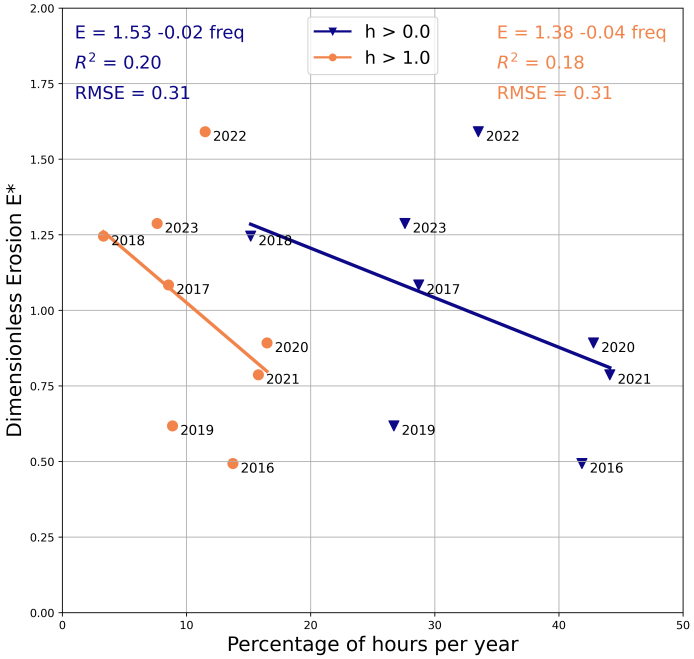

Figure 4.15: Relation between dimensionless erosion rate (E^*) and percentage of hours that the water depth exceeds the thresholds (h > 0 m and h > 1.0 m) including linear fits.

There is a negative relationship between erosion rate and inundation frequency for both water depth thresholds. The slopes of the graphs are -0.02 for h > 0.0 m and -0.04 for h > 1.0 m, which appears to be very gentle slopes, but this is due to the different scales of the axes in the Figure 4.15. This negative relation means that as the time the marsh is inundated increases, the lateral erosion decreases. This does not immediately make sense: apparently the duration of water presence at the cliff does not influences lateral erosion rate. This result is further discussed in Chapter 5.

4.3 Marsh Section Scale

4.3.1 Retreat rate

Figure 4.16 shows the marsh width and yearly retreat rates of the six sections, using the final dataset as determined in Section 4.2.1. This means that until the data point in the middle of 2022 the PDOK images are used and for the last three data points the drone DEM data is used to locate the marsh edge and determine the erosion rate with. Table 4.4 gives the average marsh width, retreat rate and cliff height per section, where marsh sections B, D and E have a cliff at the marsh edge and marsh sections A, C and F do not.

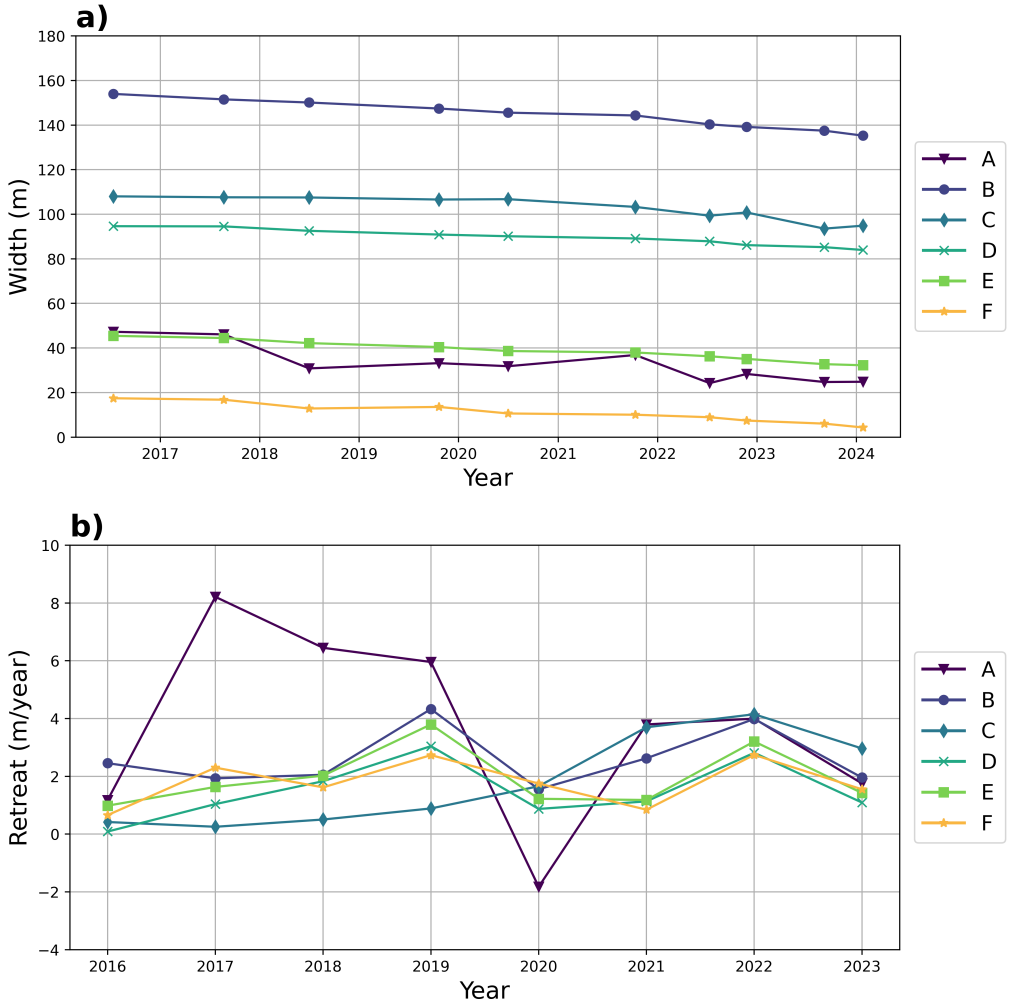

Figure 4.16: (a) Marsh width of the different sections and (b) yearly retreat of the different sections.

Table 4.4: Average marsh width, retreat rate and cliff height of the sections.

Section	**A**	**B**	**C**	**D**	**E**	**F**
Average width (m)	33.60	145.35	103.28	89.78	39.39	11.67
Average retreat rate (m/year)	2.82	2.06	1.81	1.18	1.59	1.42
Cliff height (m)	0.10	0.51	0.25	0.54	0.55	0.24

All sections except for A show a continuous decrease in marsh width and a positive retreat rate. The time-average retreat rate over the years are given in Table 4.4. The time-average retreat rate is largest for

section A and smallest for section F. Moreover, except for section A, the retreat rate of the marsh sections follows the same order as marsh width. The influence of the summer dike does not seem to be very large. The sections without summer dike (sections E and F) are much less wide compared to most of the other sections, but the retreat trend is not significantly different. Lastly, section A behaves very differently than the other sections, which is probably because there is no clear marsh edge at that section and because it is located in the dent in the sea dike. This resulted in very differently determined locations of the marsh edge and unreliable retreat rates. Furthermore, sections A and C show very low values in cliff height, indicating that there is no notable cliff at those locations. As mentioned in Section 4.1.1 and Figure 4.2, the cliff heights in section F are not always reliable. Leaving those inaccurate measurements out results in a cliff height of 0.24 m, which is interpreted as no cliff. For the analysis in Section 4.3.3, only the sections that have a cliff at the seaward marsh edge are included (Sections B, D and E), using the respective cliff height from Table 4.4.

4.3.2 Hydrodynamic forcing

The hydrodynamic forcing is assumed to be very similar over the whole marsh edge, so the same data as before is used.

4.3.3 Relations between cliff erosion and hydrodynamic forcing

The relation between dimensionless erosion rate (E^*) and dimensionless hydrodynamic forcing (P^* and T^*) is made for the sections with a cliff at the marsh edge. Figure 4.17 shows the plots of dimensionless wave power against dimensionless erosion rate per marsh section, taking into account the cliff heights of these different sections as presented in Table 4.4.

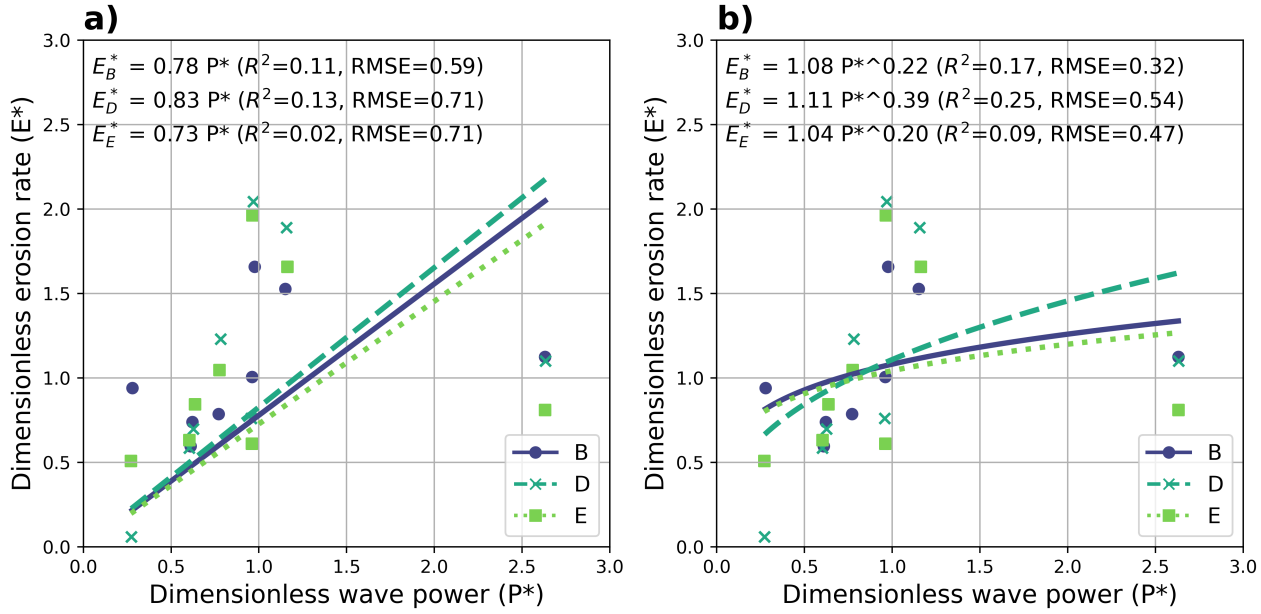

Figure 4.17: Dimensionless erosion rate plotted for dimensionless wave power divided per marsh section including a linear fit (a) and a power law fit (b) through the data points.

It is clear from the plots and the table that there is a slight difference between the sections. Although the slopes of the linear trend lines are quite close, there are large differences in the goodness-of-fit metrics. Section D shows the best fit to the data with also the largest slope in the linear fit (α^* = 0.83) and the largest parameter values in the power law fit (n = 1.11, k = 0.39). Section E shows a very poor fit of the linear trend line to the data

points with a large RMSE (0.71) and an R-squared close to zero (0.02). This R-squared is so close to zero that it should be interpreted as the absence of a relationship. These observations are reflected in the power law fit. Again section E fits worst (RMSE = 0.49, R^2 = 0.09). In general, the power law function provides a better fit to the data points than the linear function for all three sections with smaller RMSE and a larger R-squared. The average RMSE is 0.23 lower and the R-squared is 0.08 higher and closer to 1.0 for the power law fit than the linear fit.

The sections with dike (marsh sections B and D) show a slightly higher erosion rate with increasing wave power than the section without dike (marsh section E), which is reflected in the higher α^*, k and n of the sections with summer dike than the section without summer dike. However, the differences are very small and highly influenced by the results of section D.

Figure 4.18 shows the results of the relation between marsh edge erosion rate and incoming wave thrust for the different marsh sections. The plots are structured the same as for the erosion rate - wave power relation.

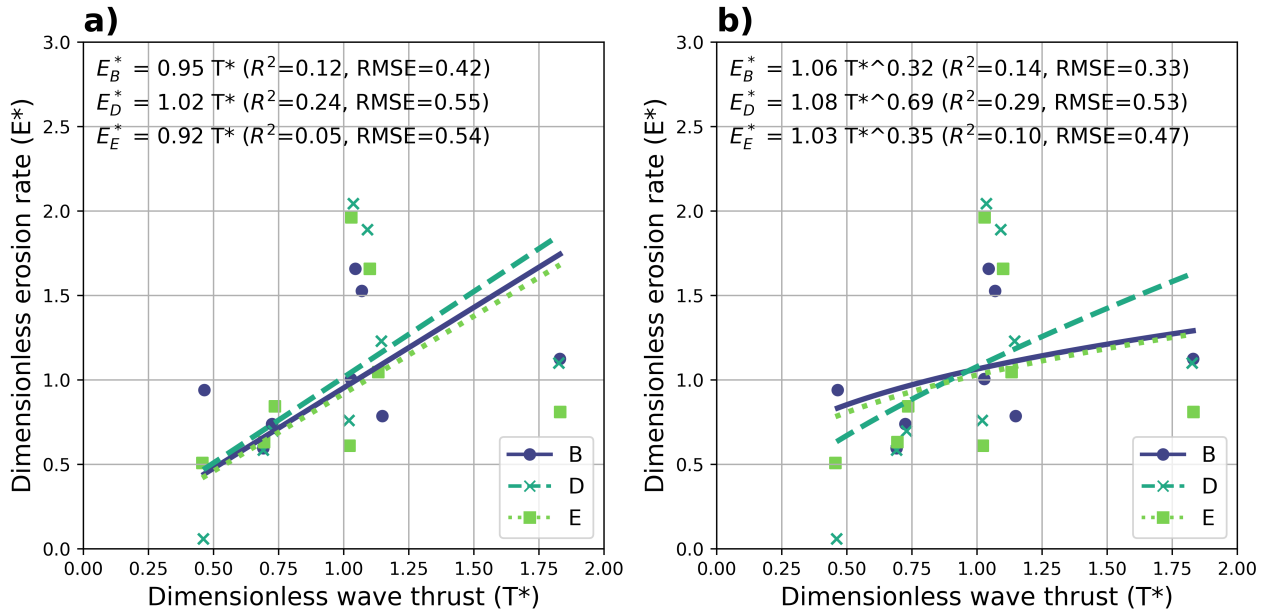

Figure 4.18: Dimensionless erosion rate plotted for dimensionless wave thrust divided per marsh section including a linear fit (a) and a power law fit (b) through the data points.

The results for the linear erosion rate - wave thrust relationship show that there is a slight difference between the sections. On average, the power law fit to the data points shows a lower RMSE and a higher R^2 than the linear fit, indicating a better fit to the data points. Section D stands out from the other two as it has the steepest slope (α^*=1.02) in the linear fit and the highest power (n=0.69) in the power law fit. This indicates a weak resilience of the marsh against increasing wave thrust. Differences between sections with summer dike (sections B and D) and the section without summer dike (section E) are not notable. While section E does show the lowest slope in both fits, the differences are negligible and highly influenced by the results of section D.

The results of the erosion rate-wave thrust relationship are quite similar to the results of the erosion rate-wave power relationship, meaning that the differences between the sections follow a similar trend: section D shows the largest increase in erosion rate with increasing wave power or wave thrust. The α^* of the linear fits of all sections are very similar, but on average the slope of the linear erosion rate-wave thrust relationship is slightly larger than the slope of the linear erosion rate-wave power relationship (4.5%).

4.3.4 Relation between cliff erosion and marsh edge complexity

The fractal dimension (FD) is determined for the different sections (excluding section A) using the marsh shape of each year. Appendix C shows the intermediate result of this process, meaning the plots of $log(n)$ against $log(L)$ of the whole marsh and the different sections for the nine years. In general, there is not much difference in the marsh shape over the years. The FD of the whole marsh shape varies between 1.07 in 2024 and 1.14 in 2021. For reference, the shape in Figure 2.8 is a relatively simple shape and has an FD of 1.05 (Piera et al., 2005). A more complex shape such as the coastline of Great Britain has a FD of 1.31 (Peitgen et al., 2004). So, the FD of the entire Wierum marsh lies between these two values. There is no clear trend detected over the years, meaning that the FD does not increase or decrease steadily over the years. There are, however, clear differences between the different marsh sections. Table 4.5 shows the average FD for the five sections and Figure 4.19 shows the variations in FD of the sections over the years.

Table 4.5: Average fractal dimension (FD) over the years of the five marsh sections.

Section	**B**	**C**	**D**	**E**	**F**
Avg FD	1.011	1.073	1.052	1.100	1.126

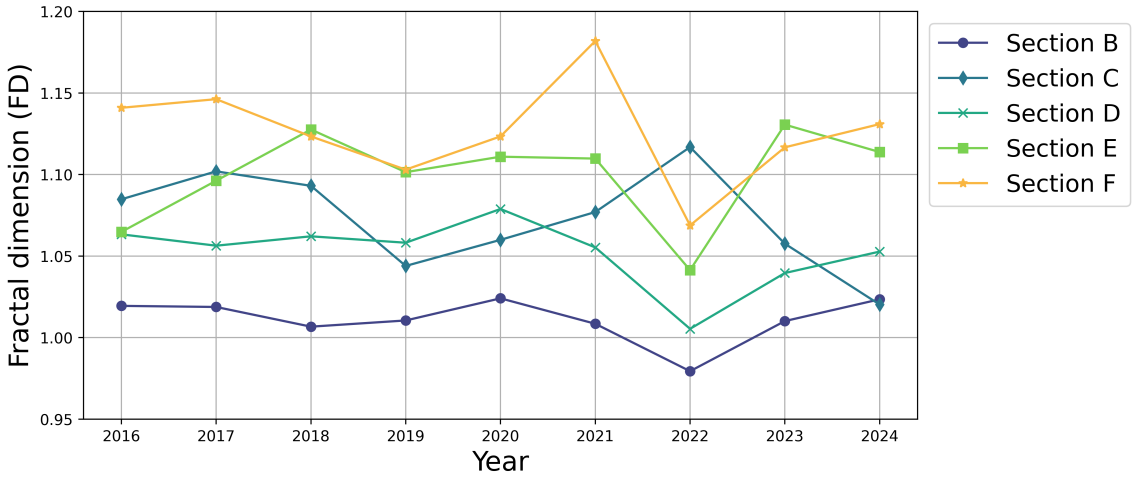

Figure 4.19: The fractal dimension (FD) of the marsh sections B-F over the years.

The time-average FD of the sections over the years shows that there is a small difference between the sections (Table 4.5). Sections E and F have the highest FD and can therefore be considered as the most complex in shape. Section B, on the other hand, has the lowest average FD which means that it is a simpler shaped marsh edge. The difference between marsh sections with and without cliff at the edge is represented as a larger variation of FD in Figure 4.19. Sections F and C vary more than the other sections. There is a difference in FD between section D (with summer dike) and E (without summer dike), as the FD of section E is constantly higher than the FD of section D (on average 0.048 higher).

The dimensionless erosion rate (E^*) of the different sections for the different years is plotted against the fractal dimension (FD) no unit) in Figure 4.20, where also a linear fitted trend line through all data points and the goodness-of-fit metrics are added.

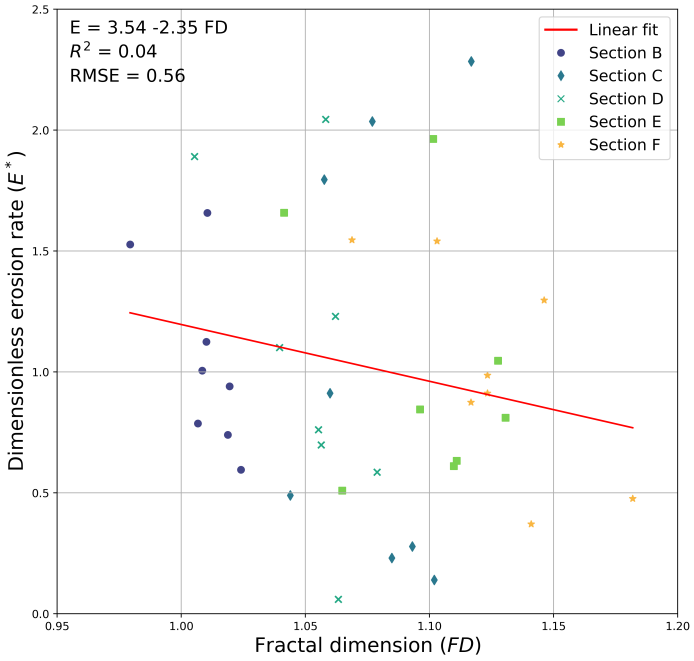

Figure 4.20: Dimensionless erosion rate plotted for the fractal dimensions of sections B-F for the different years, including a linear fit through the points.

The general trend line shows a negative relation between FD and E^*: for an increase in FD, E^* will decrease. The slope of the linear fit is -2.35. This means that a more complex marsh edge shape (larger FD) experienced less erosion. This linear fit has a R^2 of 0.04 and a RMSE of 0.56.

4.3.5 Relation between cliff retreat and vegetation

The time-averaged 90th percentile of the Normalized Difference Vegetation Index (NDVI) of the five marsh sections (so excluding section A) is presented in Table 4.6. Figure 4.21 shows the change in NDVI (90th percentile) of the sections over the years.

Table 4.6: Average NDVI near the marsh edge over the years of the five marsh sections.

Section	**B**	**C**	**D**	**E**	**F**
Avg 90th percentile NDVI	0.213	0.126	0.0955	0.00616	-0.0682

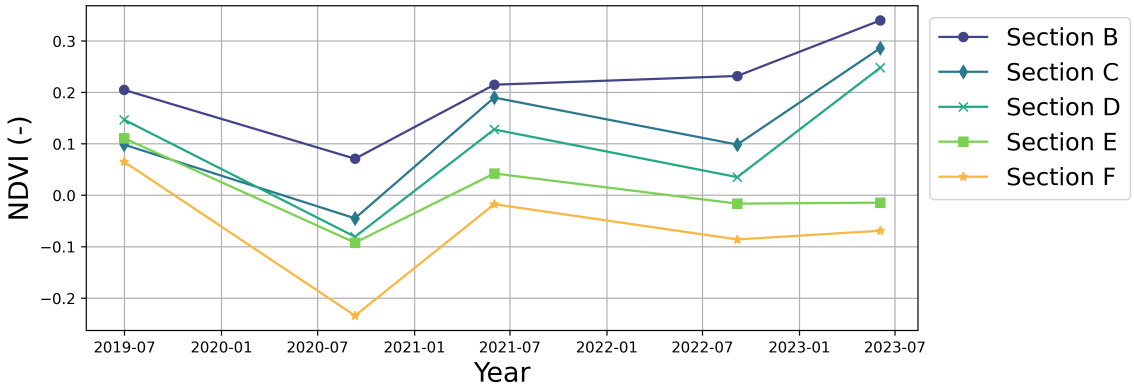

Figure 4.21: The average NDVI per section near the marsh edge plotted over the available years.

There is a clear difference in NDVI between the sections: it appears that Section B has the most vegetation growing close to the edge of the marsh and Section F has the least. In the year 2020 there was almost no vegetation detected at the marsh edge, leading to very low NDVI values (below 0.1). An NDVI below 0.1 means that there is basically no vegetation. An NDVI below 0.0 has no physical meaning, so the dataset is filtered and all values below 0.0 are removed to determine the erosion rate - vegetation density relation.

The yearly NDVI per section is plotted against the erosion rate per year and per sections in Figure 4.22. A linear fit is made to reveal any relation. Again, the goodness-of-fit between the data points and the linear fit is measured by the R^2 and RMSE.

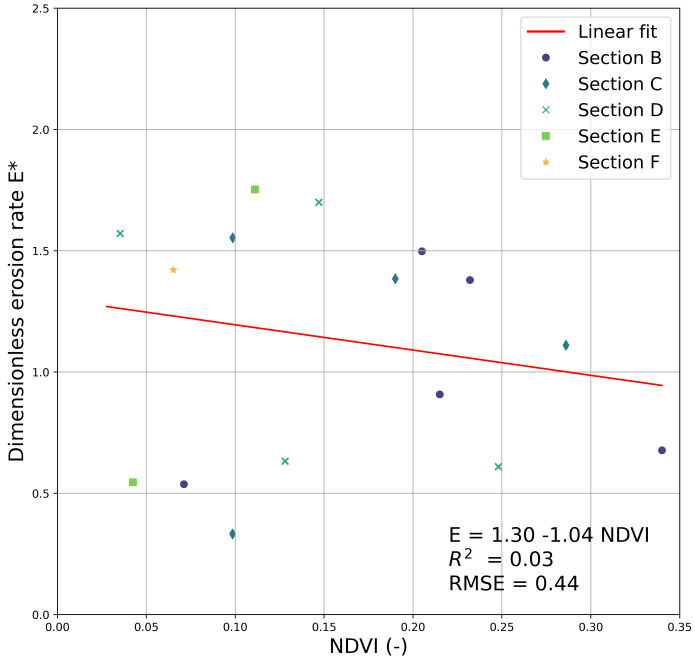

Figure 4.22: Dimensionless erosion rate plotted for the NDVI of sections B-F and the different years, including a linear fit through the points.

The linear fit through the data points has a slope of -1.04, indicating a negative relation between NDVI and erosion rate. This means that more vegetation would lead to less erosion. The level of reliability of this result needs to be questioned, because the very low values of the NDVI, indicating that there is very little vegetation present in any section.

Chapter 5

Discussion

5.1 Discussion of the results

The main limitation of the results of this study is the lack of data points. There are only eight cliff retreat data points considered and this has led to dubious results regarding the erosion rate - wave power and erosion rate - wave thrust relationships. This is reflected in the poor performance of both the linear and power law model with RMSE values between 0.28 and 0.51 and, more importantly, R^2 values of 0.33 and lower. Especially the low R^2 values indicate that the linear and power law fits are not a convincing representation of the data points.

Looking at the erosion rate - wave power depiction in Figure 4.13 there is one year that stands out: 2023. This data point influences the data greatly with its relatively large value for wave power, but its relatively low value for erosion rate. The large average wave power could be caused by the presence of storm Pia in December 2023. This storm caused high water levels and wave heights in the Wadden Sea (KNMI, 2023), which in turn result in a high wave power. Figure 4.10 reflects this partly, but the wave power was quite high during the whole year, not just at the end of December. Since the retreat rate in 2023 was not significantly higher than other years, it could be concluded that the combination of high water levels (causing deep flow over the marsh surface) and high wave heights does not influence lateral erosion that much.

The assumption was made there is no erosion when there is no wave power or wave thrust, meaning that the fits of dimensionless erosion rate against dimensionless wave power (E^*-P^*) and dimensionless erosion rate against dimensionless wave thrust (E^*-T^*) need to go through the origin (0,0). To test the effects of this assumption, a fit was made where the interception point with the y-axis was also determined by the least-square algorithm. The results of of both the linear and power law fit for both E^*-P^* and E^*-T^* are presented in Appendix B.4. The first thing that stands out is that the power law fit is almost the same for both approaches. The reason for this is probably that the original fits are already almost crossing the origin. The main difference between these fits and the original fits is that the linear fit is much closer to the power fit. This makes sense because the power fit had a lower RMSE and an R^2 closer to 1.0 (Figure 4.13 and 4.14), which means the model presents a better fit to the data. Another reason for the better fit is the fact that there is one less constraint for the least-square algorithm, hence resulting in a better fit. Removing the constraint results in the linear fit intersecting the y-axis at a height of 0.75 for the wave power and a height of 0.50 for the wave thrust. This means that even when there is no wave power or wave thrust, there would be some edge erosion. While this does not automatically make sense, this erosion could be caused by tidal flow and wetting and drying of the marsh only and not the influence of waves (Francalanci et al., 2013).

A negative relation was found between the frequency of inundation (in % of hours per year that inundation) and dimensionless erosion rate. This indicates that even when there is not often water at the cliff, there is still erosion observed. This result seems very counterintuitive and might originate from a lack of data points. Figure

4.15 shows indeed that the spread of data points is very large. However, there are theories that could explain this negative relationship. A very large water depth (h > 1.0 m) means that the salt marsh cliff is completely inundated. The waves create then less horizontal forcing on the cliff and therefore there could be less salt marsh edge retreat. However, also a negative relation is found between the frequency that there is any water at the cliff (h > 0.0 m). This suggests that instead of the duration of water presence at the marsh cliff, wave action influences cliff erosion.

The results of the E^* - P^* relation for the different marsh sections show that there are no notable differences between the sections with a cliff at the edge (marsh sections B, D and E in Figure 4.17). This could be caused by the uniform value for water depth and wave height along the marsh boundary that is used because there was no data available about spatial differences in hydrodynamic forcing. Differences in erosion rate between the sections are not drastically different. The section with the largest erosion rate (excluding section A) is section B. This could be explained by the orientation of this section: it is the section that extends the most onto the mud flat, which means that it would be subject to the hydrodynamic forcing the most out of all sections. Following the same reasoning, section C is sheltered from the waves by section B and should retreat less. For the years 2016 to 2020 this is indeed what is observed (Figure 4.16 b), but from 2021 onward section C experienced more erosion than section B. In Appendix C.2, the E^* - P^* and E^* - T^* analyses are done for all sections (Figures C.3 and C.4), to see how the linear and power law fits look. The respective cliff heights from Table 4.4 are used for the sections, which means that the applicability to the sections without cliff (marsh sections A, C and F) might be limited. This is reflected in the power law model results: marsh sections A and C show a very different trend than the sections with cliff at the edge. Section A has a negative power in both the E^* - P^* and the E^* - T^* relationship. Section C, on the other hand, presents a very steep slope. Section F seems to behave similarly to sections B and E. The linear fits of the sections without cliff are not drastically different from the fits of the sections with cliff.

The marsh edge complexity is expressed by the fractal dimension (FD) using the box counting method. The digitalization of the marsh edge is a simplification of the actual marsh edge, which generates a limitation in the box counting method. At a certain point decreasing the box size will not result in more boxes, because there is no no more detail in the drawing of the marsh edge. This might also be an explanation of the relatively low FD values that were found for the different marsh sections.

Connecting the results of erosion rate, the hydrodynamic forcing, and marsh edge complexity, an interesting observation is made. The sections with a summer dike show a higher erosion rate with increasing wave power and wave thrust than the sections without dike. At the same time, the sections with a summer dike have a more smooth edge. This shows that the results of these separate analyses complement each other. Reasons for this phenomenon are unknown, as the presence of a dike further towards the dike on the marsh should not directly influence the erosion at the boundary. Perhaps there are significant differences in elevation, soil type, or vegetation between the land in front and behind the dike.

The results of the relation between NDVI and erosion rate were disappointing. Figure 2.10 b shows that there is some vegetation present at the marsh edge, but this did not come forward in the determination of the NDVI (Figure **??** and Table 4.6) with values below 0 for some sections while using the 90th percentile of NDVI values within one section. Possible reasons for this might lie in the accuracy of the data used. The satellite images had a resolution of 0.5 m horizontally, which means that every grid cell receives one value for NDVI. If the vegetation in a particular cell is very sparse, this could lead to a very small (or even negative) NDVI value, even though there is some vegetation present. The presence or absence of one large plant also has a great influence on this 90th percentile of the NDVI.

5.2 Discussion of the input data

A major limitation follows from the input data that is used. In general, because this data is (mostly) real-world measurements, it contains uncertainties from many sources. For example, the PDOK aerial images had a time stamp in the metadata that did not always agree with the time stamp according to the PDOK website and in some cases there was no time stamp given at all. This resulted in a large uncertainty in the date that a certain image was generated, which has led to uncertainty in the marsh edge retreat rate. The spatial resolution of the PDOK images also contributed to this uncertainty. For the years 2016 to 2020 the resolution was 0.25 m, which means that the potential error in marsh edge retreat between two consecutive years is 0.5 m. In context to the average retreat rate over the years (1.56 m/year) this is a significant number that might have influenced the results. Also the human error in the digitalization of the marsh edge plays a role here. The marsh edge was digitalized by manually tracking the cliff edge. The cliff was well visible in the PDOK images (Figure 3.2), but at locations without cliff it was difficult to define a marsh edge. This difficulty might have led to a very different placement of the marsh edge for different years, resulting in an inconsistent retreat of the marsh edge. This problem was less prominent for the ANH and drone DEM's, because the elevation was used directly to determine the marsh edge. Still, locating the marsh edge where there is no cliff is a subjective matter.

The hydrodynamic input data (water depth, wave height and wave direction) also caused uncertainties. The most prominent cause is the fact that the three variables originate from different sources (Figure 3.1) that have used different methods to obtain the water depth, wave height and wave direction. As mentioned in Section 3.3.1 the data consists of a mix of observations and modelled values. The data from these sources was modified and combined to form one final time series with water depth, wave height and wave direction. In this process it was assumed that the different sources are compatible, but this might not be entirely the case. Figure 4.6 shows a direct example of this, where water depth and wave height measurements on the mudflat at Wierum are compared to the modified water depth from the Holwerd station and SWAN-generated wave heights. Locally measured data were structurally lower for both variables, which indicates that the data used in the analyses is not entirely accurate. Furthermore, Figure 4.3 shows that there are differences in the input data: there are periods where the water depth does not reach 0 at all, for example in the year 2021. This is unrealistic, because during low tide there should not be water at or near the marsh edge. This discrepancy is also visible in the time series of the wave power and wave thrust (Figure 4.10). Also in the wave height there is a difference between data sources: especially before and after mid-2022. This coincides with the start of a new dataset: Wierumerwad 3 instead of Wierumerwad 2. However, it is unknown what the difference is between those two datasets: both data sets use SWAN model-generated data extracted at the same location. Perhaps a new version of the SWAN model is used in Wierumerwad 3 that impacts the data.

5.3 Comparison to literature

5.3.1 Relation erosion rate and wave power

Linear relationship

Many studies report a linear relationship between erosion rate and wave power, using observed marsh erosion rate and modelled or observed wave characteristics. Amongst them, Leonardi, Ganju, and Fagherazzi (2016) used data from eight different marshes all over the world. Figure 5.1 shows the results of Leonardi, Ganju, and Fagherazzi (2016) and the results of this study.

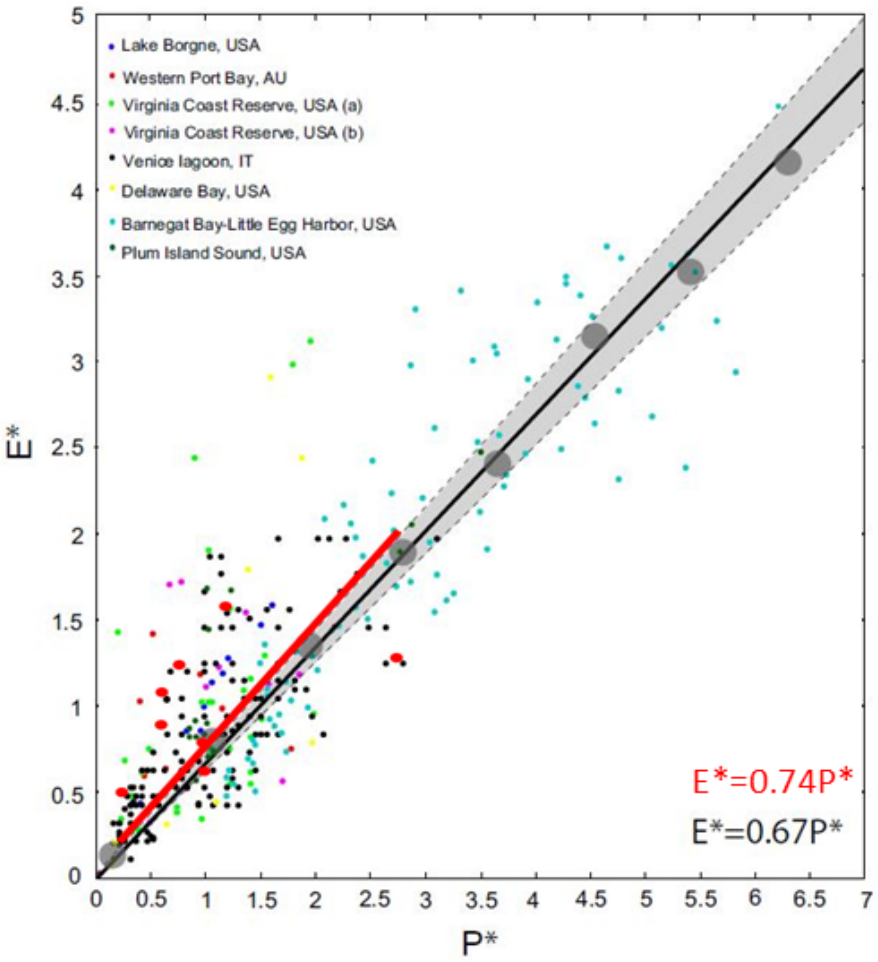

Figure 5.1: Results from this thesis (red dots with linear fit) plotted with the results of Leonardi, Ganju, and Fagherazzi (2016) of the relation between dimensionless wave power (P^*) and dimensionless erosion rate (E^*).

The data of Leonardi, Ganju, and Fagherazzi (2016) exhibit a wider spread than the results of the Wierum marsh. There is one marsh in particular that experienced both a large wave power and a rapid retreat: Barnegat Bay-Little Egg Harbor, USA. The other seven marshes follow more or less the same range as the Wierum marsh. The slope of the linear fit is larger for the Wierum marsh than for the Leonardi, Ganju, and Fagherazzi (2016) data set (0.74 and 0.67, respectively). Possible explanations for this could be the fact that Leonardi, Ganju, and Fagherazzi (2016) evaluated some salt marshes that were particularly subject to hurricanes, but they report that more frequently occurring events such as winter storms have a larger influence on the erosion rate than hurricanes. The Wierum marsh is located in a very sheltered bay (Wadden Sea), where there are no intense storms like hurricanes. Every winter, however, there are storms that hit the marsh. Following the findings of Leonardi, Ganju, and Fagherazzi (2016), this does result in a larger erosion rate, and hence a larger α^*. Other differences between the

Wierum marsh and the marshes in Leonardi, Ganju, and Fagherazzi (2016) are found in the tidal range, which is larger in the Wadden Sea (mesotidal environment, average tidal range is 2.2 m) than all the marshes in Leonardi, Ganju, and Fagherazzi (2016) (microtidal environments) (Whitfield & Elliott, 2011). A larger tidal range will not have much effect on wave power, which is largely determined by wave height. However, it could result in higher flow velocities at the edge of the marsh that cause erosion. The total erosion rate will then also be greater.

Other literature that found a relation between erosion rate and wave power use often a volumetric erosion rate, defined as marsh loss per meter edge length per year (m^3/m/year, which equals m^2/year) (Mel et al., 2022; WinklerPrins et al., 2024). To match this definition, the volumetric erosion rate for the Wierum marsh can be determined by multiplying the lateral retreat by the cliff height, using an average cliff height of 0.5 m. The results of this volumetric erosion rate are plotted against wave power including a linear fit in Figure 5.2, where also the findings of Finotello et al. (2020), Marani et al. (2011), McLoughlin et al. (2015), and Mel et al. (2022) are included. Mel et al. (2022) evaluated the processes in the Venice Lagoon between 2014 and 2018, where they measured the cliff retreat on a monthly and annual time scale by placing 26 horizontal pins in the cliff. Wave power was calculated using empirical equations with wind and water level as inputs. Finotello et al. (2020) also carried out field measurements in the Venice Lagoon. They made 83 transects along the coast and measured the retreat of the cliffs between the summers of 2015 and 2016. Wave power was determined using a numerical model (SWAN). The results of Marani et al. (2011) of three marshes in the Venice Lagoon were obtained by analyzing aerial photographs and determining the erosion rate and using the same approach as Mel et al. (2022) for the wave power. Finally, McLoughlin et al. (2015) determined the erosion rate of a marsh in Virginia, USA (Hog Island Bay) using aerial photographs and model-generated wave power.

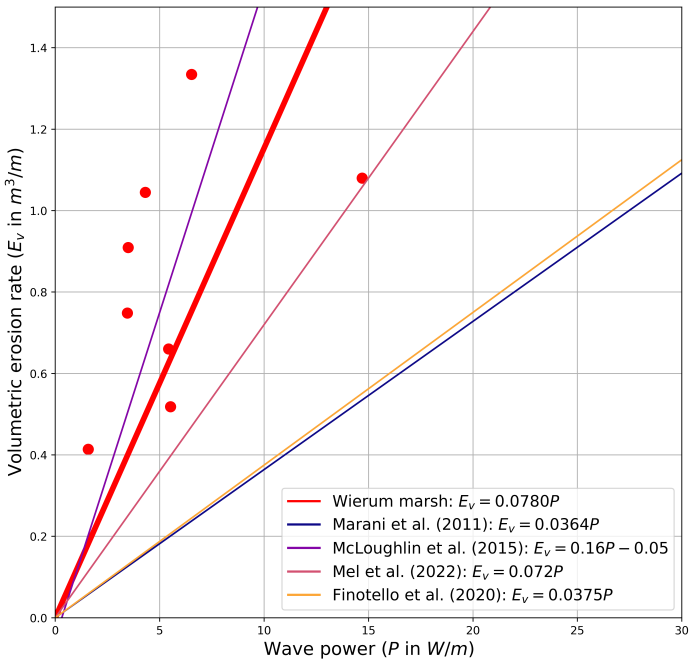

Figure 5.2: Volumetric erosion rate (E in m^3/m) plotted against wave power (P in W/m) for the Wierum marsh (red dots with linear fit), including results from Finotello et al. (2020), Marani et al. (2011), McLoughlin et al. (2015), and Mel et al. (2022).

Figure 5.2 shows that the results from this study are the most similar to Mel et al. (2022) and McLoughlin et al. (2015). Reasons for this are not straightforward: there are differences both in the type of salt marsh that was studied, the magnitude of hydrodynamic forcing and erosion rates, and methods used between the four sources.

Power law relationship

A power law relationship between wave power and wave thrust is reported less often than a linear relationship. Schwimmer (2001) evaluated two salt marshes in Rehoboth Bay, Delaware, USA at nine locations and report a power law relationship between wave power and erosion rate ($E = 0.35P^{1.1}$). The wave power that they reported is much higher than in the Wadden Sea (order of magnitude 1000 W) and therefore it is not possible to compare results directly. The function is applied to the wave power values of the Wadden Sea and plotted in Figure 5.3.

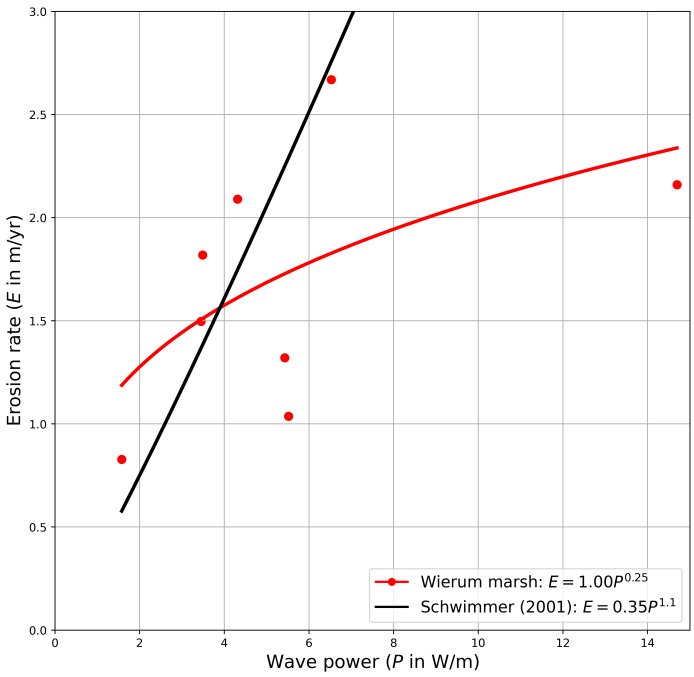

Figure 5.3: Erosion rate (E in m/year) plotted against wave power (P in W/m) for the Wierum marsh, including results from Schwimmer (2001).

The difference between the two power functions is clearly visible in Figure 5.3. The power in the function that Schwimmer (2001) report is 1.1, whereas the wave power found in this study lies well below 1 (0.25). The most plausible reason for this difference lies in the data points for the Wierum marsh. As mentioned in Section 5.1, the data point for 2023 heavily influences the power law fit. Leaving that point out, the power law fit would take a very different shape and the function from Schwimmer (2001) seems to fit quite well. However, assuming this data point is correct, it could be argued that the relationship found by Schwimmer (2001) is likely not applicable to basins with very small wave power such as the Wadden Sea. Another difference between the two marshes is the presence of vegetation. Pictures by Schwimmer (2001) show that the marsh is densely vegetated, right until the cliff. Schwimmer (2001) describes that undercutting below the roots of this vegetation has led to large blocks separating from the marsh. Perhaps this process increases greatly with increasing wave power, leading to a power of 1.1. Another conclusion that might be drawn from this difference is that the Wierum marsh is much more resilient to higher wave power than the Rehoboth Bay marsh, since for a higher wave power there is not much more erosion observed. However, again, it is hard to compare the two situations.

Houttuijn Bloemendaal et al. (2023) saw that a power curve is often a better fit to the data points than a linear line. However, they state that this depends on the distribution of the data: non-normally distributed data are first transformed in their study. This is not done with the Wierum marsh data, even though the data are not normally distributed (Figure 4.11 in Section 4.2.2). Looking at the results of the wave power - erosion rate

relationship, it appears that the power law function does result in a better fit than the linear function (Figure 4.13). Perhaps transforming the data, as Houttuijn Bloemendaal et al. (2023) did, further improves the fit.

5.3.2 Relation erosion rate and wave thrust

To the authors knowledge there is only one example in literature that presents the relationship between erosion rate and wave action in the same way as this study. Leonardi, Defne, et al. (2016) evaluated the erosion rate between 1930 and 2013 of 10 sections of the Barnegat Bay salt marsh and used modelled values of wave thrust as hydrodynamic forcing. They found a positive correlation with a slope of the linear fit of 11.92 m^2/kN yr (Figure 5.4). Using the same units for the Wierum marsh, a much steeper slope is found (70.27 m^2/kN yr). A possible explanation for this could lie in the ranges of erosion rate and wave thrust that are observed. The erosion rate of the Barnegat Bay marsh was approximately two times lower than the Wierum marsh, while the wave thrust was up to three times larger (Leonardi, Defne, et al., 2016). This makes it difficult to make a fair comparison between the two marshes.

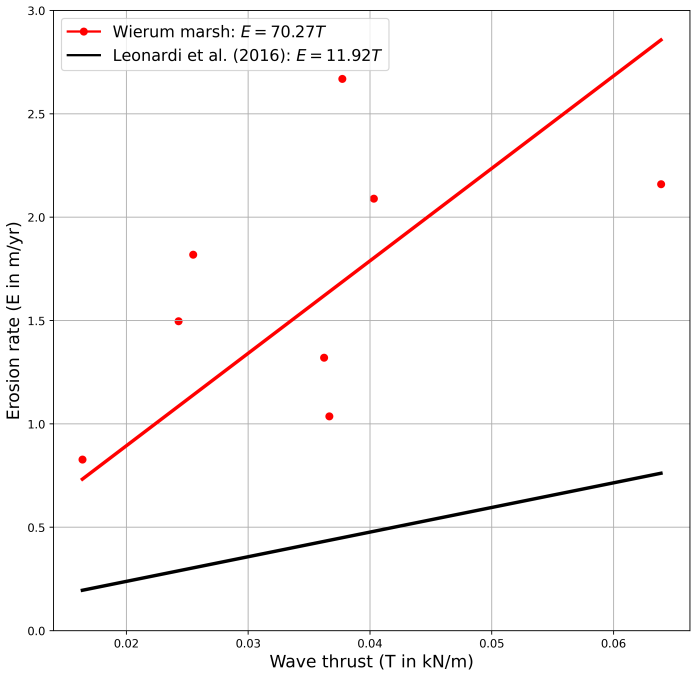

Figure 5.4: Erosion rate (E in m/year) plotted against wave thrust (T in kN/m) for the Wierum marsh, including results from Leonardi, Defne, et al. (2016).

There are various modelling studies done about the erosion rate - wave thrust relationship (Donatelli et al., 2019; Fagherazzi et al., 2013; Tonelli et al., 2010). The general consensus from these articles is that the wave thrust has the largest impact on the marsh edge when the water level is (almost) equal to the top of the marsh cliff. For the Wierum marsh, the average cliff height is 0.5 m and a water depth of 0.5 m lies in between every high and low tide (Figure 4.3 a), meaning that this water depth occurs very often. This could explain the erosion trend in the Wierum marsh, but this relationship is not studied and strong conclusions cannot be drawn. Besides relative water level, different soil and vegetation characteristics probably also have an influence on the erosion rate.

5.3.3 Spatial variability

The spatial variability of marsh edge erosion in literature is often considered in a more qualitative manner. Schwimmer (2001), for example, schematized the cliff erosion patterns of a salt marsh in Rehoboth Bay, Delaware, USA and saw a 'wavy' marsh edge pattern that they call necks and clefts. Over time the cleft widens and a small island is cut off from the neck (Figure 2.7 in Section 2.1). To a greater or lesser extent a similar process is observed in the Wierum marsh. Figure 3.1 shows this pattern. This means that the same erosion patterns that Schwimmer (2001) presented could be at play in the Wierum marsh. However, the Wierum marsh is a semi-natural marsh that was formed under man-made circumstances, which is also visible in Figure 3.1, because the necks are situated almost exactly in line with the ditches in the marsh. This could indicate that these ditches somehow influence the cleft/neck formation. Perhaps there is some flow from the ditches towards the sea that brings sediment onto the mudflat which settles just outside of the marsh, where it forms a bulge. This would heavily influence the processes that Figure Schwimmer (2001) describes.

A model study by Leonardi and Fagherazzi (2015) to the alongshore variations in erosion rate forced by wave power shows that the erosion patterns are influenced by the magnitude of wave power and the presence or absence of extreme events. Figure 2.6 shows that a more uniform erosion occurs in cases with high wave power and a more irregular erosion occurs in cases with low wave power. The presence of frequent extreme events increases the irregularity of the case with high wave power and decreases the irregularity of the case with low wave power (Leonardi & Fagherazzi, 2015). The Wierum salt marsh is subject to a low wave power (order of magnitude of 10 W) without many extreme events (winter storms). Comparing this to the results of Leonardi and Fagherazzi (2015) would mean that there should be a lot of variation in the erosion pattern. This is not necessarily observed, looking at Figure 4.1 and 4.8 b. However, it is hard to compare the results of Leonardi and Fagherazzi (2015) directly to the case of the Wierum marsh because Leonardi and Fagherazzi (2015) used a very abstract and theoretical numerical grid model that measured erosion in terms of number of grid cells instead of meters. Moreover, there are no specific definitions given for high and low wave power, nor for an extreme event.

Erosion rate - Fractal dimension

To the author's knowledge, only two studies have evaluated the salt marsh edge complexity using the fractal dimension (Leonardi, Defne, et al., 2016; Schwimmer, 2008). Leonardi, Defne, et al. (2016) report a negative correlation between fractal dimension and erosion rate in the Barnegat Bay marsh, which means that a more smooth marsh edge erodes faster than a more complex marsh edge shape. Figure 5.5 shows the results of Leonardi, Defne, et al. (2016) and the results of this study.

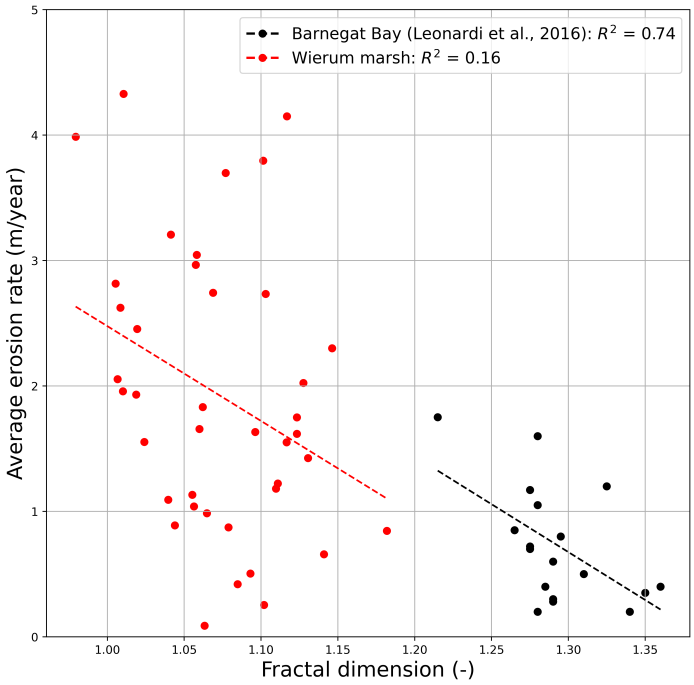

Figure 5.5: Erosion rate (E in m/year) plotted against fractal dimension (FD) for the Wierum marsh (red) and the Barnegat Bay marsh (black) (Leonardi, Defne, et al., 2016).

Both marshes show a negative relation between erosion rate and fractal dimension even though the fractal dimensions of the Barnegat Bay marsh are larger than the Wierum marsh. A difference between the two studies that could explain the different range of fractal dimension is the scale of the study area. The marsh stretch evaluated in Leonardi, Defne, et al. (2016) spans almost 140 km, which is more than 100 times longer than the Wierum marsh (1.2 km). A closer examination of the marsh shape of the Barnegat Bay marsh reveals that indeed the marsh shape is more complex on a larger scale compared to the rectangle-like shapes of the Wierum marsh. This could explain the larger fractal dimension. Another explanation lies in the simplification resulting from the box counting method, as discussed in Section 5.1. The low values of the fractal dimension in the Wierum marsh could also be the result of the method used to digitalize the marsh edge which already simplifies the shape. However, Leonardi, Defne, et al. (2016) use a very similar approach of digitalizing the marsh edge, so it can be assumed that the same simplification error is made.

The fractal dimensions in Rehoboth Bay, Delaware, USA that Schwimmer (2008) determined lie closer to the fractal dimensions of the sections of the Wierum marsh. The average FD of the six sites in Schwimmer (2008)'s study was 1.10. This is comparable to sections C and E of the Wierum marsh (Figure 4.19). Even though Schwimmer (2008) does report a negative relation between fractal dimension and erosion rate, they do not report any specifics about the nature of this relationship.

All three studies report a negative relation, which could mean that both on a small and a large scale a more complex marsh edge erodes slower. However, the amount of data points is very little and there are only two studies done about this relation. This means that there is more research needed to confirm this negative relation.

Chapter 6

Conclusion and Recommendations

6.1 Answers to research questions

How is the spatially averaged salt marsh cliff erosion rate related to the spatially averaged hydrodynamic forcing at the Wierum site?

A positive relationship was found between incoming wave power and average cliff erosion rate at the Wierum salt marsh. This is represented by both a linear fit and a power law fit to the data using dimensionless erosion rate (E^*) and dimensionless wave power (P^*). The linear model has the shape $E^* = 0.74P^*$ with a R^2 of 0.24 and a RMSE of 0.51. This linear model does not perform very well, which is represented in the relatively low value of R^2 and the relatively large RMSE. Still, the results are in line with existing literature (Leonardi, Ganju, & Fagherazzi, 2016; McLoughlin et al., 2015; Mel et al., 2022). The power law fit to the data has the shape $E^* = 1.03P^{*0.30}$ with a R^2 of 0.32 and a RMSE of 0.29. The power of the function lies well below 1.0, which indicates that the Wierum marsh is very resilient against high wave power events. The goodness-of-fit metrics (R^2 and RMSE) indicate that a power law model describes the relationship better than a linear model.

Between incoming wave thrust and average cliff erosion rate also a positive relationship was found. A linear fit and a power law fit were made through the data points of dimensionless erosion rate (E^*) and dimensionless wave thrust (T^*). The linear fit that is found has the shape $E^* = 0.90T^*$ with a R^2 of 0.30 and a RMSE of 0.34. The power law fit has the shape of $E^* = 1.00P^{*0.50}$ with a R^2 of 0.33 and a RMSE of 0.28. Again, the power law model performs the best out of the two models.

A negative relation was found between inundation frequency and erosion rate. Two thresholds were used: a water depth larger than 0.0 m, indicating any water at the cliff and a water depth of 1.0 m, indicating that the cliff is completely inundated. For both thresholds a negative relation was found between inundation frequency and dimensionless erosion rate: $E^* = 1.53 - 0.02f$ (R^2 = 0.20, RMSE = 0.31) for h > 0.0 m, and $E^* = 1.38 - 0.04f$ (R^2 = 0.18, RMSE = 0.31) for h > 1.0 m. While this negative relationship was not expected, it indicates that the wave force at the time of inundation rather than the period of inundation might influence lateral cliff retreat.

How are local alongshore variations in cliff erosion rate at the Wierum site related to spatially averaged hydrodynamic processes and local differences in marsh edge characteristics?

The Wierum marsh was divided into six marsh boundary sections with equal properties based on the presence or absence of a cliff and summer dike. The erosion rate of these sections varied between 1.42 m/year and 2.06 m/year. The three sections that had a cliff at the seaward marsh edge were used to determine a relationship between local dimensionless erosion rate (E^*) and the hydrodynamic forcing variables (dimensionless wave power (P^*) and dimensionless wave thrust (T^*)). Using a linear fitting function, positive relations were found

between both hydrodynamic forcing variables and erosion rate. The slope of the linear fit (α^*) varied between 0.73 and 0.83 for wave power and the slope varied between 0.92 and 1.02 for wave thrust, indicating that there is not a big difference between the three sections with cliff. Sections with influence of a summer dike show a higher erosion rate with increasing wave power than the sections without dike, but the difference is small. Using a power law fit through the data points gave a similar trend.

A negative relation is found between erosion rate and marsh edge complexity (slope = -2.35, R^2 = 0.04, RMSE = 0.56), which indicates that a marsh with a smoother marsh edge erodes faster than a marsh with a more complex marsh edge. This trend is in line with existing literature, even though scales and research methods vary greatly (Leonardi, Defne, et al., 2016; Schwimmer, 2008). The differences in edge complexity of the five sections further show that the presence of a summer dike has a stabilizing effect on the marsh edge shape, as sections with summer dike have a more smooth marsh edge than sections without summer dike.

Using the Normalized Difference Vegetation Index (NDVI) as metric for vegetation presence and density, it must be concluded that there is very little vegetation detected near the marsh edge, as for almost all sections very low NDVI values were found. Still, the expected negative relationship between dimensionless erosion rate (E^*) and NDVI is found with a slope of -1.04 (R^2 = 0.03, RMSE = 0.44).

6.2 General conclusion

The aim of this study was to investigate how hydrodynamic forcing influences salt marsh cliff erosion in a meso-tidal environment at both a marsh-averaged and a local scale, examining temporal variability and alongshore differences in erosion rate and marsh characteristics.

A positive relationship was identified between hydrodynamic forcing and average cliff erosion rate, with both linear and power-law fits providing plausible models. Also on a local scale this relationship was found. Furthermore, it is shown that smoother marsh edges erode faster than complex marsh edges, and vegetation played a minimal role in differences in cliff erosion rate.

6.3 Recommendations

The largest uncertainties in this study resulted from the input data, so to improve reliability of the results and performance of the linear and power model, these uncertainties should be kept as low as possible. The first action that could be undertaken is to gather more data. With only nine years of morphological marsh data, there are very little data points that the relationships are based on. Using aerial images that date further back than 2016 will decrease the spatial resolution, but will add more data points and thus a more reliable result. Hydrodynamic data from the Holwerd station is available starting from 1990 via www.waterinfo.rws.nl and could also be used to increase the number of data points.

The hydrodynamic input data is a major source of uncertainty in this study. Comparison of local measurements to the used data set showed that these are not always in line with each other. The final recommendation is therefore to do some local hydrodynamic measurements regarding the wave climate and water levels, which could also be implemented in the marsh section scale. One measurement station for each marsh section might reveal interesting differences in hydrodynamic forcing along the marsh boundary that could be included in the research. During this field campaign also the vegetation density could be evaluated, which will complement the analysis using the NDVI. Lastly, the soil properties of the Wierum marsh could be examined. This might lead to interesting differences between the six marsh sections and could help to gain new insights related to the comparison with other salt marshes.

There are likely seasonal differences in salt marsh erosion rate, with less erosion in summer and more erosion in winter (Bouma et al., 2016; Willemsen et al., 2018). This is not included in this study, but would be interesting to include. Using only the winter half year there might be stronger correlations with hydrodynamic forcing, because there is probably more erosion. This requires a smaller temporal resolution of marsh morphological data. This is not available via PDOK, but could be retrieved from www.satellietdataportaal.nl.

The Wierum salt marsh is only one of many salt marshes along the Wadden Sea (Beintema et al., 2007). Future research could focus on another salt marsh in the Wadden Sea to see whether comparable results are found. Many marshes in the Dutch Wadden Sea are protected by brushwood dams and it might therefore be hard to make a fair comparison with the Wierum marsh. More similar situations might be found along the coast of Germany and Denmark that are more suitable for comparison to the Wierum marsh.

References

Allen, J. (2000). Morphodynamics of Holocene salt marshes: A review sketch from the Atlantic and Southern North Sea coasts of Europe. *Quaternary Science Reviews*, *19*(12), 1155–1231. https://doi.org/10.1016/S0277-3791(99)00034-7

Beintema, A., Esselink, P., van Duin, W., Bos, D., & de Vries, H. (2007). Van polder naar kwelder.

Belknap, D. F., & Kelley, J. T. (2021, April). Salt Marsh Distribution, Vegetation, and Evolution. In D. FitzGerald & Z. Hughes (Eds.), *Salt Marshes* (1st ed., pp. 9–30). Cambridge University Press. https://doi.org/10.1017/9781316888933.003

Bendoni, M., Francalanci, S., Cappietti, L., & Solari, L. (2014). On salt marshes retreat: Experiments and modeling toppling failures induced by wind waves: Modeling salt marsh retreat. *Journal of Geophysical Research: Earth Surface*, *119*(3), 603–620. https://doi.org/10.1002/2013JF002967

Bendoni, M., Mel, R., Solari, L., Lanzoni, S., Francalanci, S., & Oumeraci, H. (2016). Insights into lateral marsh retreat mechanism through localized field measurements. *Water Resources Research*, *52*(2), 1446–1464. https://doi.org/10.1002/2015WR017966

Bendoni, M., Georgiou, I. Y., & Novak, A. B. (2021, April). Marsh Edge Erosion. In D. FitzGerald & Z. Hughes (Eds.), *Salt Marshes* (1st ed., pp. 388–422). Cambridge University Press. https://doi.org/10.1017/9781316888933.018

Bertassello, L. E., Rao, P. S. C., Jawitz, J. W., Botter, G., Le, P. V. V., Kumar, P., & Aubeneau, A. F. (2018). Wetlandscape Fractal Topography. *Geophysical Research Letters*, *45*(14), 6983–6991. https://doi.org/10.1029/2018GL079094

Bouma, T. J., Van Belzen, J., Balke, T., Van Dalen, J., Klaassen, P., Hartog, A. M., Callaghan, D. P., Hu, Z., Stive, M. J. F., Temmerman, S., & Herman, P. M. J. (2016). Short-term mudflat dynamics drive long-term cyclic salt marsh dynamics: Lateral Salt Marsh Dynamics. *Limnology and Oceanography*, *61*(6), 2261–2275. https://doi.org/10.1002/lno.10374

Callaghan, D., Bouma, T., Klaassen, P., Van Der Wal, D., Stive, M., & Herman, P. (2010). Hydrodynamic forcing on salt-marsh development: Distinguishing the relative importance of waves and tidal flows. *Estuarine, Coastal and Shelf Science*, *89*(1), 73–88. https://doi.org/10.1016/j.ecss.2010.05.013

Daggenvoorde, R., & Vermeulen, C.-J. (2021). *Datarapportage KIMA* (tech. rep. No. PR4443.10). HKV.

D'Alpaos, A., Finotello, A., Goodwin, G. C. H., & Mudd, S. M. (2021, April). Salt Marsh Hydrodynamics. In D. FitzGerald & Z. Hughes (Eds.), *Salt Marshes* (1st ed., pp. 53–81). Cambridge University Press. https://doi.org/10.1017/9781316888933.005

Davranche, A., Lefebvre, G., & Poulin, B. (2010). Wetland monitoring using classification trees and SPOT-5 seasonal time series. *Remote Sensing of Environment*, *114*(3), 552–562. https://doi.org/10.1016/j.rse.2009.10.009

Deltares. (2023). FACTSHEET ZESDE-GENERATIE MODELSCHEMATISATIES SWAN-Kuststrook. Retrieved February 5, 2025, from iplo.nl/thema/water/applicatiesmodellen/%20modelschematisaties/

Donatelli, C., Ganju, N. K., Kalra, T. S., Fagherazzi, S., & Leonardi, N. (2019). Dataset of numerical modelling results of wave thrust on salt marsh boundaries with different seagrass coverages in a shallow back-barrier estuary. *Data in Brief*, *25*, 104197. https://doi.org/10.1016/j.dib.2019.104197

Dzimballa, S., Willemsen, P., Kitsikoudis, V., Borsje, B., & Augustijn, D. (2025). Numerical modelling of biogeomorphological processes in salt marsh development: Do short-term vegetation dynamics

influence long-term development? *Geomorphology*, *471*, 109534. https://doi.org/10.1016/j.geomorph.2024.109534

Elias, E., Van Der Spek, A., Wang, Z., & De Ronde, J. (2012). Morphodynamic development and sediment budget of the Dutch Wadden Sea over the last century. *Netherlands Journal of Geosciences - Geologie en Mijnbouw*, *91*(3), 293–310. https://doi.org/10.1017/S0016774600000457

Elschot, K., Marinka, P., Van Der Wal, J.-T., & Sonneveld, C. (2020). *Lange-termijnontwikkeling van kwelders in de Waddenzee (1960-2018)* (tech. rep.). Wettelijke Onderzoekstaken Natuur & Milieu. Wageningen. https://doi.org/10.18174/521727

Fagherazzi, S., Mariotti, G., Wiberg, P., & McGlathery, K. (2013). Marsh Collapse Does Not Require Sea Level Rise. *Oceanography*, *26*(3), 70–77. https://doi.org/10.5670/oceanog.2013.47

Feagin, R. A., Lozada-Bernard, S. M., Ravens, T. M., Möller, I., Yeager, K. M., & Baird, A. H. (2009). Does vegetation prevent wave erosion of salt marsh edges? *Proceedings of the National Academy of Sciences*, *106*(25), 10109–10113. https://doi.org/10.1073/pnas.0901297106

Finotello, A., Marani, M., Carniello, L., Pivato, M., Roner, M., Tommasini, L., & D'alpaos, A. (2020). Control of wind-wave power on morphological shape of salt marsh margins. *Water Science and Engineering*, *13*(1), 45–56. https://doi.org/10.1016/j.wse.2020.03.006

FitzGerald, D. M., & Hughes, Z. J. (2021, April). State of Salt Marshes. In D. FitzGerald & Z. Hughes (Eds.), *Salt Marshes* (1st ed., pp. 1–6). Cambridge University Press. https://doi.org/10.1017/9781316888933.001

Francalanci, S., Bendoni, M., Rinaldi, M., & Solari, L. (2013). Ecomorphodynamic evolution of salt marshes: Experimental observations of bank retreat processes. *Geomorphology*, *195*, 53–65. https://doi.org/10.1016/j.geomorph.2013.04.026

Hladik, C., Schalles, J., & Alber, M. (2013). Salt marsh elevation and habitat mapping using hyperspectral and LIDAR data. *Remote Sensing of Environment*, *139*, 318–330. https://doi.org/10.1016/j.rse.2013.08.003

Houttuijn Bloemendaal, L. J., FitzGerald, D. M., Hughes, Z. J., Novak, A. B., & Georgiou, I. Y. (2023). Reevaluating the wave power-salt marsh retreat relationship. *Scientific Reports*, *13*(1), 2884. https://doi.org/10.1038/s41598-023-30042-y

Karimpour, A., Chen, Q., & Twilley, R. R. (2016). A Field Study of How Wind Waves and Currents May Contribute to the Deterioration of Saltmarsh Fringe. *Estuaries and Coasts*, *39*(4), 935–950. https://doi.org/10.1007/s12237-015-0047-z

KNMI. (2023, December). Terugblik hoge waterstanden en storm Pia; december 2023. Retrieved January 10, 2025, from https://www.rijkswaterstaat.nl/nieuws/archief/2023/12/storm-pia

Koppel, J. v. d., Wal, D. v. d., Bakker, J. P., & Herman, P. M. J. (2005). Self-Organization and Vegetation Collapse in Salt Marsh Ecosystems. *The American Naturalist*, *165*(1), E1–E12. https://doi.org/10.1086/426602

Leonardi, N., Defne, Z., Ganju, N. K., & Fagherazzi, S. (2016). Salt marsh erosion rates and boundary features in a shallow Bay: Indicators Salt Marsh Erosion New Jersey. *Journal of Geophysical Research: Earth Surface*, *121*(10), 1861–1875. https://doi.org/10.1002/2016JF003975

Leonardi, N., & Fagherazzi, S. (2015). Effect of local variability in erosional resistance on large-scale morphodynamic response of salt marshes to wind waves and extreme events. *Geophysical Research Letters*, *42*(14), 5872–5879. https://doi.org/10.1002/2015GL064730

Leonardi, N., Ganju, N. K., & Fagherazzi, S. (2016). A linear relationship between wave power and erosion determines salt-marsh resilience to violent storms and hurricanes. *Proceedings of the National Academy of Sciences*, *113*(1), 64–68. https://doi.org/10.1073/pnas.1510095112

Marani, M., D'Alpaos, A., Lanzoni, S., & Santalucia, M. (2011). Understanding and predicting wave erosion of marsh edges: MARSH EDGE EROSION. *Geophysical Research Letters*, *38*(21), n/a–n/a. https://doi.org/10.1029/2011GL048995

Martinez, M., Ardón, M., & Gray, J. (2024). Detecting Trajectories of Regime Shifts and Loss of Resilience in Coastal Wetlands using Remote Sensing. *Ecosystems*, *27*(8), 1060–1075. https://doi.org/10.1007/s10021-024-00938-5

McLoughlin, S. M., Wiberg, P. L., Safak, I., & McGlathery, K. J. (2015). Rates and Forcing of Marsh Edge Erosion in a Shallow Coastal Bay. *Estuaries and Coasts*, *38*(2), 620–638. https://doi.org/10.1007/s12237-014-9841-2

Mel, R. A., Bendoni, M., & Steffinlongo, D. (2022). Salt-marsh retreat on different time scales: Issues and prospects from a 5-year monitoring campaign in the Venice Lagoon. *Earth Surface Processes and Landforms*, *47*(8), 1989–2005. https://doi.org/10.1002/esp.5359

Peitgen, H.-O., Jürgens, H., & Saupe, D. (Eds.). (2004). *Chaos and Fractals: New Frontiers of Science* (Second Edition). Springer Science + Business Media, Inc. https://doi.org/10.1007/b97624

Piera, J., Parisi-Baradad, V., García-Ladona, E., Lombarte, A., Recasens, L., & Cabestany, J. (2005). Otolith shape feature extraction oriented to automatic classification with open distributed data. *Marine and Freshwater Research*, *56*(5), 805. https://doi.org/10.1071/MF04163

Quaresma, V. D. S., Bastos, A. C., & Amos, C. L. (2007). Sedimentary processes over an intertidal flat: A field investigation at Hythe flats, Southampton Water (UK). *Marine Geology*, *241*(1-4), 117–136. https://doi.org/10.1016/j.margeo.2007.03.009

Rijksdienst voor het Cultureel Erfgoed. (2023). Actueel Hoogtebestand Nederland.

Sanford, L. P., & Gao, J. (2018). Influences of Wave Climate and Sea Level on Shoreline Erosion Rates in the Maryland Chesapeake Bay. *Estuaries and Coasts*, *41*(S1), 19–37. https://doi.org/10.1007/s12237-017-0257-7

Schoonees, T., Gijón Mancheño, A., Scheres, B., Bouma, T. J., Silva, R., Schlurmann, T., & Schüttrumpf, H. (2019). Hard Structures for Coastal Protection, Towards Greener Designs. *Estuaries and Coasts*, *42*(7), 1709–1729. https://doi.org/10.1007/s12237-019-00551-z

Schwimmer, R. A. (2001). Rates and Processes of Marsh Shoreline Erosion in Rehoboth Bay, Delaware, U.S.A. *Journal of Coastal Research*, *17*(3), 672–683. https://doi.org/10.2307/4300218

Schwimmer, R. A. (2008). A Temporal Geometric Analysis of Eroding Marsh Shorelines: Can Fractal Dimensions be Related to Process? *Journal of Coastal Research*, *241*, 152–158. https://doi.org/10.2112/06-0644.1

Siemes, R. W. A., Borsje, B. W., Daggenvoorde, R. J., & Hulscher, S. J. M. H. (2020). Artificial Structures Steer Morphological Development of Salt Marshes: A Model Study. *Journal of Marine Science and Engineering*, *8*(5), 326. https://doi.org/10.3390/jmse8050326

Simon, R. M., & Simon, R. H. (1995). Mid-Atlantic Salt-Marsh Shorelines: Mathematical Commonalities. *Estuaries*, *18*(1), 199. https://doi.org/10.2307/1352630

Sun, C., Fagherazzi, S., & Liu, Y. (2018). Classification mapping of salt marsh vegetation by flexible monthly NDVI time-series using Landsat imagery. *Estuarine, Coastal and Shelf Science*, *213*, 61–80. https://doi.org/10.1016/j.ecss.2018.08.007

Thompson, E. F., & Vincent, C. L. (n.d.). Significant Wave Height for Shallow Water Design.

Timmerman, A., Haasnoot, M., Middelkoop, H., Bouma, T., & McEvoy, S. (2021). Ecological consequences of sea level rise and flood protection strategies in shallow coastal systems: A quick-scan barcoding approach. *Ocean & Coastal Management*, *210*, 105674. https://doi.org/10.1016/j.ocecoaman.2021.105674

Tonelli, M., Fagherazzi, S., & Petti, M. (2010). Modeling wave impact on salt marsh boundaries. *Journal of Geophysical Research: Oceans*, *115*(C9), 2009JC006026. https://doi.org/10.1029/2009JC006026

Viana, C. M., Oliveira, S., Oliveira, S. C., & Rocha, J. (2019). Land Use/Land Cover Change Detection and Urban Sprawl Analysis. In *Spatial Modeling in GIS and R for Earth and Environmental Sciences* (pp. 621–651). Elsevier. https://doi.org/10.1016/B978-0-12-815226-3.00029-6

Vrieling, A., Meroni, M., Darvishzadeh, R., Skidmore, A. K., Wang, T., Zurita-Milla, R., Oosterbeek, K., O'Connor, B., & Paganini, M. (2018). Vegetation phenology from Sentinel-2 and field cameras for a Dutch barrier island. *Remote Sensing of Environment*, *215*, 517–529. https://doi.org/10.1016/j.rse.2018.03.014

Vuik, V., Jonkman, S. N., Borsje, B. W., & Suzuki, T. (2016). Nature-based flood protection: The efficiency of vegetated foreshores for reducing wave loads on coastal dikes. *Coastal Engineering*, *116*, 42–56. https://doi.org/10.1016/j.coastaleng.2016.06.001

Wang, K., Wu, G., Liang, B., Shi, B., & Li, H. (2024). Linking marsh sustainability to event-based sedimentary processes: Impulsive river floods initiated lateral erosion of deltaic marshes. *Coastal Engineering*, *190*, 104515. https://doi.org/10.1016/j.coastaleng.2024.104515

Whitfield, A., & Elliott, M. (2011). Ecosystem and Biotic Classifications of Estuaries and Coasts. In *Treatise on Estuarine and Coastal Science* (pp. 99–124). Elsevier. https://doi.org/10.1016/B978-0-12-374711-2.00108-X

Willemsen, P. W. J. M., Borsje, B. W., Hulscher, S. J. M. H., Van Der Wal, D., Zhu, Z., Oteman, B., Evans, B., Möller, I., & Bouma, T. J. (2018). Quantifying Bed Level Change at the Transition of Tidal Flat and Salt Marsh: Can We Understand the Lateral Location of the Marsh Edge? *Journal of Geophysical Research: Earth Surface*, *123*(10), 2509–2524. https://doi.org/10.1029/2018JF004742

Wilson, C. A., Perillo, G. M. E., & Hughes, Z. J. (2021, April). Salt Marsh Ecogeomorphic Processes and Dynamics. In D. FitzGerald & Z. Hughes (Eds.), *Salt Marshes* (1st ed., pp. 178–224). Cambridge University Press. https://doi.org/10.1017/9781316888933.010

WinklerPrins, L., Lacy, J. R., Stacey, M. T., Logan, J. B., & Stevens, A. W. (2024). Seasonality of Retreat Rate of a Wave-Exposed Marsh Edge. *Journal of Geophysical Research: Earth Surface*, *129*(7), e2023JF007468. https://doi.org/10.1029/2023JF007468

Zhu, S., Wei, W., Zhu, Q., Wan, K., Xing, F., Yan, W., Gao, J., & Wang, Y. P. (2024). Wave attenuation and transformation across a highly turbid muddy tidal flat-salt marsh system. *Applied Ocean Research*, *147*, 103980. https://doi.org/10.1016/j.apor.2024.103980

Appendix A

Input Data

Two types of time-series data are needed to link the cliff retreat to wave power on the marsh scale: morphological marsh data and hydrodynamic forcing data. The data is collected from different sources and has a variable quality and quantity. Figure A.1 presents a timeline containing details, sources and dates of the data that is used in the analyses.

A.1 Data availability

Marsh morphology
The marsh morphology is determined using aerial images from three different sources: aerial photographs retrieved from Publieke Dienstverlening Op de Kaart (PDOK), digital elevation models (DEMs) from Actueel Hoogtebestand Nederland (AHN), and drone-generated DEMs that were made by flying a drone above the salt marsh.

PDOK photographs taken from 2016 until 2024 are used and obtained via the QGIS PDOK plugin. Aerial imagery dated before 2016 is scarcely available and has resolutions of 1.0 meters and lower (https://viewer.satellietdataportaal.nl). This means that the difference in the location of the salt marsh boundary between two years would not be well visible and it is therefore decided to start the analysis from 2016 onward. The exact dates that the images were taken are retrieved from the data room of the Dutch governmental organisation that manages aerial images of the Netherlands (www.beeldmateriaal.nl/data-room). AHN data, like PDOK, is freely available and contains detailed measurements of elevations in the Netherlands as raster data. The AHN data is downloaded from Esri Nederland (www.arcgis.com). However, these measurements are not done very frequently. For this analysis, AHN4 and AHN5 were suitable, as they were generated in 2020 and 2023, respectively (Figure A.1). The drone data was made on 24/11/2022, 05/09/2023 and 25/01/2024 (Figure A.1).

To do the analysis on vegetation at the marsh edge infrared and red-colored images were needed. These were available through sattelietdataportaal.nl for the years 2019 until 2023 ((Figure A.1).

Hydrodynamics
The second type of data needed is about the hydrodynamic forcing on the marsh edge (Figure A.1). Keeping in mind the equations for wave power and wave thrust (Equations 3.1 and 3.3) the needed variables are water depth (h in m) and significant wave height (H_s in m). For the significant wave height the spectral significant wave height (H_{m0}) is used, which is defined as four times the standard deviation of the sea surface elevation and is commonly used to describe the significant wave height (Thompson & Vincent, n.d.; WinklerPrins et al., 2024). The data is collected using the waterinfo website of Rijkswaterstaat (https://waterinfo.rws.nl/nav/publiek) and

using the online application MATROOS from Rijkswaterstaat (https://noos.matroos.rws.nl).

The waterinfo data set (RWS) contains all kinds of observed data originating from a point near the Wierum marsh (coordinates: 6.06 E, 53.41 N), including water level in m+NAP and wave height in m. The wave height time series goes from 01/07/2016 until 01/09/2019 and the water level data goes from 01/07/2016 until June 2017, both with a measurement interval of 10 minutes.

Almost directly connecting to the RWS data are the MATROOS data sets. MATROOS provides both predictive and historical observed data on sea hydrodynamic conditions in the North Sea and Wadden Sea. Two data sets are used: observed data from 04/09/2019 until 22/03/2020 and SWAN model-generated data from 06/10/2020 until 31/01/2024. The observed data set contains data about wave height (H_{m0}) in cm and water depth (h) in cm in a 10 minute interval, while for the model-generated data this is hourly. Moreover, the SWAN model includes wave direction. This is included as an extra factor in the wave power and wave thrust equations, as a wave that approaches the marsh perpendicular to the marsh edge has more impact than an oblique wave. Both the observed and SWAN data are measured/generated at the same location as the RWS data. For this thesis data until 31/12/2023 is used, which is deemed sufficient to match the marsh width data. Additional data that is used is locally measured water depth and wave height (both in m) at a location on the mudflat in front of the Wierum marsh using a wave logger. This was done from October to December 2023 (Figure A.1).

There are some gaps in the water level / water depth data that is available. As Figure A.1 shows, this gap is filled by using additional data from a station near Wierum: the Holwerd harbour, which is approximately 10 km away from Wierum in Westward direction. This data set contains the same type of data: water level in m+NAP and wave height in m with a 10 minutes time interval.

Finally, the direction that a wave has has an impact on the wave power exerted on the marsh edge. A wave perpendicular to the marsh has the most power and more oblique waves have less power, because they have experienced more energy dissipation. This is included in the wave power equation as a cosine factor. Matroos has data available on wave directions starting from 06/10/2020. For the dates before that, wind direction data of the KNMI is used, containing daily values. In both data sets, the wave/wind direction is presented in degrees with respect to the North (North is 360°).

A.2 Data quality

The quality of the marsh width data can be deduced from Figure A.1. There is a PDOK image taken every year, but there is some inconsistency in the date. The pictures of the years 2016 until and including 2020 were taken approximately one year after each other. After that, however, there are larger and smaller gaps between the images. Moreover, for some images no date was given or the date was highly unrealistic (set in another year, for example), so in that case an educated guess is made, which is presented in Figure A.1 as the date in italics. This educated guess was based on the knowledge that the images should be taken in winter. The quality of the 2024 aerial image could be a little less high, since this data was still under revision when the analysis was conducted. This could lead to inconsistencies at the edges of two separate images. The Wierum site does span over three different images, but in a close inspection of the image no inconsistencies were found. The spatial resolution of the images is deemed sufficient for the intended purpose. The images taken in 2016 until and including 2020 have a horizontal resolution of 25 cm and the newer images 8 cm. The marsh edge retreat rate is estimated to be in the order of magnitude of one to a couple meters per year, which should be visible with the given resolutions.

The other two data sets that are used are AHN data and drone DEMs. The AHN is redone every couple years, depending on the frequency of flights that are done. For the time span between 2016 and 2024 and for the area of Wierum AHN3 and AHN4 were suitable, as they were made in the years 2020 and 2023, respectively.

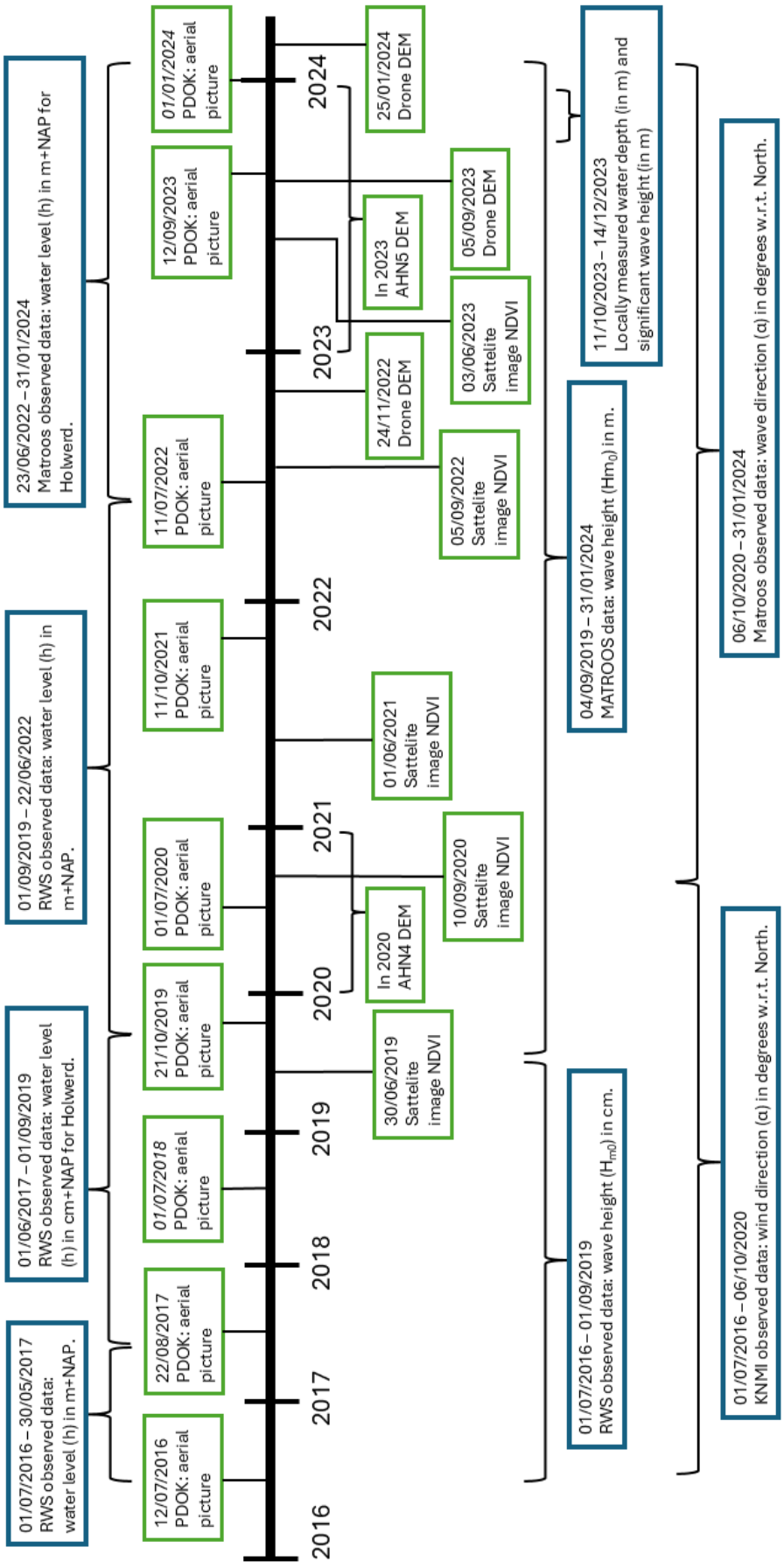

Figure A.1: Details, origin and dates of the marsh width data (green) and hydrodynamic forcing data (blue) needed for the analyses in this section. Dates in italics mean an estimated date.

The exact date that the data was measured is unknown, so the data point is placed in the middle of the year (July 1st). The resolution of the AHN data is lower than the aerial images: 50 cm in horizontal direction and 5 cm in vertical direction. The other data set contains DEMs that were made by flying a drone over the marsh. This was done three times on 24-11-2022, 05-09-2023, and 25-01-2024. The drone very accurately measures the elevation of the surface, with an accuracy of 0.5 cm horizontally and 1.0 cm vertically.

The quality of the raw hydrodynamic data is described by looking at the percentage of missing data and some general statistics such as: the average value, the standard deviation, the minimum and maximum value. This is split per variable (h, H_s, and α) and per data set. The results are presented in Table A.1, A.2 and A.3.

Table A.1: General statistics of the different hydrodynamic forcing raw data sets for water level/ water depth (h)

Location	**Wierum**	**Holwerd**	**Wierum**	**Holwerd**
Begin date	01-07-2016	01-06-2017	01-09-2019	23-06-2022
End date	30-05-2017	31-08-2019	21-06-2022	31-12-2023
Time interval	Every 10 minutes	Every 10 minutes	Every 10 minutes	Every 10 minutes
Average value	40.9 (cm depth)	3.2 (cm+NAP)	44.9 (cm depth)	0.22 (m+NAP)
Standard dev.	42.4 (cm depth)	40.7 (cm+NAP)	45.4 (cm depth)	0.80 (m+NAP)
Minimum value	-1 (cm depth)	-281 (cm+NAP)	0 (cm depth)	-2.5 (m+NAP)
Maximum value	317 (cm depth)	281 (cm+NAP)	307 (cm depth)	3.5 (m+NAP)
% missing	0.0	0.0	2.5	10.3

Table A.2: General statistics of the different hydrodynamic forcing raw data sets for significant wave height (H_s), where SB indicates stappenbaak, R indicates radar and MATROOS indicates SWAN model-generated data.

Source	**RWS Wierum (SB)**	**RWS Wierum (R)**	**Matroos Wierum**
Begin date	01-07-2016	01-07-2016	02-09-2019
End date	09-09-2018	09-09-2018	31-12-2023
Time interval	Every 10 minutes	Every 10 minutes	Every 10 minutes
Average value	7.9 (cm)	6.6 (cm)	0.074 (m)
Standard dev.	7.8 (cm)	7.8 (cm)	0.084 (m)
Minimum value	0 (cm)	0 (cm)	0 (m)
Maximum value	149 (cm)	572 (cm)	8.94 (m)
% missing	21.4	6.0	25.3

Table A.3: General statistics of the different hydrodynamic forcing raw data sets for the wave direction factor ($cos(\alpha)$)

Source	**KNMI wind direction**	**Matroos wave direction**
Begin date	01-07-2016	06-10-2020
End date	05-10-2020	31-12-2023
Time interval	15 per day	1 day
Average value	0.61	0.70
Standard dev.	0.31	0.22
Minimum value	0	0.079
Maximum value	1.0	1.0
% missing	0.0	0.0

There is some inconsistency in the units of water depth and significant wave height. The desired unit is m, both for water depth and for wave height. In the next subsections this is converted. Moreover, there are some outliers that can be spotted. Firstly, the minimum water depth in the Wierum 1 seems to be -1 cm. This is impossible, as a negative depth can never happen. The second value that stands out is the maximum wave height in the RWS Wierum (R) data set and Matroos Wierum data set, which are 5.72 m and 8.94 m, respectively. These values are probably mistakes in the data and this means that there should be checked for more outliers that need to be removed before doing the analysis.

A.3 Data preprocessing

No actual preprocessing was needed for the marsh image data. It was, however, checked whether all images were ready to use and were in the same coordinate system, which was the case.

The goal of the preprocessing step is to generate timeseries of all variables that start on July first 2016 and end on December 31st 2023. The desired time step is one day and the desired units are m for both water depth and wave height and degrees with respect to North for wave direction. Furthermore, there is looked for any unrealistic outliers that need to be removed, as mentioned before. A summary of the preprocessed data is presented in Table A.4.

To transform the water level data from Holwerd into water depth data, the level of the sea bed in front of the marsh in m+NAP is subtracted from the water level. This bed level is determined at the location of the buoy at Wierum (bed level = 0.2 m+NAP) to ensure a consistency in water depth data between the two locations. Then, any negative values are set to 0, since a negative water depth is not possible. Finally, the water depth data is converted to meter depth, a hourly average is determined and then the different parts are combined into one time series.

The wave height data obtained from Rijkswaterstaat (RWS) was measured using two different methods: stappenbaak and radar (respectively SB and R in Table A.2). A stappenbaak is a pole in the water that measures the water level by means of electrical signals generated by metal pins in the pole (Daggenvoorde & Vermeulen, 2021). To generate the final data set, the measurements from the stappenbaak were first considered, as this is a direct measurement at the exact location. If, however, for a certain data point there was no value for the stappenbaak, but there was a radar value available, that value was used. Like the water depth, the data is converted to meter height, a daily average is computed and then the two parts are combined into one time series.

The wave direction needs to be included in the wave power equation (Equation 3.1) as a factor using the cosine of the angle of incident waves. The wind and wave direction data was given as a direction in degrees with respect to North. The marsh edge is on average 5 degrees slanted with respect to North. To transform the wave direction accordingly, all values are increased by 5 degrees. Then, the factor is determined. This is also what is presented in Table A.3. Again, a daily average is computed and then the two parts are combined into one time series.

Figure A.2: Determination of the angle between North and the marsh edge on average. As background the aerial picture of 2024 is used.

The final three data sets are time series starting on 01/07/2016 and ending on 31/12/2023, containing hourly averages of water depth in m, and daily averages of wave height in m and the dimensionless wave direction factor.

Table A.4: General statistics of the different hydrodynamic forcing variables after preprocessing

Variable	**Water depth (h) in m**	**Wave height (H_s) in m**	**Wave direction factor ($cos(\alpha)$)**
Average value	0.39	0.068	0.64
Standard dev.	0.17	0.049	0.28
Minimum value	0	0.0032	0
Maximum value	1.5	0.5	1
% missing	1.1	2.4	0.0

Appendix B

Marsh averaged scale

B.1 Distributions annual retreat

The distribution of the annual retreat is visualized in a histogram for each year. Again, there are 11 bins into which the 119 data points are sorted.

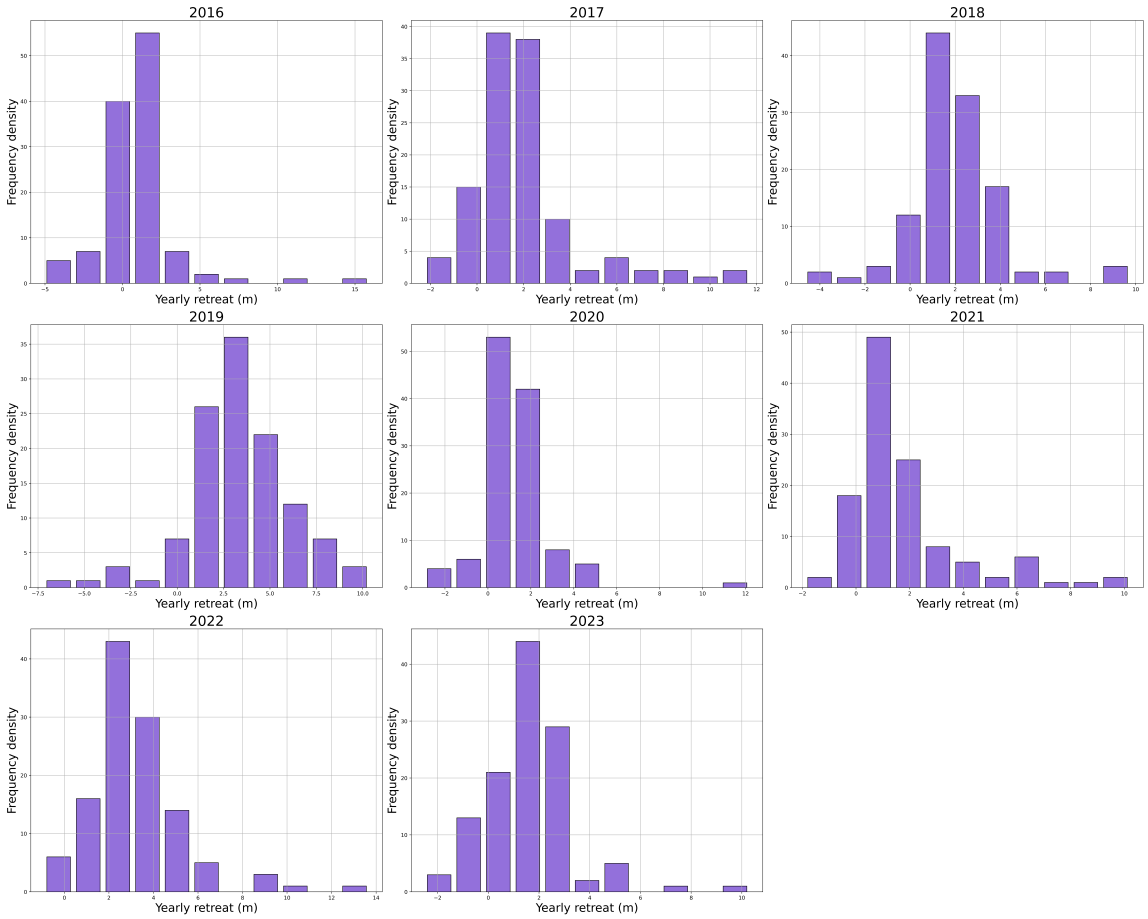

Figure B.1: Frequency density of yearly retreat for the data points

B.2 Distributions marsh width

The distributions of the marsh width are shows in histograms per year. The data of the transects is sorted into 11 bins for which the frequency is determined.

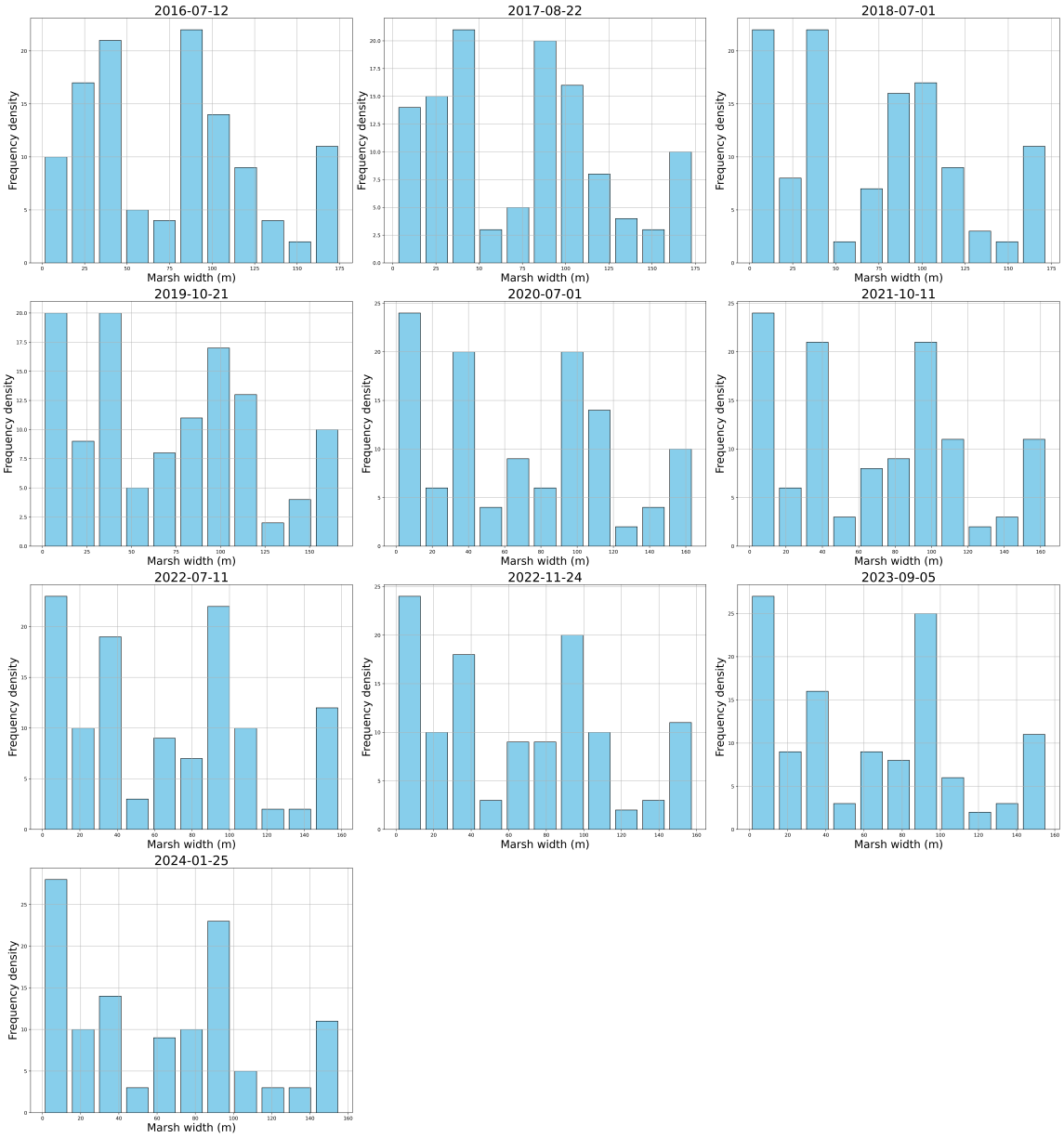

Figure B.2: Frequency density of marsh width for the data points

B.3 Cliff height

Cross-sections of the elevation of the marsh and mudflat are plotted along selected transects.

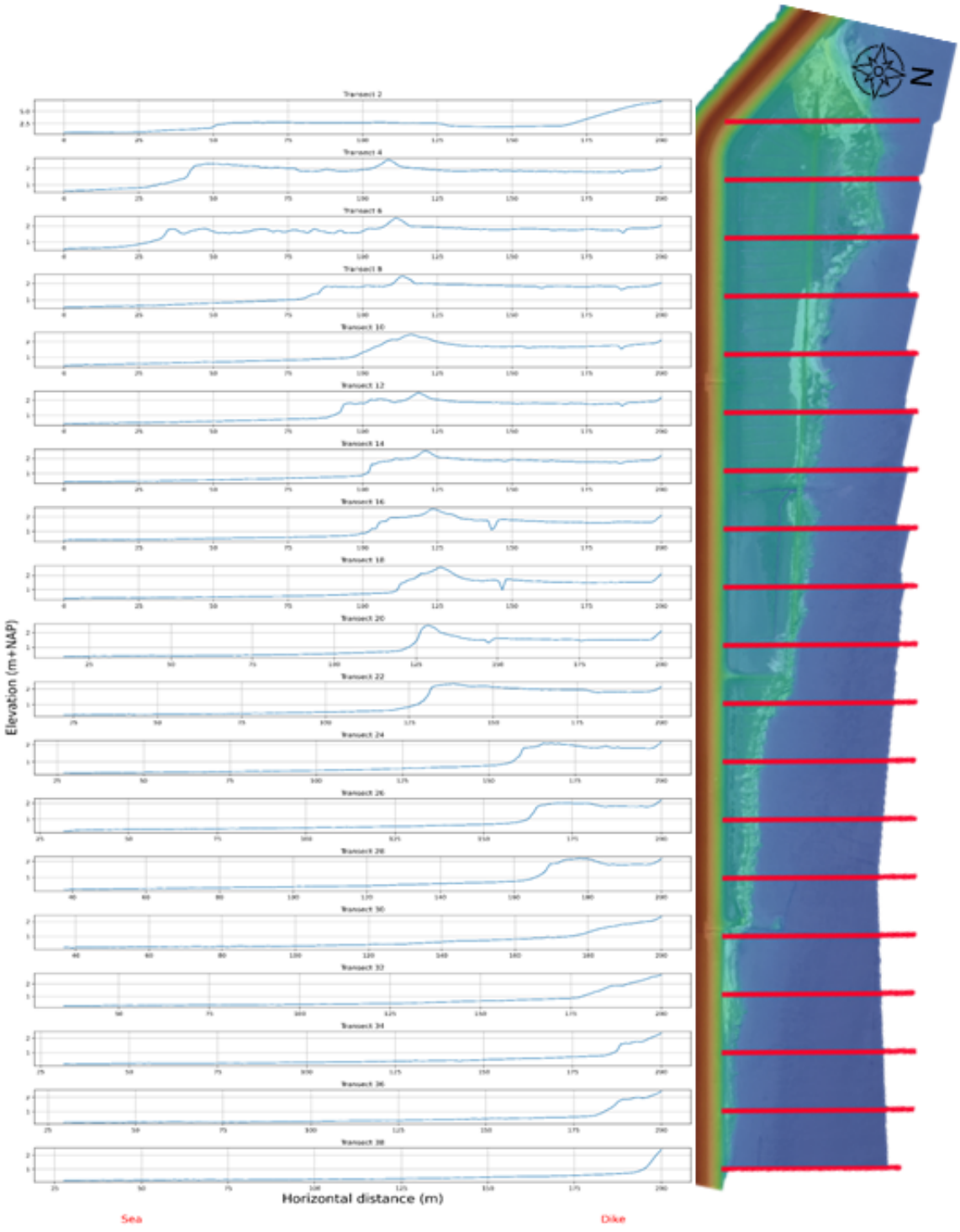

Figure B.3: Cross-sections of the marsh along selected transects (red) using AHN4 data. The marsh image is not to scale.

B.4 E^*-P^* and E^*-T^* relation without forcing the fit through the origin

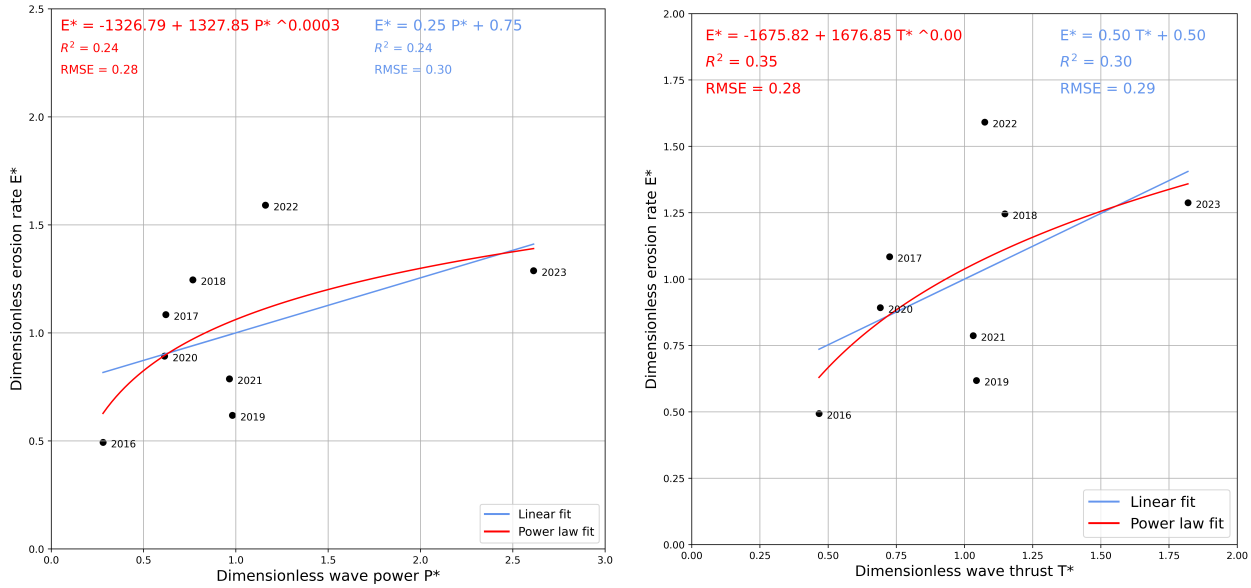

Figure B.4: Relation between dimensionless erosion rate (E*) and dimensionless wave power (P*) (left) and dimensionless wave thrust (T*) (right) including a linear fit (blue) and power law fit (red) without forcing the fits to go through the origin (0,0)

Appendix C

Marsh section scale

C.1 Fractal Dimension

For the whole marsh shape of each year the fractal dimension (FD) is determined.

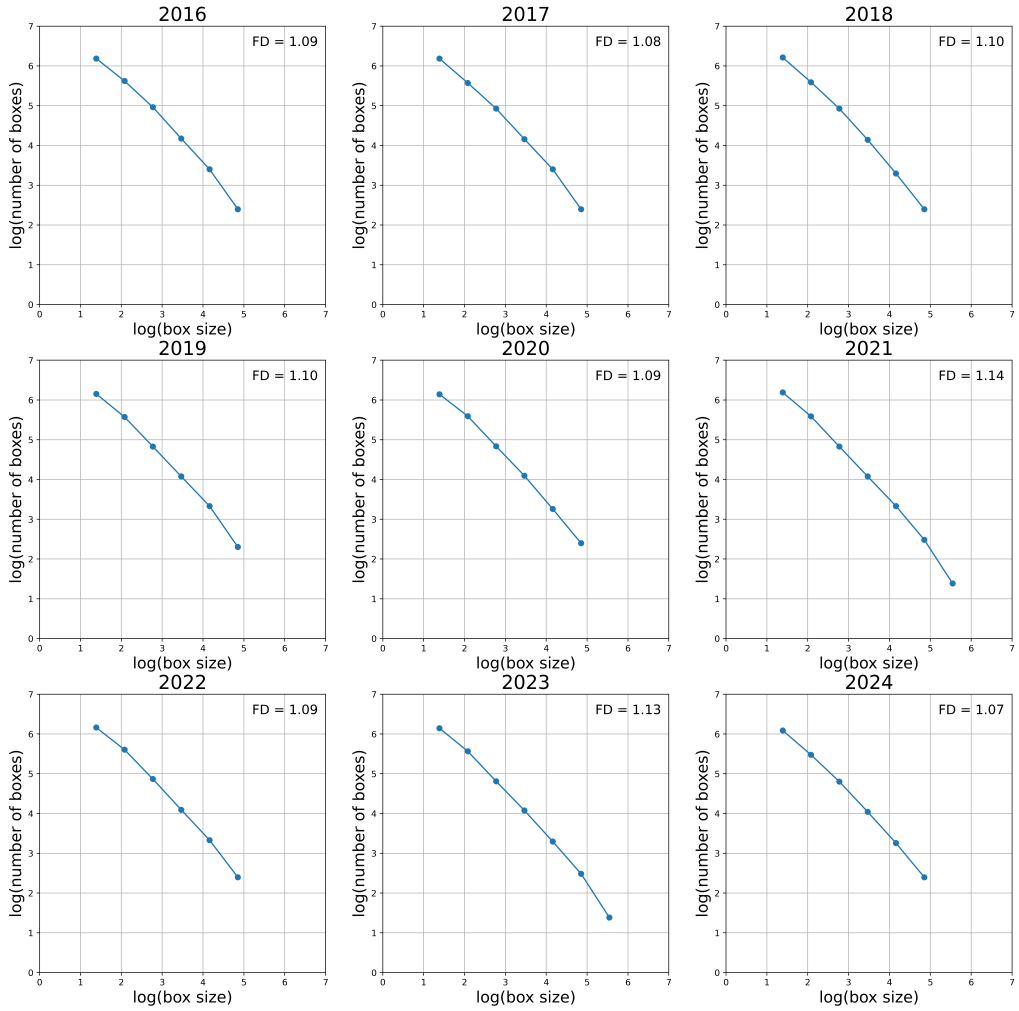

Figure C.1: Determination of the fractal dimension (FD) of the marsh area shape of the different years. FD is the slope of the graph.

Also the fractal dimension (FD) of the different marsh sections is determined.

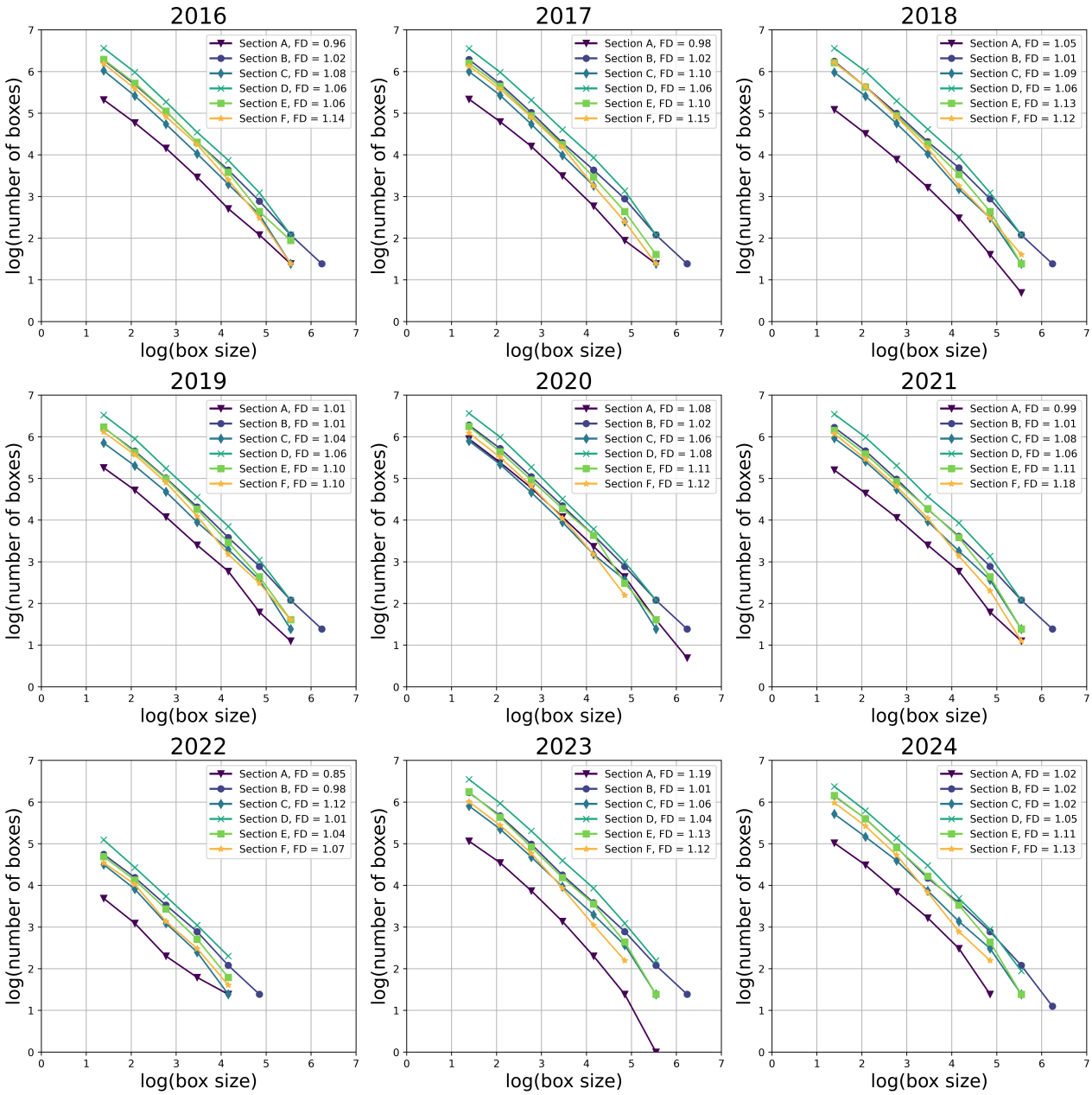

Figure C.2: Determination of the fractal dimension (FD) of the different marsh sections. FD is the slope of the graph.

C.2 Including sections without cliff

Marsh section A was behaving strangely regarding erosion rate because the exact marsh edge could not be determined consistently for every aerial image. Therefore, this section was left out of the analyses that were done in the marsh section scale. Also sections C and F were left out of the analyses, because there was no cliff at the marsh edge. Here, these sections are included to determine how this would have influenced the results. This is done for the relations of dimensionless erosion rate (E^*) with respect to dimensionless wave power (P^*) and dimensionless wave thrust (T^*). For the relation between erosion rate (E in m/year) and marsh shape complexity (fractal dimension, FD) and vegetation density (NDVI) only section A was excluded in the main study and is therefore the only section that is included extra here.

C.2.1 E^* - P^* and E^* - T^* relation

The $E^* - P^*$ and $E^* - T^*$ relation is determined for section A, C and F the same way as the other sections: using a linear fit and a power law fit. Figure C.3 shows the results for the dimensionless wave power for the sections with cliff (Figure C.3 a and b) and the sections without cliff (Figure C.3 c and d). Figure C.4 shows the results for dimensionless wave thrust for the sections with cliff (Figure C.4 a and b) and the sections without cliff (Figure C.4 c and d).

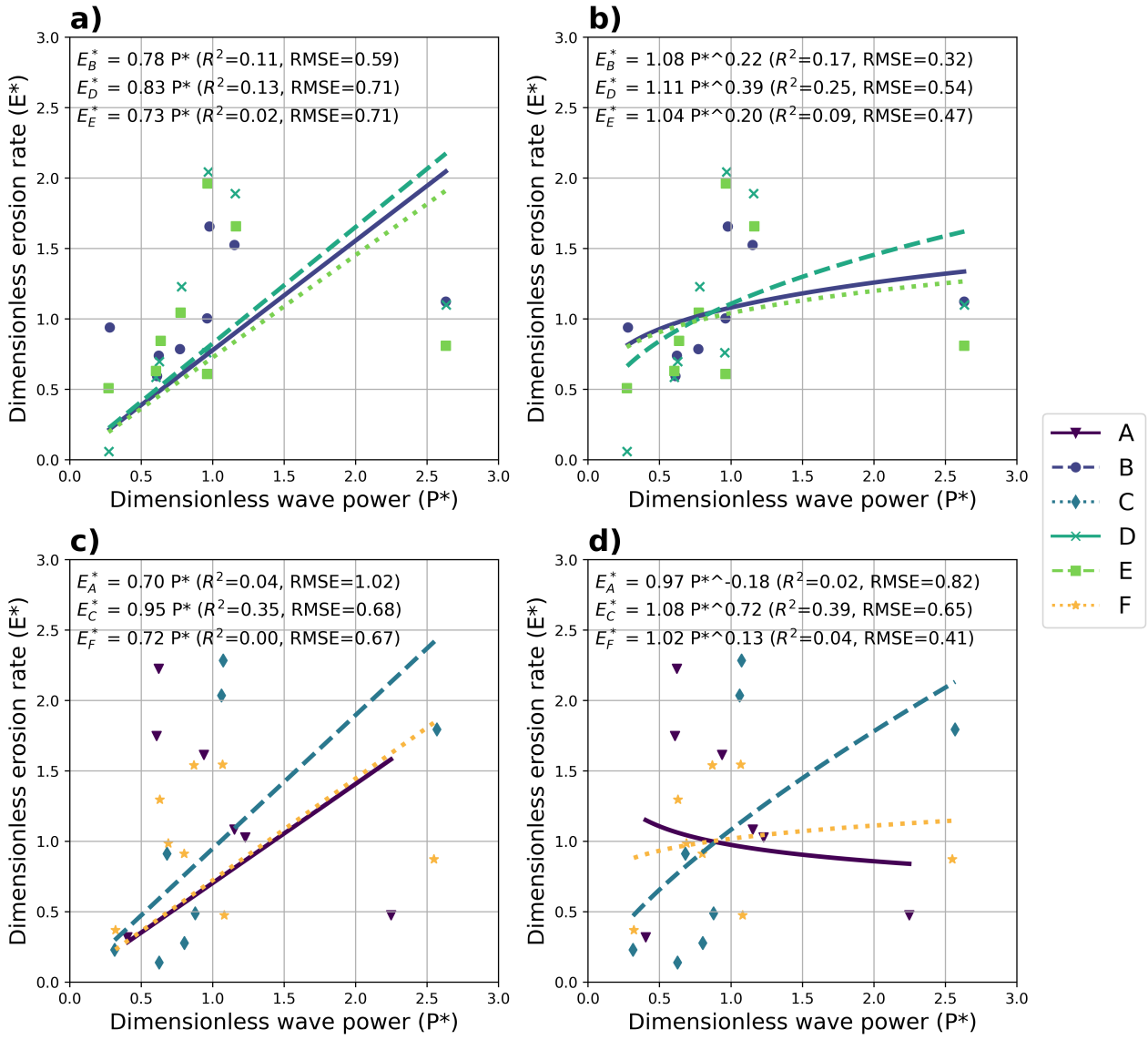

Figure C.3: Dimensionless erosion rate (E^*) plotted against dimensionless wave power (P^*) including a linear fit (a, c) and a power fit (b, d). a, b) marsh sections sections with cliff (sections B, D and E); c, d) marsh sections without cliff (sections A, D and F).

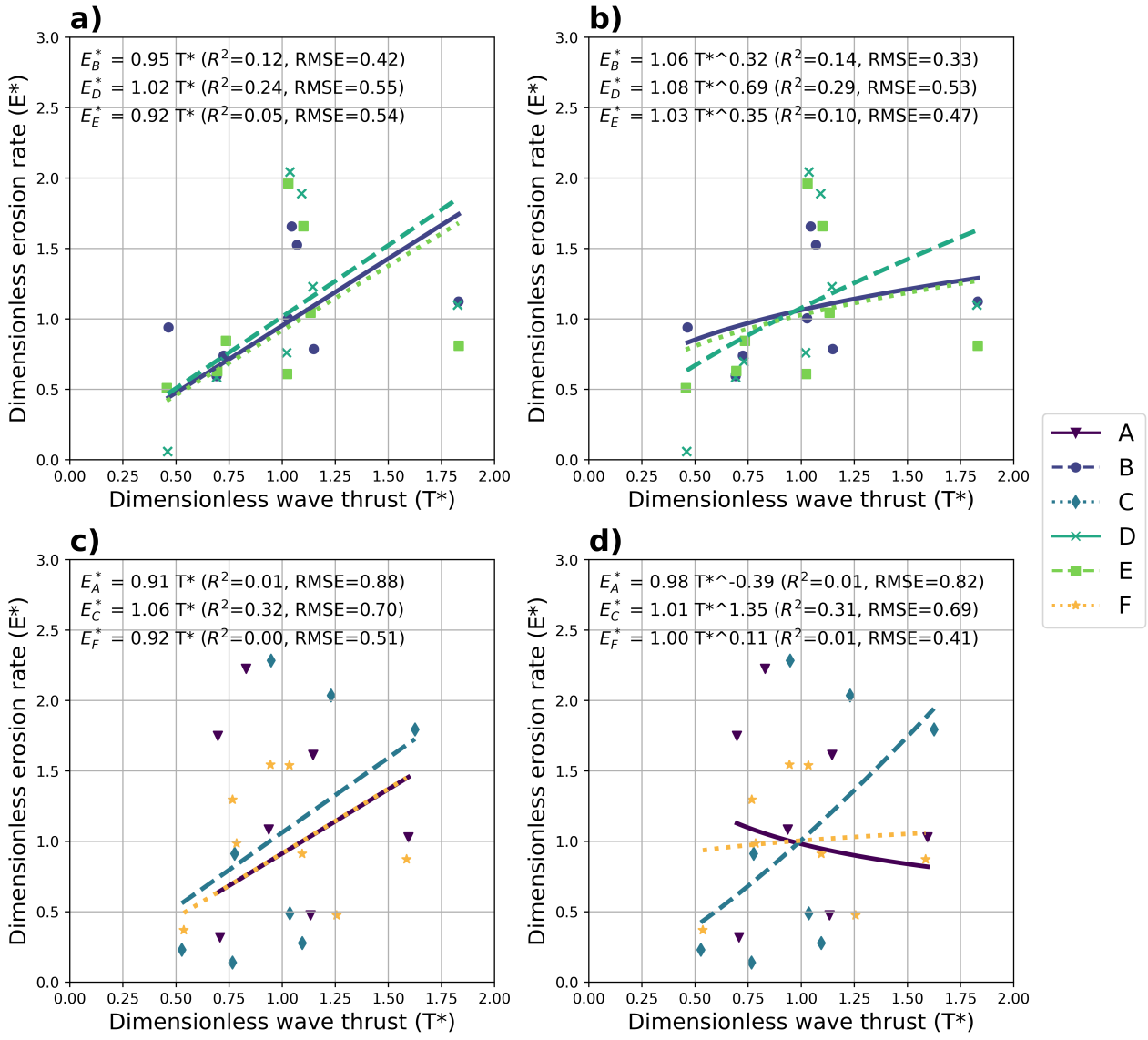

Figure C.4: Dimensionless erosion rate (E^*) plotted against dimensionless wave trust (T^*) including a linear fit (a, c) and a power fit (b, d). a, b) marsh sections sections with cliff (sections B, D and E); c, d) marsh sections without cliff (sections A, D and F).

The data points of sections A and C in Figure C.3 and C.4 c and d are more widely scattered than sections B, D and E in Figure C.3 and C.4 a and b. Section F, on the other hand, looks much alike the sections with dike. This is reflected in the linear and power law fits: section F presents similar values for α^*, k and n to the sections with cliff. Sections A and C are quite different, especially in the power law fit. Section A shows a negative relation and section C a very steep slope. Regarding the goodness-of-fit metrics, it seems that the fits of sections A and F are very poor, while section C performs quite well with a high R-squared value, but also a large RMSE. Concluding, including sections A, C and F in the results confirms the reason it was excluded in the first place: these sections behave very differently and irregularly compared to the sections with cliff.

C.2.2 E - FD relation

Table C.1 shows the average FD for all six sections and Figure C.5 shows the variations in FD of the sections over the years.

Table C.1: Average fractal dimension (FD) over the years of the six marsh sections.

Section	**A**	**B**	**C**	**D**	**E**	**F**
Avg FD	1.015	1.011	1.073	1.052	1.100	1.126

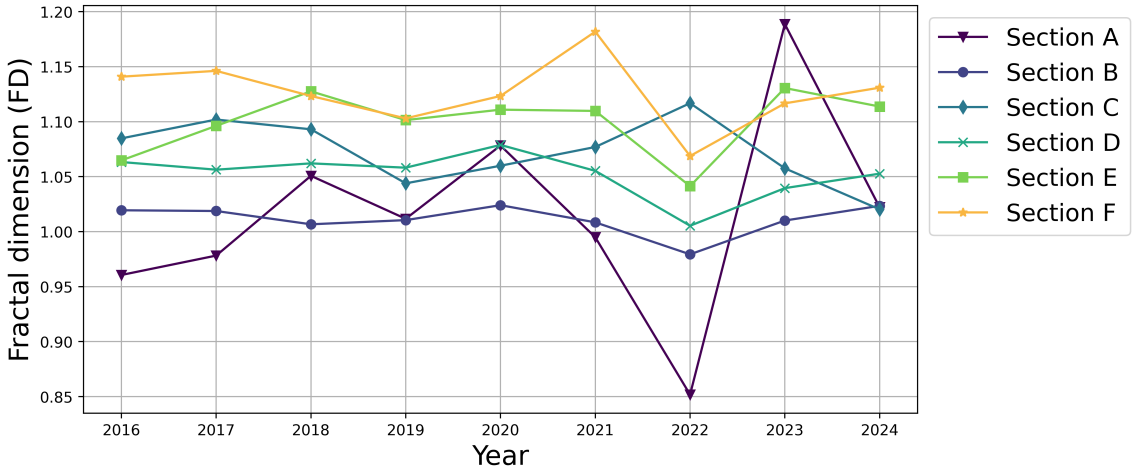

Figure C.5: The fractal dimension (FD) of the six marsh sections over the years.

The average FD of section A does not really stand out from the other sections (Table C.1). However, there is a lot of variation in FD over the years for section A compared to the other sections. Especially the data point for 2022 and 2023 have an extremely low and high value, respectively (Figure C.5).

The dimensionless erosion rate (E^*) of the different sections for the different years is plotted against the fractal dimension (FD, no unit) in Figure C.6, where also a linear fitted trend line through all data points and the goodness-of-fit metrics are added.

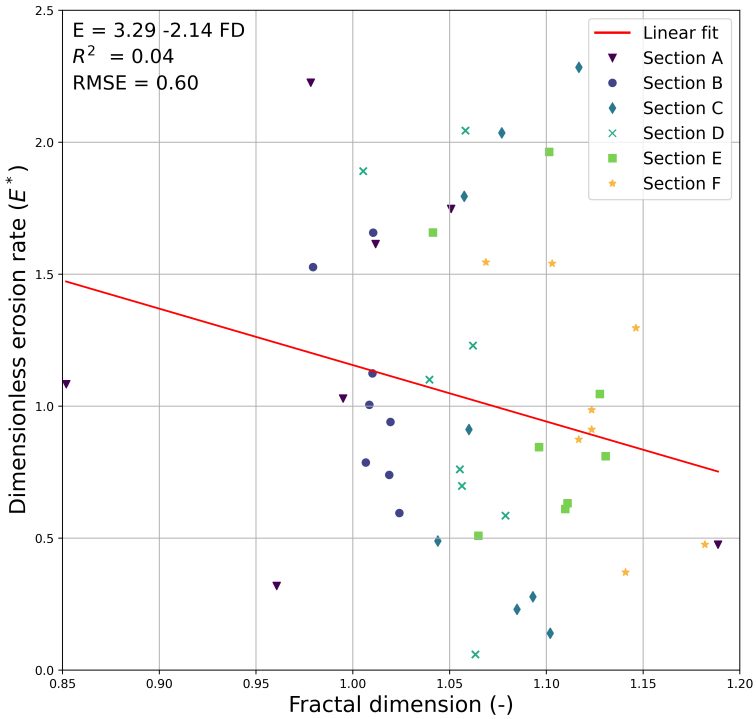

Figure C.6: Erosion rate (E in m/year) plotted for the fractal dimensions (FD, no unit) of the different sections and the different years, including a linear fit through the points.

Adding the data points from section A to the E^* - FD plot with the linear fit does not give a very different result. The slope and the point of intersection with the y-axis of the linear fits are both in the same order of magnitude whether section A is included or excluded. Including section A does not result in a difference in R^2, but the RMSE is larger: 0.60 compared to 0.56. This can be explained by the large spread of the data points of section A in the plot.

C.2.3 E - NDVI relation

Table C.2 shows the average 90th percentile value of NDVI over the years for all six sections and Figure C.7 shows the variations in NDVI of the sections over the years.

Table C.2: Average NDVI near the marsh edge over the years of the six marsh sections.

Section	**A**	**B**	**C**	**D**	**E**	**F**
Avg 90th percentile NDVI	0.010	0.213	0.126	0.0955	0.00616	-0.0682

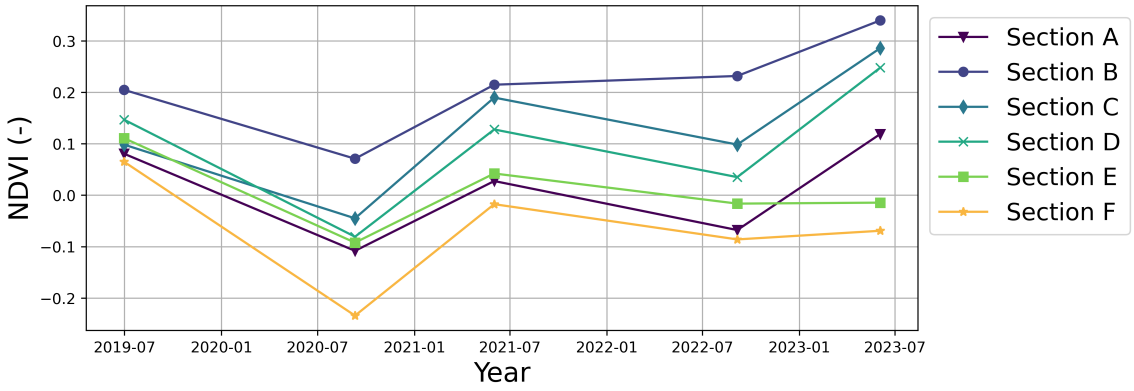

Figure C.7: The average NDVI near the marsh edge of all sections plotted over the available years.

The NDVI of section A presents a quite low value, which indicates that there is little to no vegetation near the edge of the marsh. However, the NDVI for section A does not stand out from the other years. This can be explained by the fact that in sections E and F there was also no vegetation near the marsh edge.

The dimensionless erosion rate (E^*) of the different sections for the different years is plotted against the NDVI (no unit) in Figure C.8, where also a linear fitted trend line through all data points and the goodness-of-fit metrics are added.

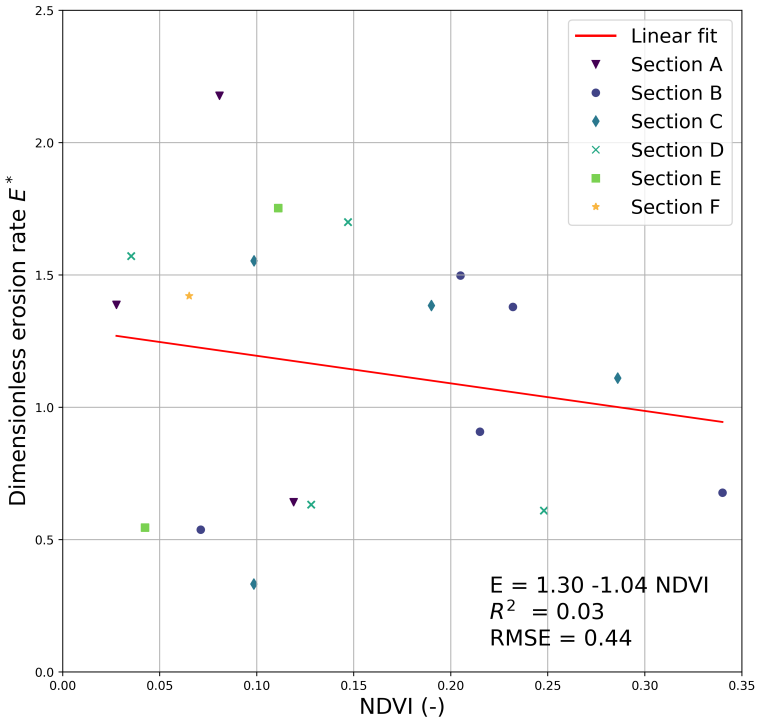

Figure C.8: Dimensionless erosion rate plotted against the NDVI of all sections and the different years, including a linear fit through the points.

Adding the data points from section A to the E^*-NDVI plot with the linear fit does not result in a different relationship. All parameters remain exactly the same. This can be explained by the fact that section A shows similar NDVI values as sections E and F and fits well in the existing spread of data points.